Isolation and Functional Analysis of Cellular Components of the Bronchiolar Stem Cell Hierarchy

by

Roxana Maria Teisanu

MD, University of Medicine and Pharmacy, Cluj-Napoca, Romania, 2002

Submitted to the Graduate Faculty of

School of Medicine in partial fulfillment

of the requirements for the degree of

Doctor of Philosophy

University of Pittsburgh

2009

UNIVERSITY OF PITTSBURGH

School of Medicine

This thesis was presented

by

Roxana Maria Teisanu

It was defended on

04-30-2009

and approved by

William Walker, Ph.D., Associate Professor, Department of Cell Biology and Physiology

Joseph Pilewski, MD, Associate Professor, Division of Pulmonary, Allergy and Critical Care Medicine

Eric Lagasse, Pharm.D., Ph.D., Associate Professor, Department of Pathology

Thomas Smithgall, Ph.D., Professor, Department of Microbiology and Molecular Genetics

Tony Plant, Ph.D., Professor, Department of Cell Biology and Physiology

Thesis Director/Dissertation Advisor: Barry R. Stripp, Ph.D., Professor, Duke University Medical Center

Isolation and Functional Analysis of Cellular Components of the Bronchiolar Stem Cell Hierarchy

Roxana Maria Teisanu, MD

University of Pittsburgh, 2009

Abstract

Mouse bronchiolar stem cells have been identified *in vivo* based on functional characteristics including naphthalene resistance, long-term retention of labeled DNA precursors, and dual expression of markers for airway (CCSP) and alveolar (pro-SPC) epithelium. Further characterization would benefit from establishment of rigorous enrichment strategies allowing analysis of their behavior in vitro and following transplantation, and the establishment of a defining gene expression signature. We have determined that Epithelial Cell Adhesion Molecule (EpCAM) and Integrin α6 are expressed on the cell surface of both alveolar and bronchiolar epithelial cells and that low levels of Sca-1 expression characterize the bronchiolar epithelium. Within the Sca-1^{low} $EpCAM^{pos}$ $Integrin\alpha6^{pos}$ population of bronchiolar epithelial cells, autofluorescence (AF) levels distinguish the facultative transit-amplifying population which is AF^{hi} from bronchiolar stem cells which are AF^{low}. Use of transgenic animal models allowing expansion or depletion of the stem cell compartment and use of lineage tracing strategies have allowed us to determine the identity of cells isolated based on their cell surface phenotype and autofluorescence characteristics. Injury models associated with depletion of terminally differentiated ciliated cells (ozone) or facultative transit amplifying population (naphthalene) were used to validate the functional characteristics of the two fractions of bronchiolar progenitors. In conclusion, we have developed and validated a fractionation approach for the generation of highly purified preparations of bronchiolar stem and Clara cells from the mouse lung. These data enable establishment of robust *in vitro* and transplantation assays to further validate the functional behavior of stem and facultative TA (Clara) cells and allows analysis of gene expression profile of the two populations towards a better understanding of unique characteristics of the bronchiolar stem cell compartment.

TABLE OF CONTENTS

LIST OF TABLES

LIST OF FIGURES

PREFACE

I would like to acknowledge Dr. Keitaro Matsumoto for his help with the naphthalene experiments, Dr. John Whitesides for his help with the flow cytometry analysis and sorting and Dr. William Foster and Erin Potts for their help with ozone exposures.

1.0 INTRODUCTION

1.1 HETEROGENEITY OF EPITHELIAL CELLS IN THE ADULT AIRWAY

The adult mammalian lung is a complex organ that evolved to facilitate gas transfer between inspired air and the blood. To accomplish this process, structural components of the lung are organized into a branching system of conducting airways and blood vessels that terminate in the gas exchange unit, the alveolus. The respiratory tract is lined by a structurally heterogeneous epithelium in which cell types are organized into specialized functional zones based upon their progenitor-progeny relationships[1-3]. This epithelium fulfills a range of secondary functions from muco-ciliary clearance[4] to secretion[5,6], metabolism, and the detoxification of either systemic or inhaled xenobiotic chemicals[7-9]. Epithelial cell types can be distinguished based upon their unique ultrastructural characteristics and gene expression profiles. The lining of tracheal and bronchial airways is a pseudo-stratified epithelium composed of basal cells, secretory cells, other less abundant nonciliated cell types such as neuroendocrine cells, brush cells and intermediate cells, and ciliated cells[10-12]. The most distal conducting airways, the bronchioles, are lined by a simple cuboidal epithelium consisting of Clara cells, ciliated cells and rare neuroendocrine cells[13]. Neuroendocrine cells are commonly organized into clusters, which are associated with nonciliated cells that lack the typical ultrastructural features of Clara cells[14]. The epithelium lining alveoli is composed of alveolar type II cells (ATII), which secrete

pulmonary surfactant, and alveolar type I cells (ATI), which are highly specialized epithelial cells with a large surface area to facilitate gas transfer[3,15].

1.2 EPITHELIAL FUNCTION

With every inspiration the lung epithelium is exposed to micro-organisms and their pyrogenic by-products, viral particles, oxidative pollutants, and particulate matter. Despite these persistent environmental challenges, the epithelial lining turns over at a very low rate due to innate hosts defense mechanisms that preserve tissue integrity[16-19]. To prevent undue injury and an unwarranted immunological response the airway epithelium provides for physical clearance of inhaled stimulants through mucociliary clearance[20]. In the event that mucociliary clearance is overwhelmed, the epithelium also plays a pivotal role in regulation of the innate inflammatory response. Recent studies highlight the fact that tight regulation of the NF-kappaB signaling pathway in epithelial cells is required for appropriate control of the inflammatory response and communication with resident lung macrophages required for an effective response[21-25].

In contrast, these processes are likely compromised in the setting of chronic lung diseases, such as cystic fibrosis and chronic obstructive pulmonary disease, resulting in chronic epithelial injury, defective repair, and subsequent remodeling of the epithelial-mesenchymal trophic unit[26]. Recently, we have demonstrated that defective epithelial repair can phenocopy aspects of chronic lung disease, such as bronchiolar and alveolar extracellular matrix (ECM) deposition and an augmented inflammatory response suggesting a role for altered progenitor cell behavior in disease etiology[27,28]. In other organ systems, it has also been shown that deregulation of the stem cell compartment leads to acute and chronic diseases[29,30]. In the

hematopoietic system, for example, increased proliferation of either stem or progenitor cells can lead to disorders such as leukemia and lymphoma[30], whereas defects in cellular differentiation can lead to severe immunological abnormalities[31]. Although evidence of a direct cause-effect relationship between different disease states and the status of the resident stem cell or the niche is currently lacking, it has been suggested that diseases such as lung cancer can arise from resident progenitor cells[29,30]. Understanding the hierarchical organization of progenitor cells within the lung and the relationship between these cells and changes in their behavior with lung disease becomes critically important. The following sections summarize what is known of progenitor cells within each of the three major epithelial compartments: the tracheal-bronchial epithelium, the intra-pulmonary airways, and the gas-exchange area.

1.3 PROGENITOR CELLS AND LINEAGE SPECIFICATION IN THE DEVELOPING LUNG

Lineage relationship amongst different cell types and progenitor-progeny relationship in the extra- and intra-pulmonary epithelium have been thoroughly studied in mouse models of lung development. One of the earliest events in lung development is formation of the two lung buds from the foregut endoderm. Growth of the lung primordia and subsequent branching morphogenesis, sacculation, and alveolarization are dependent upon appropriate interactions with the surrounding foregut mesoderm[32]. Signaling between the two compartments is mediated by a variety of growth factors, amongst which members of the FGF[33,34], Tgf-β/BMP[35], and Wnt[36,37] families of paracrine regulatory factors play central roles. The tracheal epithelium arises from different foregut endoderm progenitors located anterior to the initial lung buds forming

within the foregut endoderm. Initially the trachea and the esophagus form a common tubular structure that is subsequently partitioned into two separate tubular organs[32]. Despite the distinct origins of extrapulmonary versus intrapulmonary airways the finding that distal lung mesenchyme can redirect primitive tracheal epithelium to a distal fate suggests that early endodermal progenitor cells are multipotent and that their fate is tightly regulated by paracrine interactions with surrounding mesenchyme[38,39]. Thus, epithelial cells of the conducting and alveolar airways, including basal, ciliated, secretory, neuroendocrine, and alveolar type I and II, arise from common endodermal progenitors. However, a growing body of evidence suggests that once lung endoderm has been specified in the embryonic foregut, the ensuing process of lung development yields distinct lineages that are maintained independently of one another in the late embryonic and postnatal periods. This developmental process has been reviewed extensively elsewhere[32].

1.4 ADULT STEM CELLS AND TISSUE MAINTENANCE BY A STEM CELL HIERARCHY

The term adult tissue stem cell was coined to describe cells with the ability to proliferate and generate differentiated progeny within a tissue, yet retain the capacity for long-term self-renewal. Unlike embryonic stem cells, a pluripotent cell type that can be maintained in culture by providing medium additives but lack a stable in vivo counterpart, adult tissue stem cells generally have more restricted differentiation potential and can be maintained for prolonged periods in vivo[40,41]. Cells with these characteristics were first described in the hematopoietic system. The capacity of hematopoietic stem cells to generate all specialized cell types of the

hematopoietic lineage and undergo long-term self-renewal were only validated through use of in vivo transplantation assays[42,43]. Similar cells have since been described in other organs including the intestine[44-46], nervous system[47], epidermis[48,49], and epithelial of the cornea[50], mammary gland[51-53], lung[17,18,54,55], liver[56,57], pancreas[58], and prostate[59]. However, tissue-specific differences in the kinetics of cell replacement coupled with anatomic constraints and differences in cellular complexity have made identification and classification of stem cells difficult in many tissues. Accordingly, a range of other properties have been used to define the stem cell compartment within a tissue and the mechanisms contributing to their regulation. Such mechanisms may be less uniformly applicable and in some cases can only be applied to stem cells of a single tissue type. Relevant properties of stem cells and their more specialized derivatives are discussed below in the context of understanding stem cell behavior within the lung and other tissues, and assays commonly used for their identification and characterization.

The classical view of a stem cell hierarchy is that rare stem cells are believed to proliferate infrequently and divide asymmetrically. Asymmetric division yields one daughter that is identical to the parent cell and another that has more limited capacity for self renewal. The latter has the ability to generate large numbers of differentiating progeny and it was therefore termed the transit-amplifying (TA) cell[41,60,61]. Despite this, not all putative tissue stem cells have been shown to undergo asymmetric division. Moreover, among those tissue stem cells that have been shown to undergo asymmetric cell divisions, regulatory mechanisms have been defined for just a few[62,63]. The best described mechanism defines self-renewal of drosophila germline stem cells, for which asymmetric divisions are tightly regulated through adhesion complexes formed between stem cells and somatic cells that form the stem cell niche[64]. Even though there is support for the concept that asymmetric cell division may in some cases control long-term

maintenance of tissue stem cells, far less is known of mechanisms that govern the life span and behavior of TA cells. Tissue-specific differences are observed in the lifespan of TA cells which has potential to impact the activity of tissue stem cells. The life span of TA cells is dictated by two variables: the probability of self-renewal versus differentiation and their proliferative frequency. The impact that the probability of TA cell differentiation has on tissue homeostasis is evident in a comparison of TA cells of the intestinal epithelium and the interfolicular epidermis. Both of these tissues harbor TA pools that proliferate frequently for normal tissue maintenance but differ in their longevity. TA cells of the intestinal epithelium exhibit a relatively high probability of generating post-mitotic progeny leading to their rapid depletion and continuous requirement for stem cell proliferation to maintain regenerative capacity. In contrast, TA cells of the interfolicular epidermis have a relatively low probability of generating post-mitotic progeny leading to their long-term maintenance and infrequent activation of stem cells[65,66]. These examples serve to highlight how changes in the probability of TA self renewal versus differentiation have potential to dramatically impact the requirement for stem cell activation in tissue maintenance and help to explain tissue-specific differences in stem cell behavior.

1.5 APPROACHES TO CHARACTERIZE AND HIERARCHICALLY ORGANIZE PROGENITOR CELLS

A number of approaches have been developed to identify progenitor cells, understand their behavior in vivo, and to distinguish tissue stem cells from TA cells within a stem cell hierarchy. The more commonly used are discussed briefly below:

1.5.1 Lineage Analysis

Progenitor-progeny relationships can be defined in vivo through use of labeling methods to tag cells and determine their fate. Three principal approaches have been used. The most straight forward approach is to label the nascent DNA of S-phase cells through incorporation of nucleotide analogs. Commonly used nucleotide analogues include tritiated thymidine (TdR) or bromodeoxyuridine (BrdU), although other halogenated thymidine analogues have also been used such as chlorodeoxyuridine (CldU) and iododeoxyuridine (IdU)[1,3,67-69]. Delivery of these labeled DNA precursors into the systemic circulation results in their delivery to proliferating cells and incorporation into DNA during S-phase. Incorporation into nuclear DNA is typically assessed by either autoradiographic or immunohistochemical detection. When coupled with either ultrastructural analysis by transmission electron microscopy or immunophenotypic analysis at the light microscopic level, it is possible to determine the phenotype of proliferating cells and with an appropriate chase period in the absence of label, the fate of their progeny. Caveats with this approach are that experiments involving pulse-chase strategies do not allow for the retrospective identification of the parental cell that initially incorporated labeled DNA precursors, and that continuing proliferation of cells leads to label dilution which renders this method useless for lineage analysis.

An alternative method that allows analysis of lineage relationships is that of lineage labeling using recombinant retroviral vectors[70 71]. Mixed populations of retroviral vectors carrying different reporter genes allow for the analysis of clonality and lineage relationships. A caveat with this approach is the inability to retrospectively define the phenotype of the founding cell for a population of tagged cells that are identified after a defined “chase” period. Many of these technical hurdles have been overcome through use of lineage tracing methods involving

Cre/LoxP technologies[41,72]. Cre recombinase is a bacteriophage enzyme that catalyzes homologous recombination between adjacent LoxP sequences. Any DNA sequence that is engineered to include two adjacent copies of the LoxP sequence can serve as a substrate for Cre. Recombination catalyzed by Cre can lead to either deletion or reversal of the intervening sequence depending upon whether the LoxP elements are in the same or opposing relative orientation, respectively. A prerequisite for lineage analysis using the Cre/LoxP system is that progenitor cell-specific genes have been identified and their promoters characterized allowing the generation of transgenic mice capable of directing cell type-specific expression of Cre. Mice carrying the Cre-expressing transgene are crossed with a reporter line in which a LoxP-flanked transcriptional terminator sequence is present between an upstream ubiquitous promoter and a downstream reporter gene. In this case, Cre-mediated recombination activates the expression of the down-stream reporter, thus introducing a lineage tag within the cell that can be traced among daughter cells. When this strategy is coupled with use of ligand-regulated forms of Cre such as CreER, lineage tags can be introduced into defined cell types in a temporally controlled fashion [72,73].

1.5.2 In vivo Label-Retention

The concept that tissue stem cells proliferate infrequently compared to their transit-amplifying progeny formed the basis for assays to define these populations based upon this distinguishing characteristic. Infrequently proliferating cells have been identified in organs with high cellular turnover by labeling nuclear DNA with nucleotide analogues as discussed in detail above, followed by a chase period that dilutes the label within frequently cycling cells[74,75]. This assay has been used to define “label-retaining” cells (LRC). One pre-requisite of such

experiments is that the stem cell actively proliferates at the time of the pulse labeling. However, recent evidence in the intestinal stem cell compartment challenges the label-retaining dogma and shows that there is a population of non-label retaining stem cells at the bottom of the crypt, distinct from the classical LRC found 4 cells upstream from the bottom of the crypt (+4). Lineage tracing analysis demonstrates that these stem cells have the ability to generate the entire epithelium of the crypt and the villus, including the +4 epithelial cells[45]. Another limitation of this approach is its reliance on the difference in proliferation rate between the highly proliferative TA compartment and the relative quiescence of the stem cell. Thus, in organs with very low cellular turn-over such as the lung, pancreas, and liver, where both compartments proliferate infrequently in steady state, various injury models have been used to reveal the difference in proliferative potential of stem *vs* TA cell populations [17,18,55,58,76,77]. In these organs, chemical injury and/or tissue resection was used to reveal a population of label retaining cells with stem cell properties.

1.5.3 In vitro and transplantation assays

In vitro assays are dependent upon the existence of a set of positive and negative selection markers that allow prospective isolation of stem cell enriched populations. Once such enrichment is possible, the self-renewal and differentiating properties of these cells can be studied in clonogenic, serial-passage, and limited dilutions analysis assays[78,79]. However, *in vitro* experiments have the caveat of being dependent upon subjective medium components and are very susceptible to false interpretation due to inadequate culturing conditions that can bias progenitor cell renewal or differentiation independently of whether these cells function as tissue stem cells in vivo. Transplantation assays are rooted in the hematopoietic stem cell field where

functional validation of stem cell behavior can be verified through analysis of the capacity for long-term reconstitution of the entire hematopoietic system from one single cell[42,43,78]. This type of approach has been effectively employed in both the mammary gland and prostate to demonstrate that single cells isolated based on specific cell surface markers can reconstitute the entire gland when transplanted in immuno-compromised hosts[51,52,59].

1.6 PROGENITOR CELLS OF TRACHEOBRONCHIAL AIRWAYS

Analysis of clonogenic, differentiation, and proliferative potential of progenitor cells in the tracheobronchial epithelium have benefited from the use of *in vitro*[80] and transplantation[81] assays as well as *in* vivo models of epithelial injury and repair[82]. Transplantation studies in the trachea have been quite successful due to the relative ease of cell isolation, identification of cell surface markers for fractionation, and surgical transplantation compared to their more distal counterparts. Early work demonstrated that progenitor cells could be isolated from the tracheal epithelium, fractionated according to their ability to interact with the lectin *Griffonia simplicifolia* I (GSI)-B_4, transplanted into denuded rat tracheas, and differentiate appropriately to restore the cellular diversity of the tracheal epithelium[81,83]. From this study more sophisticated approaches have been utilized to more thoroughly define the progenitor capacity of tracheal epithelial cells. In a classical study, Engelhardt and colleagues isolated human bronchial epithelial cells, transduced these cells with retroviral constructs expressing a reporter gene for use in lineage tracing, and transplanted the cells into a denuded rat trachea. By analyzing the cell types represented in each clone, this study demonstrated that a single progenitor cell can give rise to all the cells of the airway surface epithelium in addition to the cells of the submucosal

glands[84]. These results suggest that a progenitor cell with more stem-like properties exists within the tracheobronchial compartment. In addition to these observations, this study is one of only a few to investigate human airway progenitor cell behavior. Unfortunately, the stochastic nature of retroviral transduction precluded a determination of the molecular or cellular identity of the initiating clonogenic cell. Each of these studies relied upon isolating cells from intact tissues, which could bias the experimental outcome based upon cellular viability during the isolation procedure. Therefore, a series of *in vivo* studies were initiated to better characterize the stem cell hierarchy in the tracheal epithelium.

Borthwick and colleagues repeatedly injured the tracheal epithelium through exposure to SO_2 or polydocanol and simultaneously treated with BrdU to label proliferating cells. To determine if a stem cell niche exists in the tracheal epithelium, label retaining cells in the repairing epithelium were quantified after various chase periods. These data demonstrated that label retaining cells existed in the upper and lower trachea in the sub-mucosal glands and at the junction of the inter-cartilaginous rings, respectively. This study also demonstrated that keratin 5 (*Krt5)* positive subsets of basal cells could be identified in tissue based upon activity of the β-galactosidase (β-GAL) reporter under control of the human *Krt5* promoter[16]. *Krt5* expressing cells were never immunolocalized with the label retaining cells. However, their localization to submucosal gland ducts and junctions of inter-cartilaginous rings was suggestive evidence that the label retaining cell may be *Krt5* positive. This study provided *in vivo* evidence that a stem cell niche may exist in the tracheal epithelium. The precise molecular and cellular identity of these label retaining cells remains unknown and recent studies have questioned label retention as a relevant assay for defining stem cell potential[45]. Collectively, these studies demonstrated that

epithelial progenitors exist in the tracheal epithelium, with a subpopulation of these cells sharing characteristics of resident adult tissue stem cells.

To determine the cellular identity and molecular profile of the tracheal epithelial stem cell a combination of *in vivo* lineage tracing and *in vitro* assays were utilized. These studies have demonstrated that subsets of tracheal and bronchial basal epithelial cells can be characterized by their multipotent differentiation potential. In 2004, both Schoch and colleagues as well as Hong and colleagues reported that the expression of keratins 5 and 14, respectively, demarcate cells with multipotent differentiation potential[85-87]. Using a ubiquitously expressing β-GAL transgenic mouse, Shoch and colleagues demonstrated that the mouse tracheal epithelium contains a population of cells capable of clonal expansion and multipotent differentiation when cultured *in vitro*, confirming the previous observations made by Engelhardt and colleagues in human xenograft transplantation. Based upon the previous observation that *Krt5* expression defines a subset of basal epithelial cells in the tracheal epithelium, a transgenic reporter mouse expressing EGFP under the control of the human *Krt5* promoter was used to fractionate tracheal basal cells. Fluorescent activated cell sorting and *in vitro* culturing indicated that EGFP positive cells display multipotent differentiation capacity and increased clonogenic potential relative to EGFP negative epithelial cells[85]. In contrast, Hong and colleagues used an *in vivo* lineage tracing strategy. A bitransgenic mouse line expressing the fused CRE-ERt under control of the *Krt14* promoter crossed with the ROSA26-flox-stop recombination substrate was utilized to establish differentiation and clonogenic potential. In this study, it was demonstrated that following naphthalene ablation of secretory cells, *Krt14* expressing basal cells display either multipotent or unipotent differentiation capacity[87,86]. The relationship between the *Krt5* and *Krt14* expressing basal cells is currently unknown. Further fractionation of basal cells in

conjunction with *in vitro* and transplantation assays will be required before this relationship can be effectively studied. However, data to date suggest that basal cells are a heterogeneous population that includes a subset with greater clonogenic and differentiation potential suggesting that this subpopulation of basal cells may be the equivalent of a local tissue stem cell.

If cell based therapeutic approaches are to be implemented, faithful cell surface markers that allow for fractionation of progenitor cells must be identified. Several methods have been utilized to fractionate tracheal and bronchial epithelial cells. Previous work in the hematopoietic system fractionated stem cells on the basis of the phenotypic ability to rapidly efflux Hoechst dye, termed side population (SP) cells[88]. As such, several studies in the tracheal and bronchial epithelium have adopted this approach. Unfortunately, in mouse this method has been highly irreproducible indicating that the SP cell may be either epithelial or mesenchymally derived[89,90]. Despite this, a recent study used this approach to fractionate human SP tracheal and bronchial epithelial cells and analyze their differential potential *in vitro.* The results of this study indicate that human SP cells are capable of differentiating into epithelial cells. However, whether the SP enriches for cells with clonogenic or differentiation potential remains to be determined[91]. Regardless, it is evident that adopting cell surface markers or phenotypic profiles used to fractionate stem cells in other compartments does not guarantee enrichment of airway progenitors. Recent work has also demonstrated that human airway epithelial progenitors can be isolated, grown in three dimensional culture, efficiently transduced, and are capable of restoration of the airway epithelium in denuded tracheas[92]. In addition, these progenitor cells can be fractionated based upon the expression of aquaporin-3 to enrich for progenitor cell capacity[93]. Despite the current inability to reproducibly purify subpopulations of progenitor cells, a seminal study recently demonstrated that cell based therapeutic intervention in lung disease is now a

reality. In a proof of principle study, Macchiarini and colleagues conducted the world's first human main bronchus transplant using a donor denuded trachea seeded with recipient airway epithelial cells. The patient had presented with a stenosis of the left main bronchus and severely attenuated forced vital capacity (FVC) and FEV_1 (forced expiratory volume in 1 second) levels due to tuberculosis infection. Four months following transplantation, the epithelium was completely restored, FVC and FEV_1 levels returned to normal, and no signs of allograft rejection were apparent[94]. Although the study cannot rule out invasion of the recipient's own epithelial cells into the transplanted trachea, it yields great promise for the future of lung regenerative medicine. Collectively, these data indicate that despite the low rate of epithelial turnover in the tracheal and bronchial epithelium, this compartment maintains a sub-population of epithelial cells with incredible differentiation and clonogenic potential. Future studies are needed to adequately harness the potential of these cells in the treatment lung disease.

1.7 PROGENITOR CELLS OF BRONCHIOLAR AIRWAYS

The identity of bronchiolar progenitor cells and their differentiation potential was initially studied using TdR labeling methods to mark proliferative cells in the normal and repairing epithelium. Evans and colleagues, using Ozone and NO2 injury models to selectively injure ciliated cells in rat airways demonstrated that epithelial renewal is accomplished through a wave of proliferation. Pulse-chase experiments involving systemically delivered [^{3}H]-thymidine (TdR) were used to demonstrate that nonciliated bronchiolar (Clara) cells represented the only proliferative cell type that responded to ciliated cell injury and that daughter cells gave rise to either mature Clara or ciliated cells[2]. Furthermore, the authors very thoroughly describe the

morphological changes that secretory cells go through in order to enter the cell cycle and replenish the pool of terminally differentiated ciliated cells. Thus, the name Type A Clara cell was used in reference to Clara cells that have lost both secretory granules and smooth endoplasmic reticulum, ultrastructural changes that were accompanied by cell cycle progression through S-phase[1]. These findings indicated that secretory cells are multifunctional, fulfilling roles in secretion and metabolism in the resting state, yet proliferating in response to injury to effect renewal of the epithelium. This duality of function for airway progenitor cells is in contrast to the obligate progenitor function observed among transit-amplifying cells in classical stem cell hierarchies, thus the term facultative transit-amplifying (TA) cells.

The existence of bronchiolar stem cells and their contribution to repair has been suggested from analysis of airway injury models involving selective ablation of mature Clara cells. Clara cells of mammalian airways constitutively express phase I metabolizing enzymes such as cytochrome P450 that render them susceptible to injury by their enzymatic substrates. Clara cells of the mouse airway express cytochrome P450 isoenzymes 2B2 and 2F2 that metabolize naphthalene to toxic metabolites leading to selective cell death[95]. This model of naphthalene-induced airway injury has been used to investigate mechanisms of repair following depletion of this abundant pool of facultative TA cells [18,55,96-99]. Clara cell ablation is followed by a proliferative response, the magnitude, spatial context, and kinetics of which are dictated by the extent of injury and airway location, leading to renewal of the epithelium[97,100]. Repair of the Clara cell depleted bronchiolar epithelium is accomplished through activation of putative tissue stem cells that localize to two discrete microenvironments including bronchoalveolar duct junctions (BADJ) and neuroepithelial bodies (NEB)[17,97]. Using this injury-repair model, Hong et al and later Giangreco et al identified naphthalene-resistant CCSP-expressing cells that

incorporate labeled DNA precursors into nuclear DNA during the early repair response and show a long-term label-retaining phenotype indicative of an infrequently cycling tissue stem cell[18,55]. The term variant CCSP-expressing (vCE) cell was used to differentiate this population of naphthalene-resistant cells from naphthalene-sensitive Clara cells. A direct role for vCE cells in repair of naphthalene-injured airways was further supported through use of a transgenic mouse model allowing ablation of the entire CCSP expressing population[18,96]. In this model, conditional ablation of all CCSP-expressing progenitor cells, both naphthalene-sensitive Clara cells and the putative bronchiolar stem cell, was accompanied by complete abrogation of bronchiolar repair[18,96]. More recently, naphthalene-resistant vCE cells residing at the BADJ were found to exhibit the unique molecular property of expressing the alveolar type II epithelial cell marker gene pro-surfactant protein-C[99]. Cells with this CCSP/Pro-SPC expressing phenotype have been proposed as a multipotent bronchioalveolar stem cell based upon *in vitro* data suggesting that they can generate cells expressing either airway or alveolar marker genes when cultured *in vitro*[99]. It has not been determined whether resident bronchiolar stem cells, either those defined based upon their resistance to naphthalene or other putative stem cells, have the capacity to generate and renew alveolar epithelium in addition to that of the bronchiole.

Localization of naphthalene-resistant vCE cells to defined microenvironments within bronchioles suggests that these regions are analogous to stem cell niches described in other organs [48,101]. However, what actually constitutes the stem cell niche and what local factors regulate maintenance and activation of the stem cell population remain unknown. Neuroepithelial body-associated CCSP-expressing cells have the distinguishing properties of both naphthalene-resistance and unique electrophysiological properties suggesting that local microenvironmental factors regulate cellular behavior[102]. Properties of NEB-associated CCSP-

expressing cells that may confer resistance to naphthalene-induced airway injury include reduced expression of phase I xenobiotic metabolizing enzymes such as CYP2F2 [17]. Collectively, these data argue that extrinsic factors controlled by the local microenvironment impact the behavior of bronchiolar progenitor cells for maintenance of the stem cell phenotype, and that this phenotype confers intrinsic resistance to environmental agents such as naphthalene.

Insight into molecular pathways that regulate the behavior of bronchiolar progenitor cells come from studies involving use of mouse models carrying genetic perturbations of specific signaling pathways. Experiments using a Cre recombinase-activated form of the K-ras gene were the first to suggest that activation of this transducer of pro-mitotic signaling pathways had the potential to impact the behavior of bronchiolar progenitor cells[103]. Epithelial hyperplasia coupled with an increase in the abundance of CCSP/SP-C dual positive cells suggested that active K-ras signaling led to expansion of cells with some characteristics of the bronchiolar stem cell prior to formation of adenomas and peripheral lung adenocarcinomas. In addition to providing insight into possible mechanisms regulating stem cell pool size, this study also provided support for the idea that tissue stem cells may be the cell of origin for lung cancer. In contrast, activation of Wnt/β-catenin signaling, a pathway directly linked to epithelial carcinogenesis and stem cell maintenance in the gut, led to expansion of bronchiolar stem cells without evidence of hyperplastic/neoplastic transformation[104]. In this study, potentiation of β-catenin signaling at the time of bronchiolar epithelial cell specification that occurs during the late embryonic period of lung development resulted in the expansion of a cell population that is naphthalene resistant, highly proliferative in response to airway injury, and co-expresses CCSP and SP-C. The ability of Wnt/β-catenin pathway to expand the pool of airway stem cells through altering the maturation of developmental progenitor cells suggested that down-regulation of this pathway in

the developing airway is necessary for establishment of the normal balance between stem cells and specialized cell types of the bronchiolar epithelium[105,106]. Changes in the abundance of the putative bronchiolar stem cell population defined by co-expression of CCSP and SP-C were also seen in mice homozygous for a null allele of the Gata-6 gene[107]. Gata-6 deficient mice displayed enhanced Wnt/β-catenin signaling in the developing lung suggesting that β-catenin can function as a common transducer for multiple signaling pathways that have potential to regulate airway progenitor cell behavior. However, the finding that specific deletion of β-catenin within the airway epithelium late in development did not impact epithelial maturation or the capacity to undergo repair following injury suggests that β-catenin is not necessary for the bronchiolar stem cell activation or maintenance[106]. These findings suggest that multiple signaling pathways have the potential to impact stem cell pool size and differentiation potential. Other potential molecular regulators of the stem cell compartment studied to date include p38α MAP kinase, PI-3 kinase, Bmi-1, and PTEN[108-111]. However, even though disregulation of these pathways impacts the behavior of stem/progenitor cells in vivo, the pathway/s involved in physiological regulation of the stem cell within the niche have not yet been defined.

Further efforts to characterize cellular components of the bronchiolar stem cell hierarchy and their regulation have involved isolation and fractionation of airway progenitor cells. Caveats with this approach are that dissociation of lung tissue eliminates spatial cues that aid in the definitive identification of the bronchiolar stem cell defined by naphthalene resistance, and the common problem that gene expression analysis suffers from potential artifacts introduced during the isolation procedure. However, some of these difficulties have been overcome through use of genetically modified mouse models to introduce lineage tags and regulate progenitor cell pool size. Methods used for preparation of lung cells either enrich for certain epithelial cell types

through use of defined protease cocktails coupled with application to lung tissue in a manner that restricts enzymatic activity to a localized compartment [8,112], or have used methods for isolation of all lung cells[113].

Enrichment of different members of the bronchiolar stem cell hierarchy is highly dependent upon the existence of specific positive and negative selection strategies that exploit either biochemical or molecular characteristics to effect fractionation of a mixed population of cells[89,99,113-115]. The use of known markers for tissue stem cells, such as stem cell antigen-1 (Sca-1), has been used most frequently[89,99]. A strategy based upon positive selection for Sca-1 and CD34, and negative selection for CD45 and CD31, was used to enrich cells that were immunoreactive for both CCSP and SP-C from crude preparations of cells isolated using a method for enrichment of alveolar epithelial cells[96]. When placed in culture these cells have the ability to express aquaporin 5, CCSP and SP-C, markers for alveolar and airway epithelium, leading to the proposal that these cells have potential for either alveolar or airway differentiation and hence may represent a bronchioalveolar stem cell (BASC).

A significant hurdle to progress is the lack of novel marker genes that define the stem cell and more abundant facultative TA cell compartments. Recent studies in the gut have provided novel molecular markers that distinguish subsets of intestinal progenitor cells with stem cell activity[45]. However, validation of these marker genes is complex and requires rigorous *in vivo* lineage tracing. A number of strategies have been used to broaden the repertoire of molecular markers for analysis of epithelial cell differentiation in the developing and adult lung. Microarray analysis of lung tissue during naphthalene injury and repair led to the identification of novel genes that define the naphthalene-sensitive Clara cell population. Many of these genes including Claudin10, FMO3, PON1, AO3, are expressed in a developmental sequence within maturing

airway secretory cells[116]. However, these strategies have not revealed genes that specifically define the bronchiolar stem cell due to the rarity of this cell population in the lung.

1.8 PROGENITOR CELLS OF THE ALVEOLAR COMPARTMENT

The gas exchange area of the lung is lined by alveolar epithelial cells. There are two types of alveolar epithelial cells with different functional and morphological features. Alveolar type I (ATI) cells are thin flat cells that line the alveolus and juxtapose the endothelial cells, together forming the gas exchange area. They are the predominant epithelial cell type in the alveolar compartment and can be identified based on T1α (RTI40), caveolin 1 and aquaporin 5 expression[15]. Alveolar type II (ATII) cells are larger, cuboidal cells whose main function is surfactant production and they can differentiate into ATI cells[3]. Alveolar type II cells can be distinguished at the ultrastructural level by the presence of lamellar bodies and microvilli[117]. Although in the adult mouse ATII produce surfactant proteins A, B and C (SP-A, SP-B and SP-C), SP-C expression is considered to be a unique marker for mature ATII cells[118,119]. Despite this, SP-C is one of the earliest genes expressed in the lung epithelium[15]. In the developing mouse lung, cells expressing SP-C appear at the tips of epithelial branches as early as E 10.5 indicating that expression of this gene product has potential to mark immature lung progenitor cells in addition to mature ATII cells[32]. These cells are highly proliferative in the developing lung and give rise to both mature epithelial cell types of the alveolar compartment. However, the alveolar epithelium turns over very slowly in uninjured mature alveolus[120].

A number of injury models have been used as tools to investigate mechanisms of alveolar repair. Commonly used agents to elicit alveolar injury include hyperoxia[5,121] and NO2[3], resulting in predominantly ATI and endothelial cell injury. Repair mechanisms have been investigated largely through use of strategies to label proliferative cells such as the use of labeled DNA precursors such as TdR or BrdU[3]. In such models, ATII cells represent the only labeled epithelial cell population immediately after *in vivo* delivery of labeled nucleotide analogues[3]. However, studies using a labeling period followed by a chase in the absence of label have shown that proliferating ATII cells can either self-renew or give rise to ATI cells, thus demonstrating the progenitor-progeny relationship between these two cell types[3]. Very similar findings have been observed following isolation and culture of ATII cells, in which their capacity to proliferate and generate ATI cells has been clearly demonstrated[118,122]. Further *in vitro* studies have also raised the possibility that ATI cells may, under some conditions, exhibit the capacity proliferate and contribute to epithelial renewal[123]. However, the question from these experiments is whether cells cultured *in vitro* that exhibit some features of ATI cells, either morphological and/or molecular, are truly representative of their *in vivo* counterpart.

Studies similar to those performed in conducting airways identifying putative local tissue stem cells have not been performed in the alveolar compartment. Despite this, it is clear that not all ATII cells proliferate in response to alveolar damage and there is evidence of heterogeneity among ATII cell population [121,124,125]. It has been proposed that a bronchioalveolar stem cell exists that at least *in vitro* has the capacity for long-term maintenance and the generation of progeny that express some genes indicative of both bronchiolar and alveolar differentiation[99]. However, a cell type capable of contributing to both bronchiolar and alveolar epithelial lineages has not been demonstrated in vivo. Furthermore, evidence arguing that bronchiolar and alveolar

lineages are maintained as distinct regenerative compartments in the adult lung has been generated using *in vivo* lineage tracing studies[115]. These in vivo observations in animal models support the finding in human patients suffering from distal lung diseases with either alveolar wall destruction or fibrosis, that the alveolar compartment has a limited ability to repair and restore normal function.

1.9 RATIONALE

The lung epithelium turns over slowly in normal conditions but has significant regenerative capacity that can be activated following injury[1,2]. This regenerative capacity is critical for homeostasis due to continual exposure of the lung to injurious stimuli by either systemic or inhalation routes. Chronic injury leads to the establishment of disease states such as idiopathic pulmonary fibrosis, asthma, chronic obstructive pulmonary disease, and lung cancer[126]. Treatments with curative rather than palliative intent are currently unavailable for most of these diseases and our understanding of their pathogenesis is limited. In this regard, deciphering the molecular phenotype and mechanisms governing behavior of different components of the bronchiolar stem cell hierarchy becomes crucial in designing effective therapeutic interventions.

The main goal of the work presented here is to develop and validate methods that allow for prospective isolation and molecular and functional characterization of airway stem and progenitor cells. Transgenic animal models associated with either expansion or depletion of the bronchiolar stem cell compartment together with lineage tracing approaches enabled us to identify and fractionate lung epithelial progenitor and stem cells. Injury and repair models

confirmed their hierarchical organization according to their *in vivo* proliferative and differentiation potential.

2.0 MATERIAL AND METHODS

2.1 ANIMAL HUSBANDRY

Mice were bred and maintained in AAALAC approved facilities at the University of Pittsburgh and at Duke University. Animals used for experiments were maintained in pathogen free conditions with unrestricted access to food and water on a 12h light/dark cycle. All experiments were performed according to IACUC approved protocols on mice between 2-6 months of age.

2.2 TRANSGENIC ANIMAL MODELS AND GENOTYPING

Genotyping was performed by PCR amplification of genomic DNA isolated from the mouse tail by previously published method. Primer pairs and PCR conditions have been previously described[104,127,128]

Table 1. Transgenic animal models

Genotype	Acronym	Use of transgene
CCSP Herpes simplex virus thymidine kinase	CCTK	Ablation of the stem and facultative TA population following ganciclovir treatment
CCSPcre Catnb $^{floxE3/flox\ E3}$	ΔE3	Amplification of the stem cell population
CCSPcreRosa26$^{FloxSTOP\ EYFP}$	CCSPcre LSL EYFP	Lineage tracing of the bronchiolar epithelium (green bronchiolar epithelium)
SP-Ccre Rosa26TdTomato$^{Flox/FloxEGFP}$	SP-Ccre TdTomato/EGFP	Lineage tracing of the intrapulmonary lung epithelium (green alveolar and bronchiolar epithelium)
Rosa26TdTomato$^{Flox/FloxEGFP}$	TdTomato/EGFP	Ubiquitous TdTomato mice
FoxJ1 GFP	FoxJ1 GFP	GFP expression in ciliated cells
SP-C GFP	SP-C GFP	GFP expression in alveolar type II cells and bronchiolar stem cells

2.3 GANCICLOVIR TREATMENT OF CCTK ANIMALS

Ganciclovir (GCV) was administered using a miniosmotic pump (Alzet, CA) loaded with 50mg/ml solution (w/v) in PBS for delivery at a rate of 8µl/hour over a 24 hour period[18]. Miniosmotic pumps were primed in sterile saline (0.9% NaCl) for 2hours prior to subcutaneous implantation. Mice were anaesthetized with Ketamine (100mg/kg body weight) and Xylazine (10mg/kg of body weight). Pumps were placed subcutaneously through a 1.5cm incision in the back skin. Mice were recovered for 6 days in normal cage environment.

2.4 BROMO-DEOXY-URIDINE ADMINISTRATION

Bromo-deoxy-Uridine (BrdU) (Sigma, St.Luis, MO) was resuspended in pirogen free 0.9% NaCl solution (B.Brown Medical Inc., Irvine, CA) at a concentration of 6mg/ml and administered i.p. at 50mg/kg body weight at 12 hours intervals.

2.5 OZONE INJURY

For ozone exposures, 14 weeks old C57B6 males were exposed to 1.5ppm ozone for 12 hours and control mice were exposed to filter air for the same period of time. Mice were removed from their housing cages, and placed separately into individual stainless-steel wire cage units; these units were placed into 55-liter stainless-steel Hinners-style exposure chamber. The chamber was equipped with a high efficiency filtered air supply, such that chamber air (50-60% relative humidity air and a temperature of 20-22 C) was renewed at the rate of approximately 20 changes/h. Ozone was generated by passing 100% oxygen gas through an ultraviolet light source that was positioned upstream of the air supply to the chamber. Ozone is metered into the inlet air supply and the ozone concentration was monitored continuously within the chamber with an ozone ultraviolet light photometer (Dasibi model 1003AH; Dasibi Environmental Corporation, Glendale, CA). The photometer was calibrated regularly against a standard ozone source[129-131].

2.6 NAPHTHALENE INJURY

Naphthalene exposures were performed using 10 weeks old male C57B6 mice. Naphthalene (Fisher Scientific) was dissolved in corn oil (Mazolla) at a concentration of 25mg/ml and it was administered i.p. at a dose of 250mg/ kg body weight (see also Appendix A3)[18,55,104].

2.7 CELL ISOLATION

Airway epithelial cells were isolated based on a previously published method[8,104]. Mice were anesthetized and exsanguinated, the thoracic cavity was opened, the lungs were exposed and the trachea cannulated. Lungs were perfused with 10ml PBS and lavaged 4 times with 1ml PBS 0.2µM EGTA. One ml of 4U/ml Elastase solution (Worthington) was instilled in the airways and incubated for 5 minutes at 37^{o}C followed by three 0.5ml instillations for 5 minutes each. Lung lobes were removed following Elastase digestion, minced, and incubated with DNase I solution (0.5mg/ml) for 10 minutes at 37^{o}C. Cells were resuspended in 30mls ice cold HBSS(Gibco), pipetted up and down to release the epithelial cells and passed through a 100µm or a 70µm cell strainer. Five milliliters of FBS were added slowly at the bottom of each tube and the samples were spun by centrifugation at 500g for 8 minutes. Red blood cells (RBC) were lysed in RBC lysing buffer (eBioscience) on ice for 1 minute. Following RBC lysis, cells were resuspended in 25mls of HBSS 10mMHEPES, 2% fetal bovine serum and centrifuged at 500g for 8 minutes. Cells were resuspended in 500µl of HBSS 10mMHEPES, 2% fetal bovine serum and live cells were counted based on Trypan blue exclusion. For a detailed protocol, see Appendix A1.

2.8 FLOW CYTOMETRY

Isolated cells were resuspended at 1 x 10^6 cells in 100µl HBSS, 10mM HEPES, 2% fetal bovine serum (staining solution), and incubated with the indicated antibodies for 30 minutes at 4^oC in the dark. For antibodies description see table 2. Cells were washed with 1ml staining solution, resuspended in 300µl staining solution and analyzed using either a FACSVantage (BD Biosciences, San Jose, CA), a FACS Canto(BD Biosciences, San Jose, CA) or FACS CantoII (BD Biosciences, San Jose, CA). Propidium iodide (PI) (2µl/100µl cell suspension) or 7-Amino-Actinomycin D (7-AAD) (5µl/100µl cell suspension) was used for dead cell discrimination. Sorting experiments were performed using a FACS Vantage (BD Biosciences, San Jose, CA) or a FACS Aria (BD Biosciences, San Jose, CA) sorter. Data was analyzed using FlowJo 7.2.4 software (Tree Star, Inc).

For CCSP intracellular staining, cells were permeabilized using a 0.1% (v/v) Tween20 solution for 30min on ice, followed by incubation with FITC directly conjugated rabbit anti-CCSP antibody (1:10000 in house). To directly conjugate the CCSP antibody we used Zenon Direct Conjugation kit (Invitrogen, CA) according to the manufacturer instructions.

BrdU staining was performed using the BrdU FITC kit from BD Biosciences (San Jose, CA) according to the manufacturer instructions. For details on the staining procedure, necessary controls and data analysis see Appendix A2.

2.9 IMMUNOFLUORESCENCE

Cells were cytospun onto glass slides and fixed in 10% NBF for 30 minutes. Cells were permeabilized using 0.5% TritonX100 (v/v) in PBS for 30 minutes, blocked in 5% BSA (w/v) in PBS for 30 minutes and incubated with the primary antibody for one hour at room temperature: polyclonal rabbit anti-CCSP (in house,1:10000) and polyclonal goat anti-CCSP (in house, 1:10000) and rabbit anti-Pro-SPC (1:2500, kind gift from Y.P. Di, U. Pittsburgh) (see table2). A fluorescently labeled secondary antibody was added for one hour and slides were mounted using Fluoromount G (SouthernBiotech) with 4, 6, diamidino-2-phenylindole (DAPI , 2µg/ml) as a nuclear counterstain. Alternatively, paraffin embedded lung tissue was sectioned (5 µm thickness), deparaffinized in Xylene and rehydrated in decreasing concentrations of ethanol in PBS. Tissue used for frozen sections was cryprotected in 30% Sucrose in PBS for 3 to 4 hours with continuous shaking, followed by overnight degassing at room temperature. Tissue was then embedded in OCT, frozen at -80^{o}C, and sectioned at 5µm thickness. Cryo-sections were dehydrated in 100% ethanol and rehydrated in decreasing concentrations of ethanol in PBS. When necessary, antigen retrieval was performed using the microwave method followed by incubation in 0.05% Trypsin/EDTA tissue culture grade (Cellgro, Mediatech Inc, Manassas, VA) for 10 minutes at 37^{o}C. Slides were blocked in 5% BSA (w/v) in PBS and the primary antibody was added for 3 hours at room temperature (see Table 2). Slides were incubated for 1 hour at room temperature with a fluorescent secondary antibody and mounted in DAPI containing Fluoromount-G (2µg/ml). Fluorescent images were acquired using an Olympus Provis AX70 microscope equipped with a Spot RT digital camera. The same acquisition and analysis parameters were used for all samples in each experiment. Images were processed and analyzed using AdobePhotoshop (Adobe Systems Inc., San Jose, CA).

Table 2. Primary antibodies used for flow cytometry and tissue histology

Antigen	Host	Titer	Source
CCSP	Goat polyclonal	1:10000 (IF), 1:20000 (FC)	In house
CCSP	Rabbit polyclonal	1:10000 (IF)	In house
proSP-C	Rabbit polyclonal	1:3000 (IF)	Kind gift from P.Y. Di
FoxJ1	Mouse IgG1	1:1500 (IF)	Kind gift from S. Brody
BrdU	Rat IgG2A	1:500 (IF)	Accurate Chemical
BrdU	Mouse	1:100 (FC)	BD Biosciences
GFP	Rabbit polyclonal	1:1000 (IF)	Abcam
Sca-1	Rat IgG2A Clone D7	2:100(FC-eBiosciences) and 1:200 (FC-Biolegend)	eBioscience and Biolegend
Sca-1	Rat IgG2A Clone 13-161.7	2:100 (FC)	Biolegend
EpCAM (FITC, PE-Cy7)	Rat IgG2A Clone G8.8	1:200 (FC), 1:100 (IF)	Biolegend
Integrin alpha6 (CD49f PE and Alexa Fluor 647)	Rat IgG2A Clone GoH3	5:400 (FC) , 1:200 (IF)	eBioscience and Biolegend
CD45 (PE-Cy7, Biotinylated)	Rat IgG2B Clone 30-F11	1:200 (FC-BD Biosciences) and 3:200 (FC-eBioscience)	BD Biosciencies, eBioscience
CD31 (PE-Cy7, Biotinylated)	Rat IgG2A, Clone 390	2:100 (FC)	eBioscience and Biolegend
CD34 (Alexa Fluor 647, Biotinylated)	Rat IgG2A, Clone RAM34	13:200 (FC)	eBioscience

2.10 RNA ISOLATION AND REAL TIME PCR

Total RNA was isolated from single cell suspension using Promega SV Total RNA (Promega, Madison, WI) isolation kit, following manufacturer's instructions. RNA was reverse-transcribed using Superscript First Strand Synthesis Kit (Invitrogen, Carlsbad, CA) according to

the manufacturer's protocol and relative mRNA abundance of genes of interest was assessed using TaqMan FAM labeled probes (Applied Biosystems, Foster City, CA) and AB TaqMan 7000 Real Time System (Applied Biosystems, Foster City, CA).

3.0 SCA-1 AND CD34 EXPRESSION AND AUTOFLUORESCENCE CHARACTERISTICS OF EPITHELIAL CELLS OF THE RESPIRATORY EPITHELIUM

3.1 INTRODUCTION

. In previous work by us and others, bronchiolar stem cells were characterized as naphthalene resistant, label retaining, CCSP expressing cells that are spatially localized to either broncho-alveolar duct junctions or branch point-associated neuroepithelial bodies [18,55,97,99]. Based upon these criteria bronchiolar stem cells have either been termed variant Clara cells (Clara(v)) according to their unique functional properties but similarity with Clara cells in their expression of CCSP[18,55], or bronchioalveolar stem cells (BASC's) due to their co-expression of the airway marker CCSP and alveolar marker Pro-SPC , their Sca-1^{pos} CD34^{pos} cell surface phenotype, and their ability to express marker genes for both airway and alveolar epithelium *in vitro*[99].

In the present study, we used transgenic animal models allowing ablation[18,96], lineage tagging[104,132], and expansion[104] of the stem cell population to verify the cell surface phenotype of bronchiolar stem cells. We found that Sca-1 does not distinguish bronchiolar stem cells from the more abundant pool of facultative TA (Clara) cells and that neither population express cell surface CD34. We determine that bronchiolar stem and facultative TA (Clara) cells share the common property of low cell surface expression of Sca-1 that distinguished them from Sca-1^{high}

lung cells, and can be distinguished from each other based upon their autofluorescence (AF) characteristics. Accordingly, bronchiolar stem cells can be defined based upon their $CD45^{neg}$ $CD31^{neg}$ $CD34^{neg}$ $Sca\text{-}1^{low}$ AF^{low} phenotype.

3.2 RESULTS:

3.2.1 Sca-1 and CD34 expression in single cell preparations of lung cells

It has previously been proposed that the bronchiolar stem cells can be distinguished from other lung epithelial cell types by virtue of their cell surface expression of Sca-1 and CD34. In their analysis Kim and colleagues prepared lung epithelial cells using methods that enrich for alveolar epithelial cells[99]. We sought to determine whether cell surface expression of Sca-1 and CD34 allowed the prospective fractionation of bronchiolar stem cells from the abundant pool of facultative TA (Clara) cells. To address this question we interrogated expression of Sca-1 and CD34 on the surface of lung epithelial cells isolated using established methods that enrich populations of airway epithelial cells[8,104]. Single cell preparations were obtained by Elastase digestion of normal mouse lung and further enriched based upon negative selection for cell surface CD45 and CD31, and positive selection for viable cells based upon exclusion of PI or 7AAD (Figure 1). The profile of the $CD45^{neg}$ $CD31^{neg}$ live population prior to staining for Sca-1 and CD34 (Figure 2A, upper left panel) revealed two distinct populations based on their autofluorescence in the AF647 and PE channels. Staining of this population for Sca-1 (Figure 2A, upper right panel) revealed two distinct Sca-1 positive populations: a less abundant $Sca\text{-}1^{high}$ (R4 gate=5.33% of $CD45^{neg}$ $CD31^{neg}$ live population) and a more abundant $Sca\text{-}1^{low}$ population

(R3 gate =18.3% of $CD45^{neg}$ $CD31^{neg}$ live population). The Sca-1^{high} population was comprised exclusively of low autofluorescent (AF^{low}) cells, while the Sca-1 low population was comprised of both AF^{high} and AF^{low} cells. Staining the $CD45^{neg}$ $CD31^{neg}$ PI^{neg} population for CD34 (Figure 2A, lower left panel) revealed a $CD34^{pos}$ fraction (R1 gate = 12.11%) derived exclusively from the AF^{low} population. Staining for the combination of all markers and analysis of the $CD45^{neg}$ $CD31^{neg}$ live population revealed that Sca-1^{pos} $CD34^{pos}$ cells (R2 gate) accounted for 4.62% of the population (Figure 2A, lower right panel, and Figure 2A). We next determined the spatial localization of Sca-1 positive cells by immunofluorescent staining of lung tissue sections (Figure 2C). Sca-1 immunoreactivity was evident in cells outside the airway epithelium with apparently high expression levels detected within endothelial cells lining blood vessels. Consistent with this pattern of immunolocalization was the observation that more than 95% of the CD31 (PECAM) positive cells from lung cell preparations were Sca-1 positive (data not shown and Kotton et al.,[133]). Within the airway epithelium, Sca-1 immunoreactivity was only detected on the basolateral membrane of epithelial cells residing within proximal intrapulmonary airways. Epithelial cells of the distal conducting airway showed no evidence of Sca-1 immunoreactivity above baseline levels in this analysis. Taken together, these data demonstrate that Sca-1 is a broadly expressed marker in the lung, and that levels of Sca-1 immunoreactivity vary significantly between cell types. The high proportion of $CD45^{neg}$ $CD31^{neg}$ Sca-1^{pos} $CD34^{pos}$ cells in isolated cells raised the question of whether Sca-1 or CD34 are appropriate and/or specific cell surface markers for rare bronchiolar stem cells.

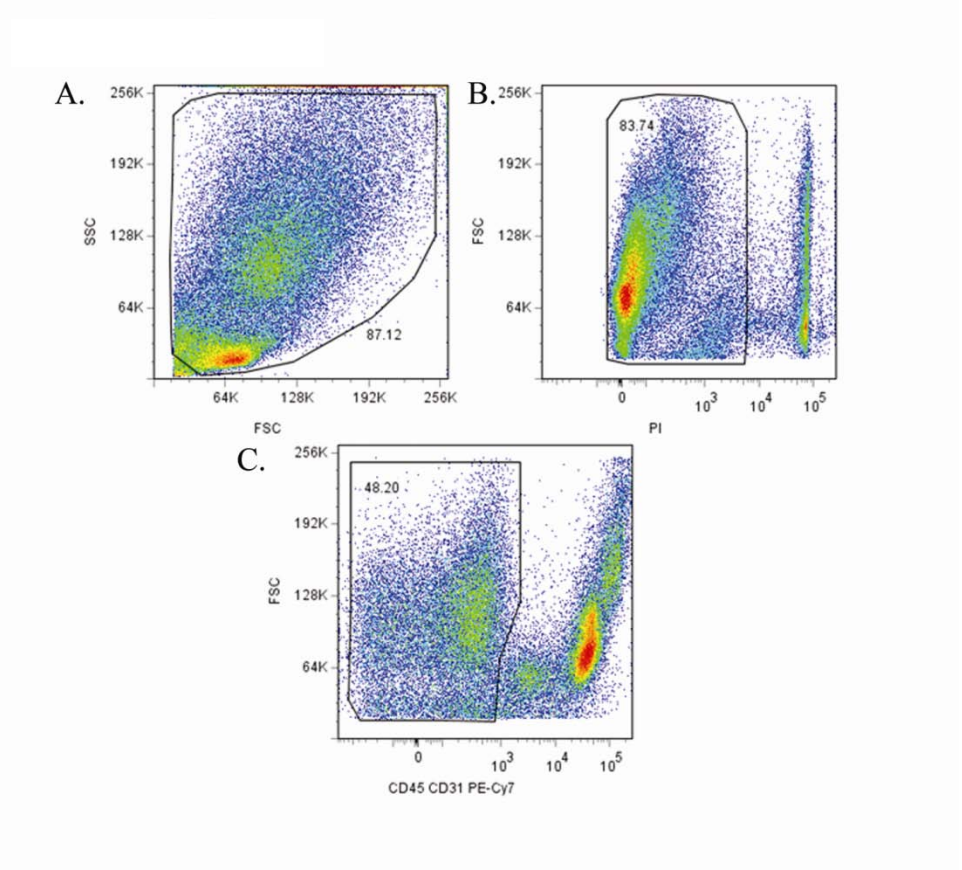

Figure 1. Exclusion of CD45pos CD31pos and dead cells.

Flow cytometry analysis of isolated lung cells showing the side scatter forward scatter profile (A), exclusion of PI^{pos} dead cells (B), and $CD45^{pos}$ $CD31^{pos}$ cells (C).

A.

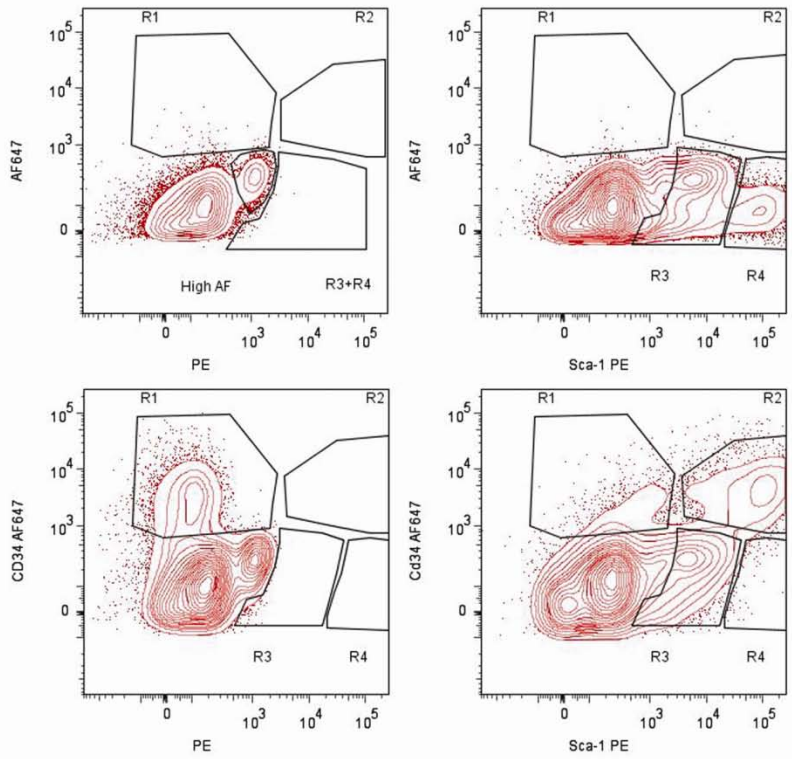
R1
R2
AF647
High AF
R3+R4
PE
Sca-1 PE
R3
R4
CD34 AF647
Cd34 AF647

B.

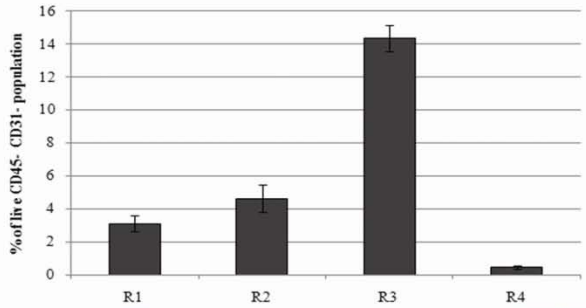
%of Lin e CD45- CD31- population
R1
R2
R3
R4

C.

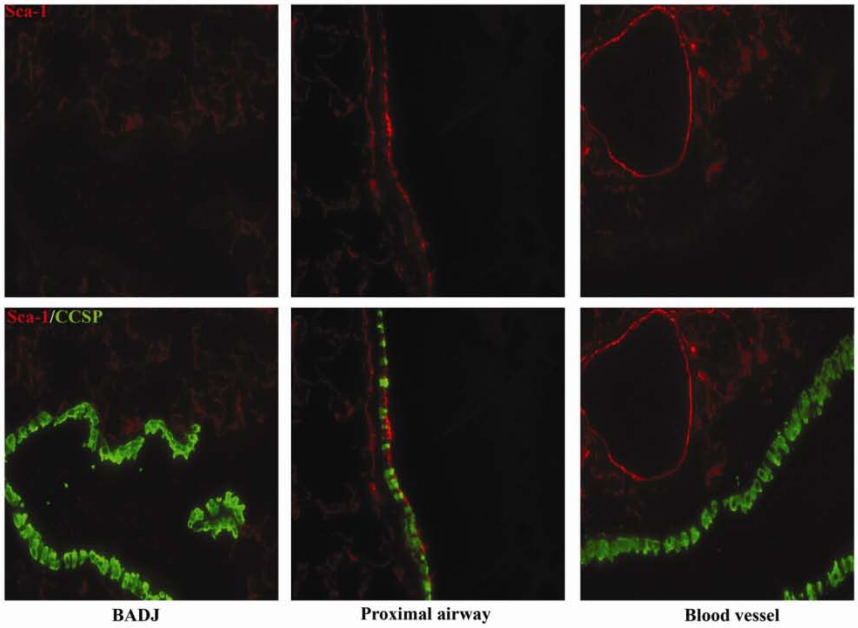
Sca-1
Sca-1/CCSP
BADJ
Proximal airway
Blood vessel

Figure 2. Sca-1 and CD34 expression in the lung

(A) Flow cytometry analysis of Sca-1 and CD34 expression on the cell surface of $CD45^{neg}$ $CD31^{neg}$ live single cell preparations from mouse lung (See Figure 1 for parameters used for initial selection of cells to be interrogated). Panels represent unstained control (upper left), Sca-1 stained sample (upper right), CD34 stained sample (lower left) and Sca-1 and CD34 stained sample. Gates identify populations as follows: R1 – CD34 positive population, R2 – Sca-1 and CD34 dual positive population, R3 – Sca-1^{low} population, R4 – Sca-1^{high} population. Unstained sample: R1=0.27%, R2=0.00, R3+R4=0.17%; Sca-1 stained sample: R1=0.14% R2=0.01% R3=18.3 R4=5.33%, CD34 stained sample: R1=12.11% R2=0.00% R3=0.38% R4=0.00% Sca-1 CD34 dual stained sample: R1=2.75% R26.07% R3=11.94% R4=0.30%. (B) Quantitative representation of data in (A). Data represent averages with standard error of the mean for 7 samples from 3 separate experiments. Data represent % of live $CD45^{neg}$ $CD31^{neg}$ population: R1=3.1% R2=4.62% R3=14.34% R4=0.46%. (C) Immunofluorescence staining of lung sections demonstrating the spatial localization of Sca-1 positive cells in the lung. Top row: Sca-1 (red) immunolocalization. Bottom row: overlay of Sca-1 staining with the nonciliated airway epithelial cell-specific marker CCSP (green). BADJ: broncho-alveolar duct junction. Images were taken at 200x magnification.

3.2.2 Sca-1 expression in Clara cell depleted lungs.

To further examine the population of lung epithelial cells that are positive for cell surface Sca-1 immunoreactivity we used a transgenic approach to ablate Clara cell secretory protein (CCSP)-expressing cells of the airway epithelium. In this model, expression of Herpes Simplex virus thymidine kinase under the mouse CCSP promoter allows ablation of the entire CCSP expressing population following GCV treatment. We have previously demonstrated that GCV exposure of CCSP-HSVtk (CCTK) transgenic mice results in ablation of both the abundant facultative TA (Clara) cell population and rare bronchiolar stem cells[18]. At day 6 post GCV treatment CCSP-expressing cells were significantly depleted (Figure 3). Isolated lung cells recovered from either untreated or GCV treated mice were interrogated by flow cytometry. After exclusion of dead and $CD45^{pos}$ $CD31^{pos}$ cells, Sca-1 and CD34 expression was analyzed and compared between treated and untreated animals (Figure 4A). In the absence of CCSP-expressing cells the size of the $CD45^{neg}$ $CD31^{neg}$ $Sca\text{-}1^{pos}$ $CD34^{pos}$ population did not change while the number of $CD45^{neg}$ $CD31^{neg}$ $Sca\text{-}1^{pos}$ $CD34^{neg}$ population increased, suggesting that other cells in the lung have the ability to express and upregulate Sca-1 in response to this mode of injury (Figure 4A and C).

Ganciclovir treatment resulted in loss of the AF^{high} population (unstained sample in Figure 4A and Figure 4B), suggesting that some or all CCSP-expressing cells have the property of high autofluorescence. To further explore this possibility, isolated cells from wild type animals were analyzed by flow cytometry for intracellular CCSP expression and their autofluorescence characteristics determined (Figure 4D). Overlay of the autofluorescence profiles of the CCSP-immunoreactive population and the no primary antibody control sample demonstrates that the majority of the CCSP-expressing cells belong to the AF^{high} population.

Importantly, a less abundant fraction of CCSP-expressing cells were localized to the AF^{low} population, suggesting that there are distinct sub-populations of CCSP-expressing cells in the airway epithelium. In conclusion, these data confirm that Sca-1 expression is not unique to the airway epithelium and that the AF^{high} population contains a sub-population of secretory cells. By inference, these data suggest that an abundant CCSP-expressing cell population with the characteristics of high autofluorescence accounts for a significant fraction of Sca-1^{low} $CD34^{neg}$ cells identified within the $CD45^{neg}$ $CD31^{neg}$ live fraction of lung epithelial cells.

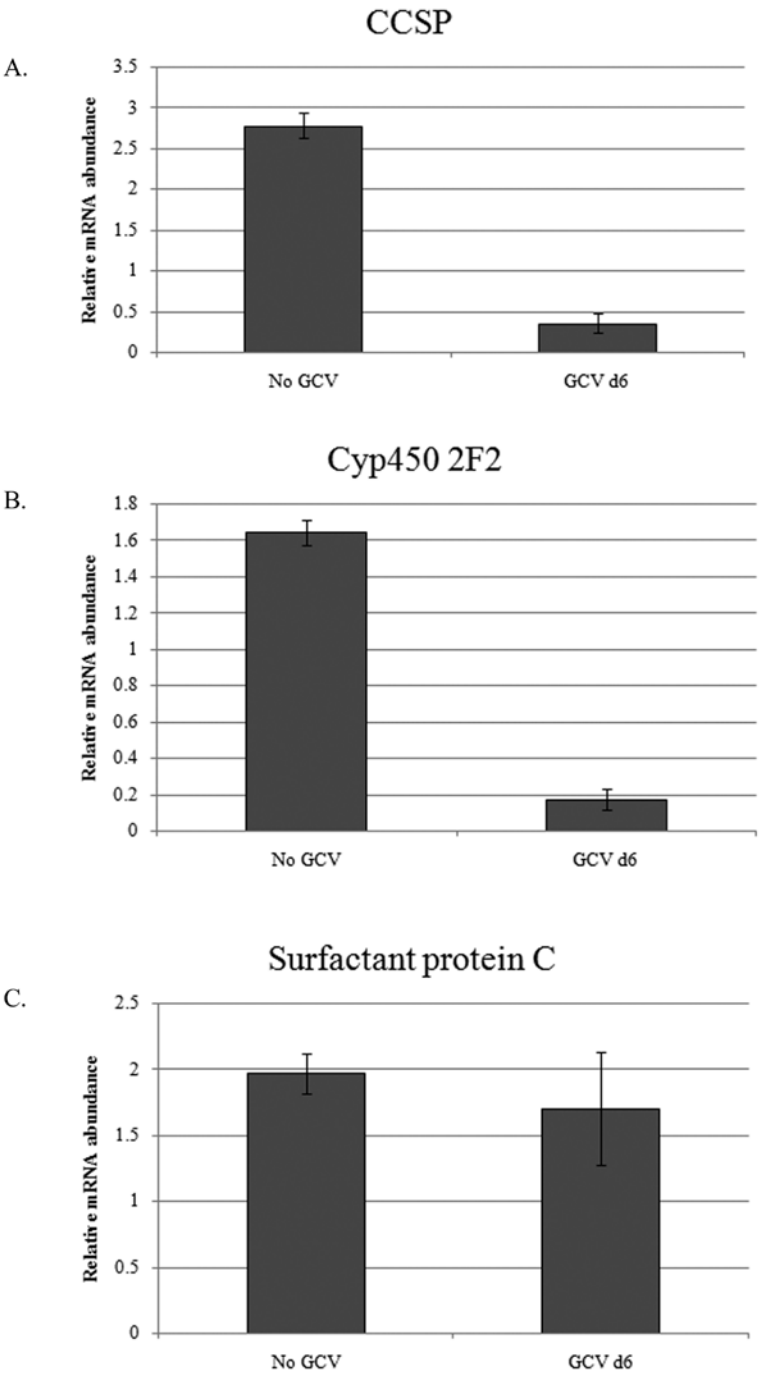

Figure 3. Assessment of the level of injury 6 days post GCV treatment

Real time PCR quantification of relative mRNA levels of airway specific genes CCSP and *Cyp2f2* and the alveolar type II cell marker SP-C.

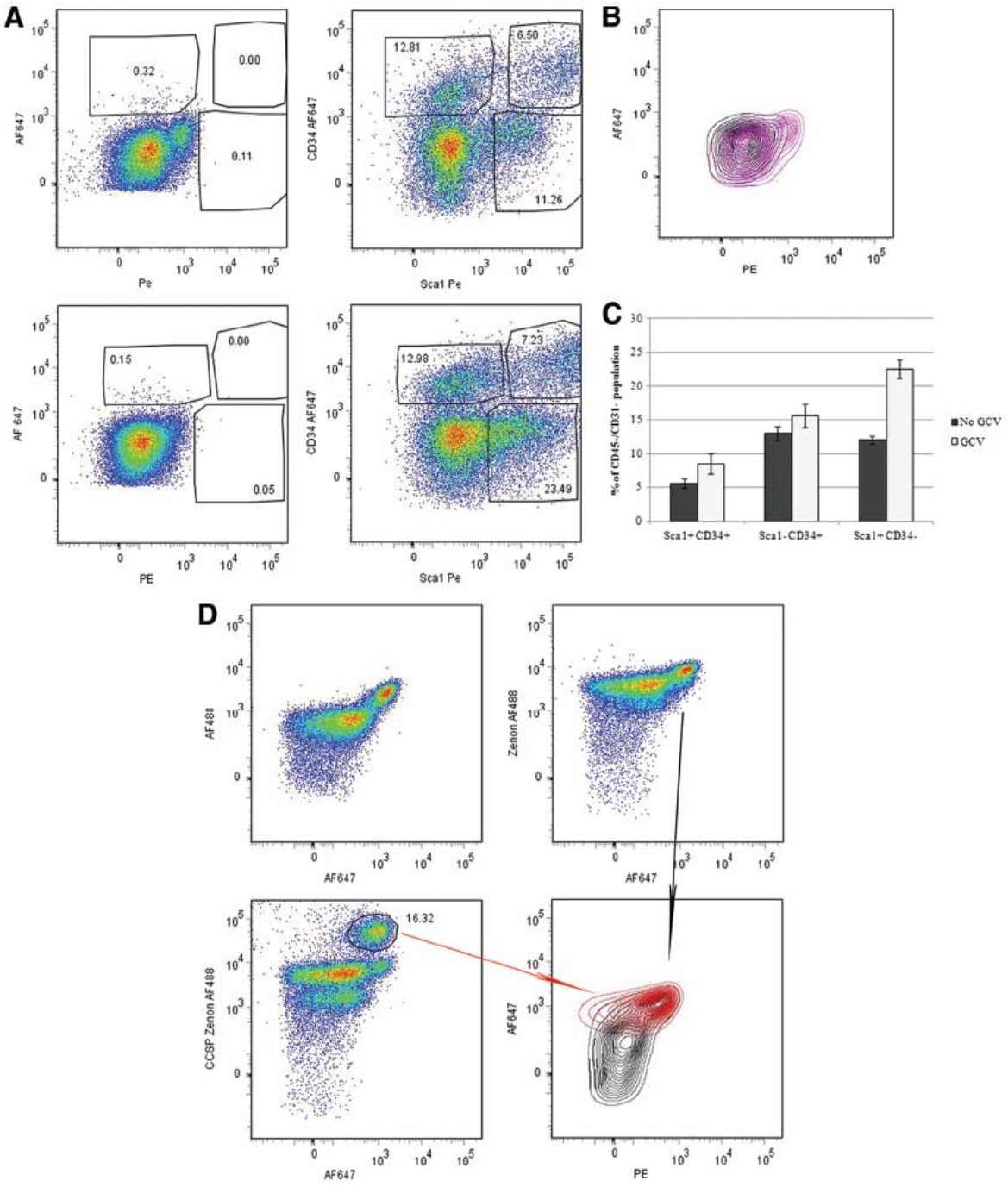
A
AF647
Pe
0.32
0.00
0.11
CD34 AF647
Sca1 Pe
12.81
6.50
11.26
AF 647
PE
0.15
0.00
0.05
CD34 AF647
Sca1 Pe
12.98
7.23
23.49
B
AF647
PE
C
%of CD45-/CD31- population
Sca1+CD34+
Sca1-CD34+
Sca1+CD34-
No GCV
GCV
D
AF488
AF647
Zenon AF488
AF647
CCSP Zenon AF488
AF647
16.32
AF647
PE

Figure 4.Sca-1 and CD34 expression following depletion of CCSP-expressing cells

Flow cytometry analysis of Sca-1 and CD34 expression on the surface of $CD45^{neg}$ $CD31^{neg}$ live cells isolated from untreated mice (top row) or CCSP-HSVtk transgenic mice recovered for 6 days post ganciclovir (GCV) treatment (bottom row). Left column represents unstained samples and right column represents Sca-1 CD34 dual stained sample. (B) Overlay of the autofluorescence (AF) profile (unstained sample) of $CD45^{neg}$ $CD31^{neg}$ live cells isolated from untreated mice (purple contour) or CCSP-HSVtk transgenic mice recovered for 6 days post ganciclovir (GCV) treatment (black contour) demonstrating the disappearance of the AF^{high} population following ablation of CCSP-expressing airway epithelial cells. (C) Quantification of data in (A). The percentages of cells in each of the three gates ($Sca\text{-}1^{pos}$ $CD34^{pos}$, $Sca\text{-}1^{neg}$ $CD34^{pos}$ and $Sca\text{-}1^{pos}$ $CD34^{neg}$) were compared between untreated (dark grey bars) and GCV treated (light grey bars) samples. (D) Intracellular staining for CCSP of cells isolated from a wild type animal showing the presence of CCSP-immunoreactive cells in the AF^{high} population. The panels represent unstained sample (top left), no primary control (top right), CCSP stained sample (bottom left) and overlay of the autofluorescence profiles of the CCSP positive (red contour) and no primary control (black contour plot) samples (bottom right).

3.2.3 The cell-surface phenotype of lineage tagged airway epithelial cells.

To clarify the cellular origins of different populations of isolated lung cells, a lineage tracing mouse model was employed. In these mice, tagging of secretory cells and their progeny was achieved by CCSP-Cre mediated recombination of a floxed stop sequence knocked into the Rosa 26 locus (ROSA-LSL-eYFP). Excision of the stop sequence allowed expression of eYFP protein[132]. Analysis of eYPF expression within CCSP-Cre/ROSA-LSL-eYPF demonstrated a pattern of recombination that was airway-specific and accounted for approximately 90% of bronchiolar epithelial cells as has been reported previously for other Cre substrates (Figure 5 and reference[104]). Lineage tagged bronchiolar cells included both CCSP-expressing cells and ciliated cells, consistent with the known lineage relationship between these cell populations[1]. Flow cytometry analysis of isolated lung cells from CCSP-Cre ROSA-LSL-eYFP mice and analysis for autofluorescent characteristics identified two distinct populations of $eYFP^{pos}$ cells: one showing high autofluorescence and one showing low autofluorescence (Figure 6A).

To address the lineage relationship between the two populations of $CD45^{neg}$ $CD31^{neg}$ $Sca\text{-}1^{pos}$ cells, we analyzed eYFP expression in the $Sca\text{-}1^{low}$ and $Sca\text{-}1^{high}$ populations (Figure 6B). The $Sca\text{-}1^{low}$ population (12.74% of the $CD45^{neg}CD31^{neg}$ live population) had 23.6% $eYFP^{pos}$ cells while the $Sca\text{-}1^{high}$ population (1.85% of the $CD45^{neg}CD31^{neg}$ live population) had very few $eYFP^{pos}$ cells (6.97%). These data demonstrate that $Sca\text{-}1^{low}$ but not $Sca\text{-}1^{high}$ cells contain CCSP-expressing cells and their derivatives. Analysis of $CD45^{neg}$ $CD31^{neg}$ $CD34^{pos}$ cells indicated that the $CD34^{pos}$ population did not belong to the bronchiolar lineage, as the vast majority of $CD34^{pos}$ cells were eYFP negative. Moreover, in the Sca-1 CD34 stained sample, the $CD45^{neg}$ $CD31^{neg}$ $Sca\text{-}1^{pos}$ $CD34^{pos}$ population lacked $eYFP^{pos}$ cells, demonstrating that cell surface staining for both Sca-1 and CD34 identified a population of cells independent of the

bronchiolar lineage (Figure 6B). Together these data demonstrate that expression of Sca-1 and CD34 is not a characteristic of airway epithelial cells, but that low levels of cell surface Sca-1 defines two populations of bronchiolar epithelial cells that can be segregated according to their autofluorescence characteristics.

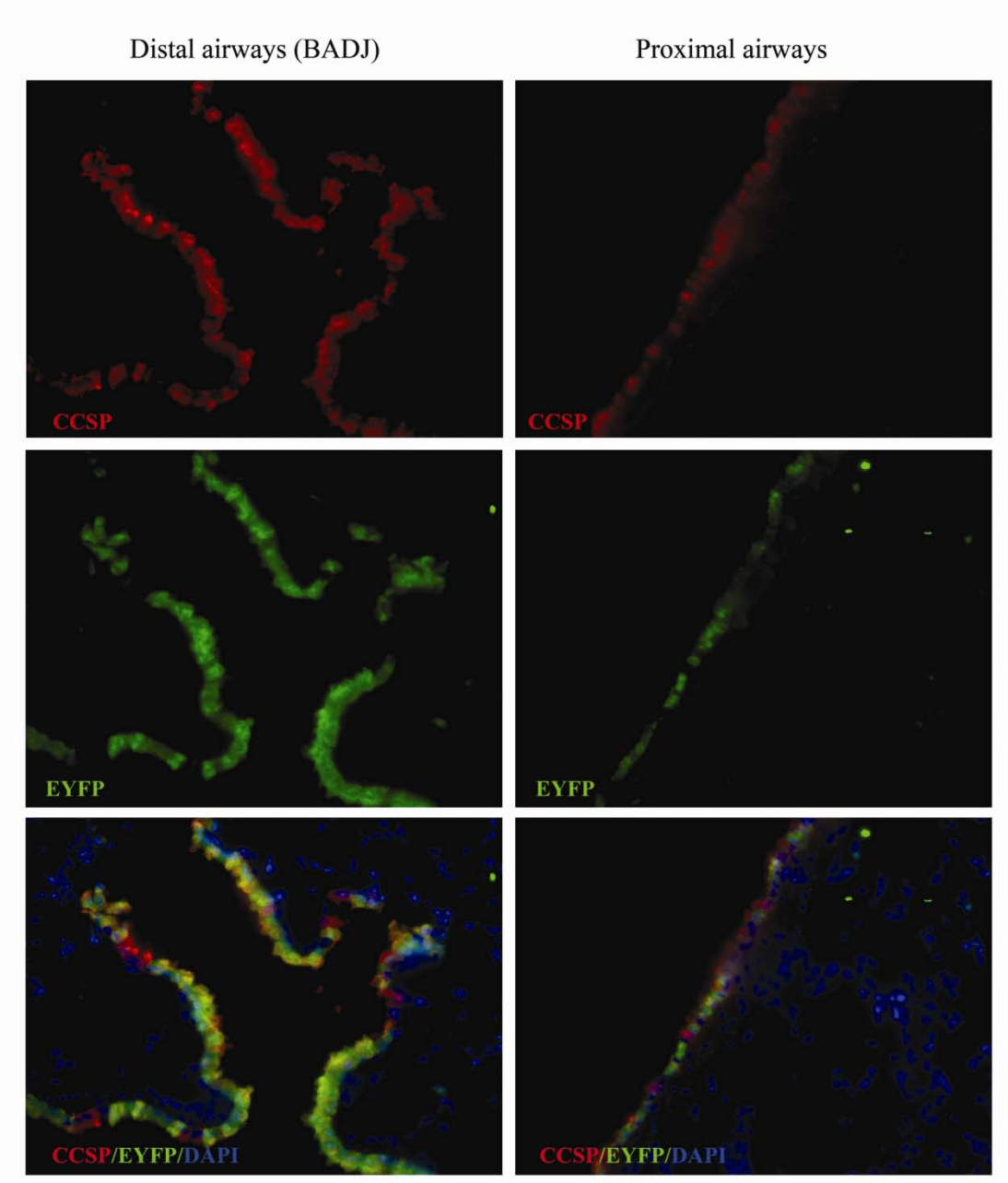

Figure 5. Recombination frequency in the airways of CCSPcre Rosa26-LSL-EYFP

Representative immunofluorescence images of lung sections from CCSP-Cre Rosa26^{EYFP} mice stained for CCSP (red) and eYFP (green). Right column shows images of distal airway epithelium and the left column shows images of the proximal airway epithelium (200 x magnifications).

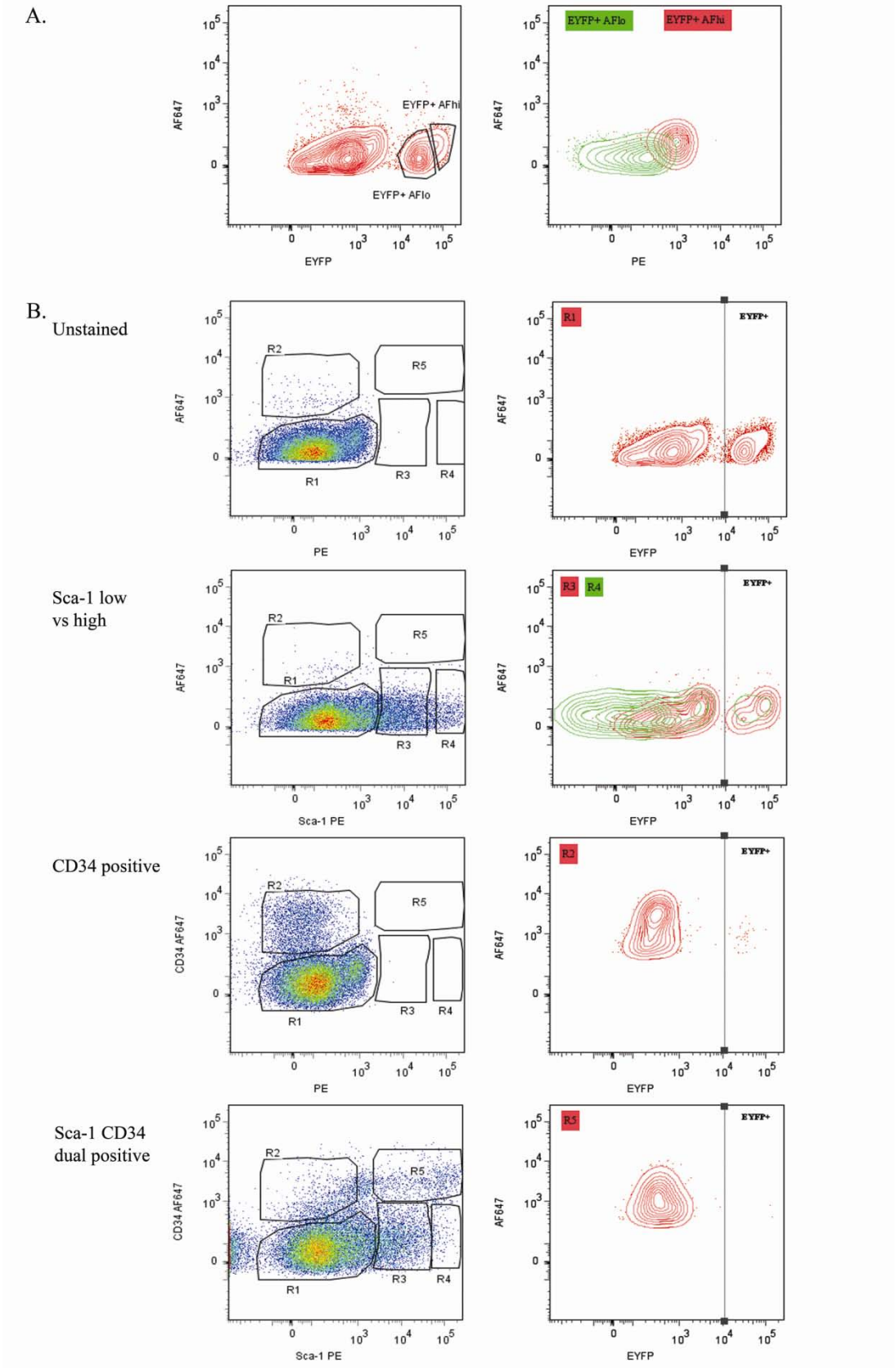
A.
EYFP+ AFhi
EYFP+ AFlo
AF647
EYFP
PE
B.
Unstained
Sca-1 low
vs high
CD34 positive
Sca-1 CD34
dual positive
R1
R2
R3
R4
R5
Sca-1 PE
CD34 AF647

Figure 6. Lineage tracing to identify cell types contributing to cell fractions defined by cell surface Sca-1 and CD34

(A) Flow cytometry analysis of the lineage tag (eYFP) in cells isolated from CCSP-Cre Rosa26-LSL-eYFP lungs. Left panel shows eYFP expression in the live CD45 CD31 negative population. Two distinct $eYFP^{pos}$ populations were identified ($eYFP^{pos}$ AF^{high} and $eYFP^{pos}$ AF^{low}). Overlay of the autofluorescence profiles of the two populations ($eYFP^{pos}$ AF^{high} - red contour and $eYFP^{pos}$ AF^{low} - green contour) demonstrates that they correspond to the high and low autofluorescence populations, respectively (right panel). (B) Sca-1 and CD34 expression among isolated, lineage tagged, airway epithelial cells. Left column: Sca-1 and CD34 staining; right column: eYFP analysis of cells in the indicated gates. Unstained: eYFP expression in an unstained sample; Sca-1 low vs high: eYFP expression in the $Sca\text{-}1^{low}$ population (R3, red contour) and the $Sca\text{-}1^{high}$ population (R4, green contour) in a Sca-1 stained sample; CD34 positive: eYFP expression in the CD34 positive population (R2, red contour) of a CD34 stained sample; Sca-1/CD34 dual positive: eYFP expression in the $Sca\text{-}1^{pos}$ $CD34^{pos}$ population (R5, red contour). In all experiments dead and $CD45^{pos}$ $CD31^{pos}$ cells have been excluded from the analysis.

3.2.4 Bronchiolar stem cells are defined by their CD45^{neg} CD31^{neg} CD34^{neg} Sca-1^{low} cell surface phenotype and low autofluorescence.

The absence of definitive assays to identify bronchiolar stem cells in isolated cell preparations required the use of genetic models of stem cell expansion to verify their molecular phenotype. We have previously shown that stabilization of β-catenin in the airway epithelium late in lung development resulted in the appearance of supernumerary bronchiolar stem cells based upon the resistance of these cells to naphthalene, their proliferative potential and expression of putative stem cell markers[104]. Histologically, the lungs of ΔE3 mice (mice expressing stabilized β-catenin) have significantly more CCSP/Pro-SPC dual positive cells compared to wild type lungs (reference[104] and Figure 7A). Single cell suspensions were prepared from lungs of wild type and ΔE3 mice, and the properties of bronchiolar epithelial cells interrogated by flow cytometry. No differences were observed between cell preparations isolated from wild type and ΔE3 mice in the abundance of Sca -1^{pos} CD34^{pos} cells within the CD45^{neg} CD31^{neg} live fraction (Figure 7B and C). These data are consistent with our earlier demonstration that cells of the bronchiolar lineage exhibit a Sca-1^{pos} CD34^{neg} phenotype (Figures 6B). To confirm that airway epithelial cells are not found in the Sca-1^{pos} CD34^{pos} fraction but mostly in the Sca-1^{pos} CD34^{neg} fraction, cells were sorted according to their Sca-1 and CD34 expression profiles into four fractions: CD45^{neg} CD31^{neg} Sca-1^{pos} CD34^{pos}, CD45^{neg} CD31^{neg} Sca-1^{pos} CD34^{neg}, CD45^{neg} CD31^{neg} Sca-1^{neg} CD34^{pos} and CD45^{neg} CD31^{neg} Sca-1^{neg} CD34^{neg}. Immunofluorescence analysis of epithelial markers CCSP and Pro-SPC revealed that the CD45^{neg} CD31^{neg} Sca-1^{pos} CD34^{neg} fraction had 57.74% CCSP Pro-SPC dual positive cells in wild type and 51.18% in ΔE3 fraction (Figure 8B). Morphologically, CD45^{neg} CD31^{neg} Sca-1^{pos} CD34^{neg} cells isolated from ΔE3 mice were smaller and had a lower cytoplasmic/nucleus ratio

compared to wild-type cells (Figure 8A). This finding was consistent with our previous demonstration that potentiation of β-catenin in bronchiolar cells of ΔE3 mice results in cells that lack cytoplasmic organelles typical of the facultative TA (Clara) cells[104]. We noted that in both genotypes the majority of CCSP positive cells were also Pro-SPC positive. This unexpected finding was in contrast to the molecular phenotype of cells characterized in situ, in which only ΔE3 mice show expansion of the bronchiolar pool of CCSP/ Pro-SPC dual positive cells. The $CD45^{neg}$ $CD31^{neg}$ $Sca\text{-}1^{pos}$ $CD34^{pos}$ fraction contained a population of large cells that were positive only for Pro-SPC, suggesting that mature alveolar type II cells localized to this fraction. In conclusion, we show that Sca-1 and CD34 dual-expression failed to capture the increase in stem cell pool size in ΔE3 animals. This finding is consistent with our earlier analysis in which cells of the bronchiolar lineage were localized exclusively to the $CD34^{neg}$ fraction.

Since autofluorescence characteristics of bronchiolar cells represented another parameter allowing their segregation we sought to test whether inclusion of this parameter provided a tool for identification of stem cells. We speculated that autofluorescence might relate to the high metabolic activity of facultative TA (Clara) cells and as such, represents a physical property that distinguishes Clara cells from bronchiolar stem cells. Comparison of the autofluorescence characteristics of the $CD45^{neg}$ $CD31^{neg}$ live cells isolated from wild type and ΔE3 mice revealed a dramatic decrease in the size of the autofluorescent population recovered from ΔE3 mice (Figure 7B unstained sample and Figure 9A). To determine if the combination of positive and negative markers that we determined so far is instrumental in revealing the increase in stem cell numbers in the ΔE3 mice, we further interrogated cell surface expression of CD34 and Sca-1 as a function of autofluorescence levels within the $CD45^{neg}$ $CD31^{neg}$ live population (Figure 9). Comparison of the $Sca\text{-}1^{pos}$ population between wild-type and ΔE3 cells

demonstrated a slight increase in Sca-1^{pos} cells in the ΔE3 genotype (Figure 9B vs 9E, 17.94% vs 22.94% respectively). Exclusion of CD34^{pos} cells and AF^{high} cells allowed us to compare the CD45^{neg} CD31^{neg} CD34^{neg} Sca-1^{low} AF^{low} population between wild-type andΔE3 genotypes (Figure 9C and F). The ΔE3 CD45^{neg} CD31^{neg} CD34^{neg} Sca-1^{low} AF^{low} population was dramatically expanded over its wild type counterpart (Figure 9G, 18.04% vs 9.2% of live CD45^{neg} CD31^{neg} respectively, p=0.0002), reflecting the stem cell expansion associated with stabilization of β-catenin. Since our previous analysis of this fraction of cells indicated that both epithelial and non-epithelial cell types are represented, the approximately two-fold increase in cells localizing to this population underrepresented the actual change in stem cell pool size that accompanies potentiation of β-catenin in ΔE3 mice. These data strongly suggest that bronchiolar stem cells can be distinguished from the more abundant pool of facultative TA (Clara) cells based upon their low autofluorescent characteristics, and provide a strategy for their prospective fractionation and analysis.

A.

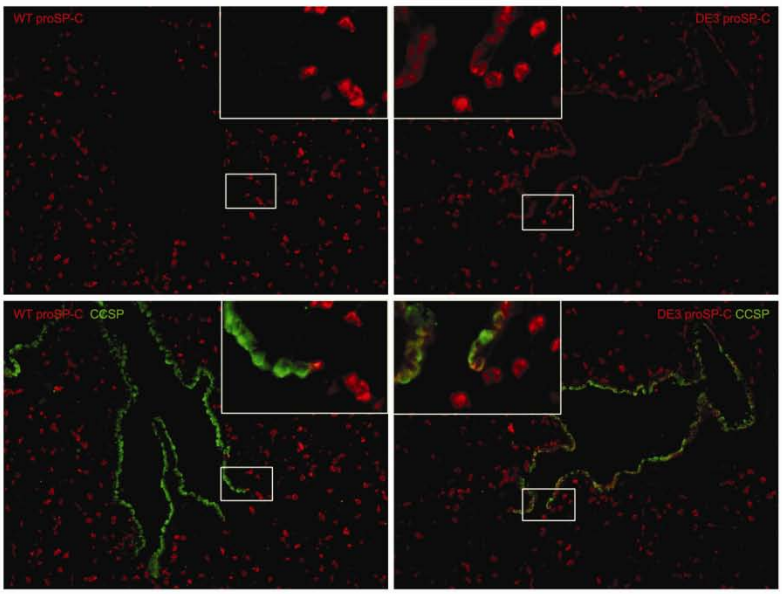
WT proSP-C
DE3 proSP-C
WT proSP-C CCSP
DE3 proSP-C CCSP

B.

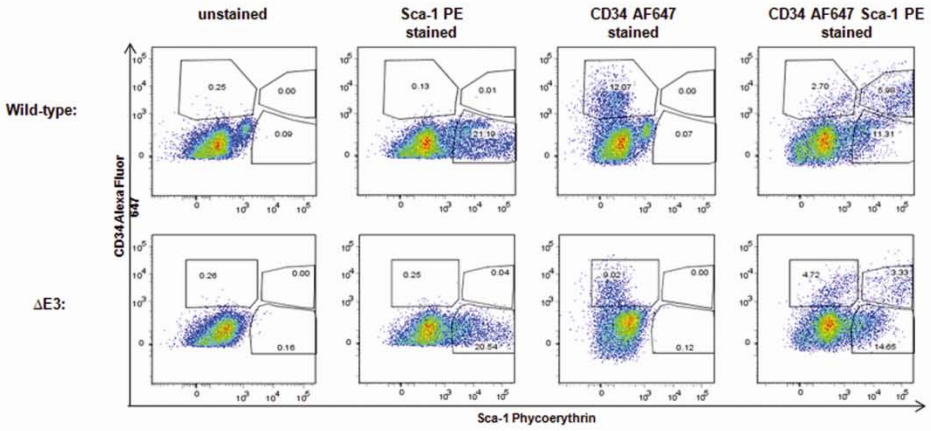
unstained
Sca-1 PE stained
CD34 AF647 stained
CD34 AF647 Sca-1 PE stained
Wild-type:
ΔE3:
CD34 Alexa Fluor 647
Sca-1 Phycoerythrin

C.

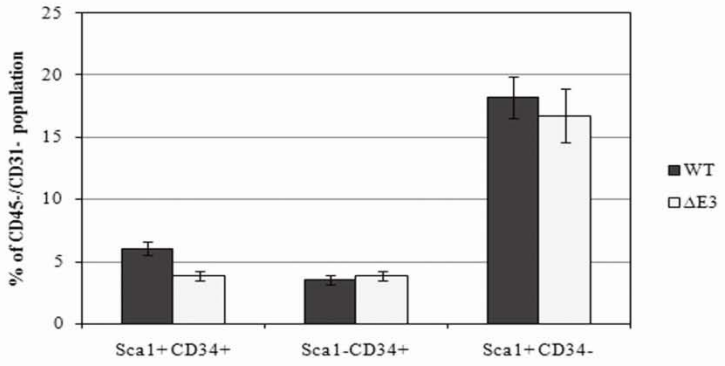
% of CD45-/CD31- population
25
20
15
10
5
0
Sca1+CD34+
Sca1-CD34+
Sca1+CD34-
WT
ΔE3

Figure 7. The cell surface phenotype of wild type and ΔE3 cells

Immunofluorescence analysis of Pro-SPC (red) and CCSP (green) in lung section from wild type (left column) and CCSP-Cre, *Catnnb*$^{floxE3/floxE3}$ (ΔE3) animals (right column). The top row shows Pro-SPC staining and the bottom row represents merged images of Pro-SPC and CCSP staining (200x magnification). Insets represent higher magnification images of the outlined areas. (B) Sca-1 and CD34 expression on the surface of cells isolated from wild type (top row) andΔE3 animals (bottom row). In left to right order, each column represents unstained, Sca -1 stained, CD34 stained and Sca-1 and CD34 dual stained samples respectively. Dead and CD45^{pos} CD31^{pos} cells have been excluded from this analysis. (C) Quantification of data in (B), comparing the percentages of cells in each population of Sca-1/CD34 dual stained samples from wild type (grey bars) and ΔE3 (white bars) mice.

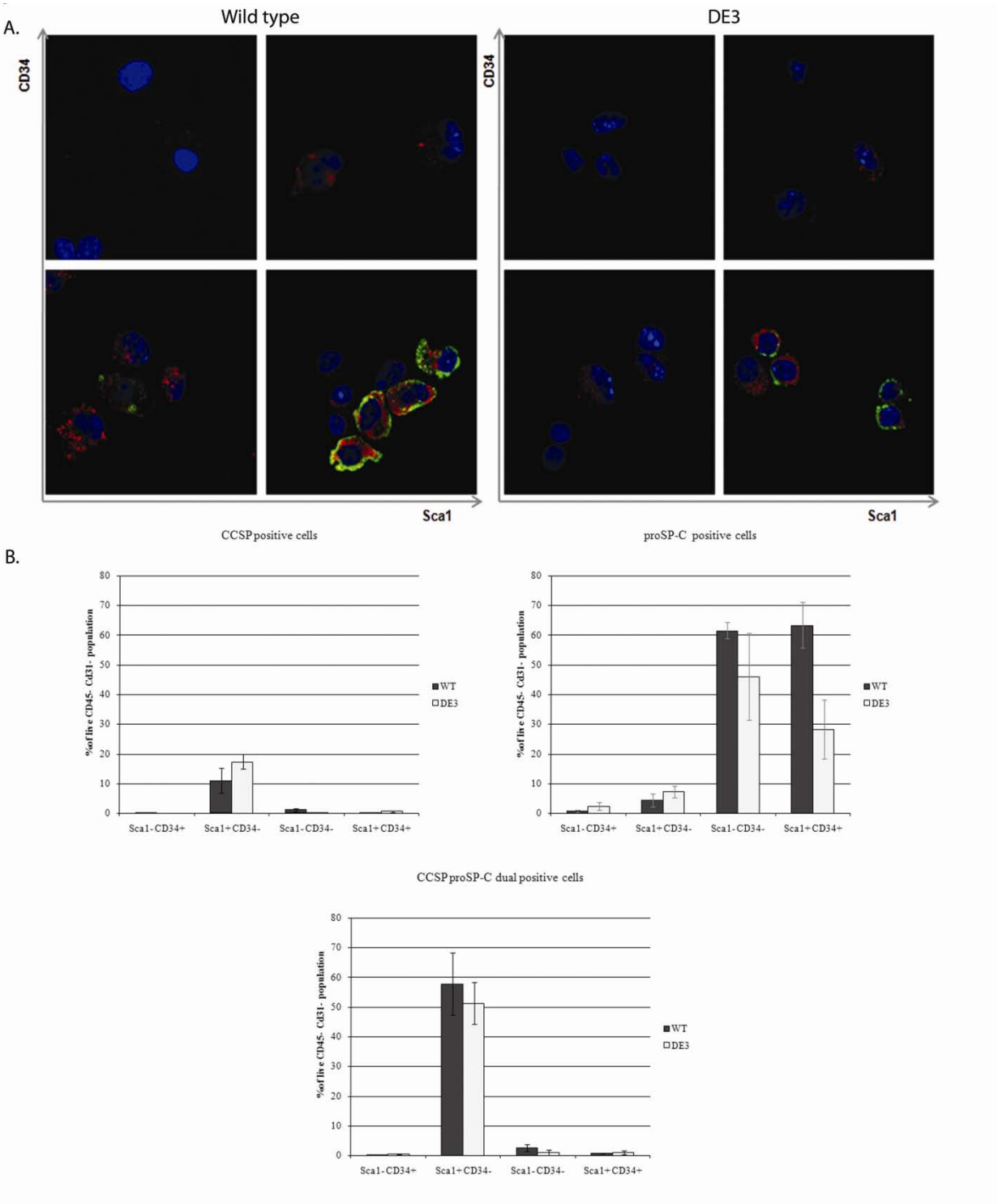
A.
Wild type
DE3
CD34
CD34
Sca1
Sca1
CCSP positive cells
proSP-C positive cells
B.
%of live CD45- Cd31- population
WT
DE3
Sca1-CD34+
Sca1+CD34-
Sca1-CD34-
Sca1+CD34+
CCSP proSP-C dual positive cells

Figure 8.CCSP/ Pro-SPC staining of cells sorted according to their Sca-1/CD34 cell surface expression.

Cells in each of the Sca-1^{neg} $CD34^{pos}$, Sca-1^{neg} $CD34^{neg}$, Sca-1^{pos} $CD34^{neg}$ and Sca-1^{pos} $CD34^{pos}$ populations were sorted. Cytospins from each fraction were stained with CCSP (green) and Pro-SPC. (A) 400x images of CCSP/ Pro-SPC stained cytospins demonstrating the presence of CCSP Pro-SPC dual positive cells in the Sca-1^{pos} $CD34^{neg}$ fraction. (B) Cells in each fraction were counted and classified either as CCSP positive (upper left graph), Pro-SPC positive (upper right) or CCSP and Pro-SPC dual-positive (lower graph). The graphs represent data from 3 wild type animals (black bars) and 3 ΔE3 animals (hatched bars).

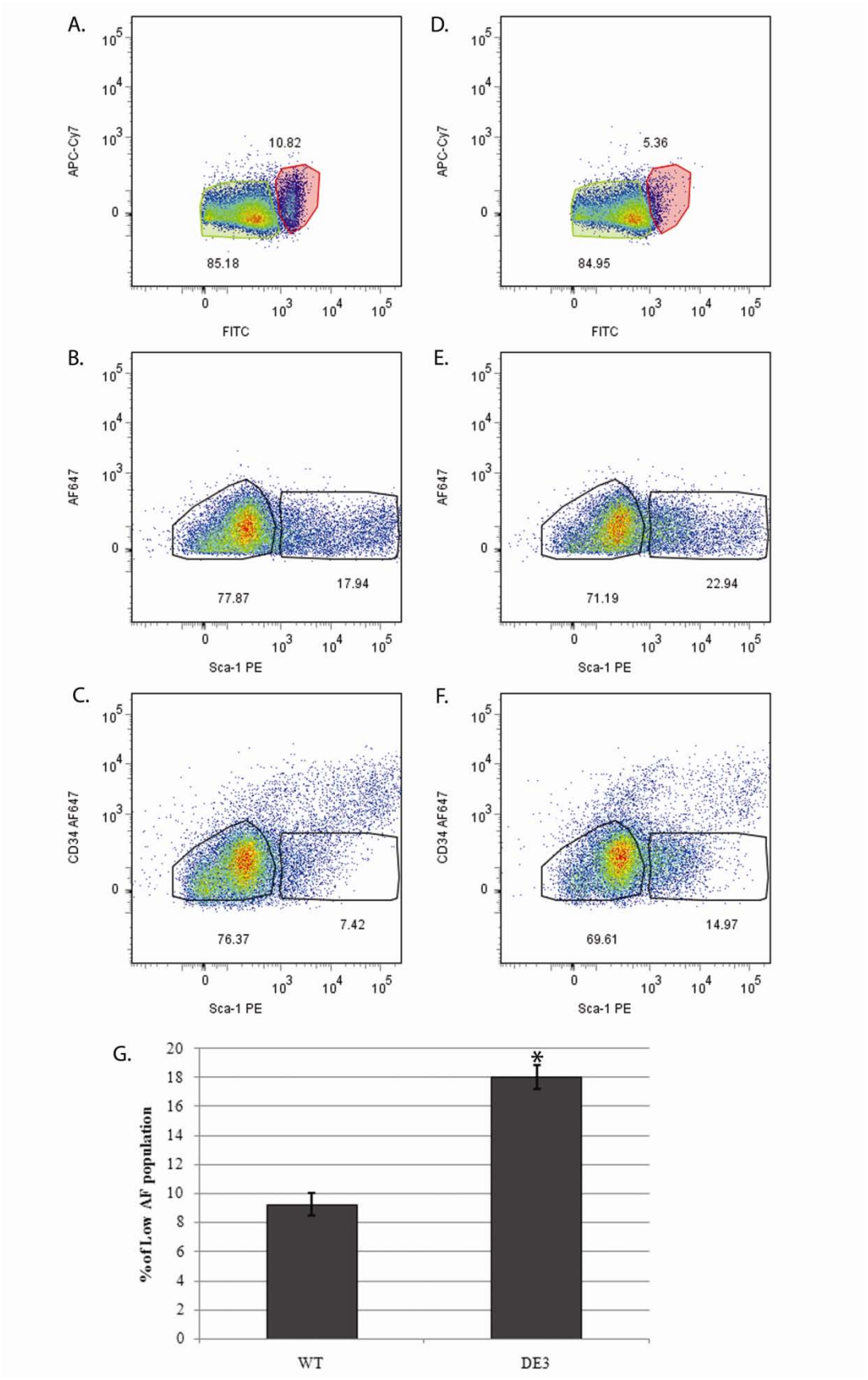
A.
APC-Cy7
FITC
10.82
85.18
D.
APC-Cy7
FITC
5.36
84.95
B.
AF647
Sca-1 PE
77.87
17.94
E.
AF647
Sca-1 PE
71.19
22.94
C.
CD34 AF647
Sca-1 PE
76.37
7.42
F.
CD34 AF647
Sca-1 PE
69.61
14.97
G.
%of Low AF population
WT
DE3
*

Figure 9. Expansion of the stem cell population in theΔE3 mice results in an increase in the number of AFlow, Sca-1pos cells

Cells were isolated from either wild type (A-C) or ΔE3 (D-F) mice, depleted of dead and $CD45^{pos}$ $CD31^{pos}$ cells, and Sca-1 expression analyzed in the AF^{low} population (green shaded gate). (A) and (D) The AF^{high} (red) and AF^{low} (green) populations of cells from wild-type and ΔE3 mice were identified in the FITC / APC-Cy7 channels. (B) and (E) Expression of Sca-1 in the AF^{low} population of Sca-1 stained samples was analyzed and compared between genotypes.(C) and (F) Sca-1^{pos} $CD34^{neg}$ populations in the AF^{low} population of Sca-1 CD34 stained samples was compared between genotypes. (G) Quantification of data in (C) and (F). The number of cells in the Sca-1^{pos} $CD34^{neg}$ population of 6 wild-type and 6ΔE3 animals from three independent experiments, shows the enrichment in Sca -1 positive cells in the ΔE3 phenotype ($p<0.0005$).

3.3 DISCUSSION

We show that Sca-1, a previously described cell surface marker for the bronchioalveolar stem cell[99], is a common cell surface marker for a broad population of bronchiolar epithelial progenitor cells that include the abundant pool of facultative TA (Clara) cells and naphthalene-resistant bronchiolar stem cells. We found that bronchiolar progenitor cells could be distinguished from many other epithelial and mesenchymal cell types based upon their Sca-1^{low} phenotype. Bronchiolar cells could be further subdivided based upon their autofluorescence (AF) characteristics; facultative TA (Clara) cells displaying an AF^{high} phenotype whereas bronchiolar stem cells exhibited an AF^{low} phenotype. This fractionation approach was validated using strategies involving targeted cell ablation, lineage tagging, and stem cell expansion, and provides a robust set of criteria for further investigation of isolated bronchiolar stem cells at molecular and functional levels.

Our demonstration that bronchiolar stem cells can be enriched for within dissociated mouse lung preparations based upon their $CD45^{neg}$ $CD31^{neg}$ $CD34^{neg}$ Sca-l^{low} AF^{low} phenotype differs from the previously described characteristics of isolated bronchioalveolar stem cells detailed by Kim and colleagues[99]. Differences between our findings are that in our study Sca-1 did not distinguish between subsets of CCSP-expressing cells (facultative TA versus stem cells), that the epithelial Sca-1^{low} fraction was a relatively abundant component of the total cell preparation, and that epithelial cells defined by a CCSP-Cre activated lineage tag were negative for CD34. The basis for these differences may be related to methods used for cell isolation and/or antibodies used to define cell surface phenotype. Lung cell preparations used for analysis by Kim and colleagues were generated using dispase/collagenase digestion coupled with methods optimized for the isolation of alveolar type II pneumocytes [99]. In contrast, lung cell

preparations used herein were generated through use of Elastase and methods optimized for inclusion of a broad population of epithelial cells from the conducting airway and alveolus[8]. Importantly, bronchiolar stem cells from both bronchoalveolar duct junction and neuroepithelial body microenvironments in addition to the abundant pool of facultative TA (Clara) cells should be represented among dissociated cell preparations used in this study. This would not be the case using preparations that largely exclude epithelial cells from conducting airways. Furthermore, explanations for the differences in cell surface CD34 reactivity observed herein and that of Kim and colleagues remain to be determined. The possibility that absence of CD34 reactivity among lung epithelial cell types in this study results from conditions used for proteolytic dissociation of cells would seem unlikely as this antigen is preserved on the surface of other non-epithelial cell types.

Stem cells are commonly thought to exhibit less differentiated character than their transit-amplifying progeny. Whereas this distinction is difficult to make for rapidly renewing tissues such as the epithelium of the small intestine, for which both populations appear to proliferate frequently and lack characteristics of specialized epithelial cells[45], it is more apparent within the progenitor cell hierarchy of the bronchiolar epithelium. We demonstrate that Clara cells, an abundant facultative TA cell type of bronchiolar airways, exhibits the distinguishing characteristic of high autofluorescence. This characteristic of Clara cells is supported through: 1) loss of the AF^{high} fraction of lung cells following ablation of CCSP-expressing cells (including Clara and stem cells) in GCV treated of CCSP-HSVtk transgenic mice, and 2) loss of AF^{high} cells following airway potentiation of β-catenin signaling. Autofluorescence is a well known characteristic of the airway epithelium[134]. In human patients autofluorescence bronchoscopy is used as a screening tool for lung cancer[134-136]. Malignant cells in lung cancer patient, which are

poorly differentiated in character, are detected as low level autofluorescence fields within a high autofluorescent background of healthy epithelial cells[134-136]. Collectively these data argue that stem cells can be distinguished from their more differentiated derivatives based upon autofluorescence characteristics and that this property is common between airway stem cells and tumor cells.

Bronchiolar epithelial cells observed in airways of mice following constitutive potentiation of β-catenin signaling lack differentiated features (cytoplasmic organelles and differentiation markers) typical of facultative TA (Clara) cells, are resistant to naphthalene injury, and show a CCSP/Pro-SPC dual expressing phenotype, all characteristics of the bronchiolar stem cell[99,104]. However, even though co-expression of CCSP and Pro-SPC has the potential to distinguish bronchiolar stem cells from more abundant facultative TA (Clara) cells *in vivo*, our data suggest that this may not be the case following enzymatic dissociation and sorting of lung cells. We find that all CCSP-immunoreactive cells present within the Sca-1^{low} fraction (both AF^{high} and AF^{low} populations) show a Pro-SPC-immunoreactive phenotype. These data suggest that Pro-SPC immunoreactivity does not distinguish between facultative TA (Clara) cells and bronchiolar stem cells following enzymatic dissociation of lung tissue and subsequent fractionation of isolated cells. This is consistent with our observation of a similar frequency of CCSP/Pro-SPC dual positive cells between isolated wild type and ΔE3 cell preparations. We conclude that use of CCSP/Pro-SPC dual positivity alone as a basis to investigate the impact of signaling pathways on isolated bronchiolar epithelial cells does not provide a basis for discrimination between rare bronchiolar stem cells and abundant facultative progenitor (Clara) cells[107-109]. We show that despite up-regulation of Pro-SPC within mature Clara cells, their

distinguishing morphological features coupled with unique high autofluorescence characteristics provide a basis for their separation from low autofluorescent bronchiolar stem cells.

Standard methods in stem cell biology include *in vivo* and *in vitro* assays to demonstrate self-renewal and differentiation potential of the proposed stem cell population. Even though *in vitro* models have been developed allowing propagation of tracheobronchial epithelial cells[80], bronchiolar epithelial cells are extremely difficult to maintain and propagate *in vitro*. Moreover, no *in vivo* transplantation studies have been reported that allow faithful establishment of bronchiolar epithelium from fractionated preparations of bronchiolar cells. Fractionation methods allowing enrichment of bronchiolar stem cells described herein will allow further analysis of gene expression to define a unique molecular phenotype and will provide a basis upon which to build in vitro and transplantation models to assess mechanisms of self-renewal. Together with transgenic animal models for identification and manipulation of the stem cell compartment, these assays will provide critical tools to unravel the bronchiolar stem cell phenotype and mechanisms governing their behavior in normal and diseased lung.

4.0 CELL SURFACE PHENOTYPE AND FUNCTIONAL ANALYSIS OF BRONCHIOLAR STEM CELLS

4.1 INTRODUCTION

Data presented in the previous chapter indicates that CD34 is not expressed on the surface of epithelial cells of the lung. Moreover we showed that low levels of Sca-1 are expressed on the cell surface of airway epithelial cells and that high autofluorescence is a property of mature Clara cells of the bronchiolar epithelium. Using a transgenic animal model in which the bronchiolar stem cell population has been expanded, we demonstrate that bronchiolar stem cells are characterized by AF^{low}, Sca-1^{low}, $CD45^{neg}$, $CD31^{neg}$, $CD34^{neg}$ phenotype. *In vivo* data suggests a significant expansion of stem cells in ΔE3 animals based upon the number of CCSP pro-SPC dual positive cells. Use of autofluorescence characteristics and cell surface phenotype revealed only a twofold amplification of the stem cell population. These data suggested that other epithelial and non-epithelial cell types are present in the AF^{low}, Sca-1^{low}, $CD45^{neg}$, $CD31^{neg}$, $CD34^{neg}$ fraction of bronchiolar stem cells. Thus we sought to further enrich the stem cell fraction using other potential cell surface markers for epithelial and non-epithelial cell types.

Stem cell behavior is at least in part dictated by interactions with neighboring cells and subtending basement membrane that together form the stem cell niche[101]. Integrin and cadherin

family of proteins are an important part of the sensing mechanisms that dictate the proliferation, migration and differentiation of epithelial cells [137]. Integrin expression and function have been widely studied in the follicular and interfollicular epidermis. Different members of the family are expressed constitutively or can be induced in response to epidermal injury [138]. Amongst these, integrin α6, a member of hemidesmosomal complexes, has been shown to be expressed at high levels on a population of mouse epidermal and follicular stem cells, allowing their prospective isolation and characterization of their *in vivo* and *in vitro* properties [139,140].

Another mediator of inter-cellular interactions shown to be expressed in other stem cell compartments is Epithelial cell adhesion molecule (EpCAM). EpCAM (also known as CD326) is a cadherin-like transmembrane protein expressed by most epithelial cells[141], including the lung[142]. Moreover, human non small cell lung carcinomas express high levels of EpCAM, leading to its utilization to monitor tumor progression and as a therapeutic target for tumor reduction[143-145]. EpCAM expression has been demonstrated on the surface of oval cell population of liver progenitors[146]. Interestingly, in the human mammary gland, EpCAM and Integrin α6 co-expression allowed the isolation of bi-potent progenitors that *in vitro* have the ability to give rise to colonies consisting of both luminal and basal mammary cells[53,147,148].

Evidence that EpCAM and Integrin α6 can be used as cell surface markers for epithelial stem cells in other organ systems led us to hypothesize that epithelial-specific cell adhesion molecules will enable us to further enrich the bronchiolar stem cell fraction in the AF^{low}, Sca-1^{low}, $CD45^{neg}$, $CD31^{neg}$, $CD34^{neg}$ population. We show that both EpCAM and Integrin α6 are expressed on the cell surface of bronchiolar and alveolar epithelium and that Sca-1 expression allows the distinction between bronchiolar and alveolar epithelium. Moreover, we find that ciliated cells co-purify with the bronchiolar stem cell population in the AF^{low}, Sca-1^{low}, $CD45^{neg}$,

$CD31^{neg}$, $CD34^{neg}$ fraction. Functional analysis of the proliferative behavior of cells in this population during injury and repair allowed its localization at the top of the stem cell hierarchy.

4.2 RESULTS

4.2.1 Validation of EpCAM and Integrin alpha 6 as cell surface markers for lung epithelial cells

EpCAM and Integrin α6 expression has been previously described in lung epithelial cells[142]. To validate this and enrich the epithelial fraction of the AF^{low}, Sca-1^{low}, $CD45^{neg}$, $CD31^{neg}$, $CD34^{neg}$ population we interrogated the expression of EpCAM on the surface of lung cells isolated from wild type mice. EpCAM was not expressed on the surface of CD45, CD31 or CD34 positive cells (Figure 11). Low levels of EpCAM and CD31 or CD34 antibodies were co-expressed on the surface of a distinctive population (Figure 11 E and F). The EpCAM low population also expresses high levels of CD45, suggesting that they most likely represent a population of hematopoietic origin (Figure 11D). Thus, this data suggests that EpCAM is not expressed on the surface of $CD45^{pos}$, $CD31^{pos}$, $CD34^{pos}$ cells, and that the low levels of EpCAM in that fraction represent non-specific uptake by $CD45^{pos}$ cells, most likely macrophages. Therefore, for the remainder of the study the $CD45^{pos}$, $CD31^{pos}$, $CD34^{pos}$ population was excluded from the analysis.

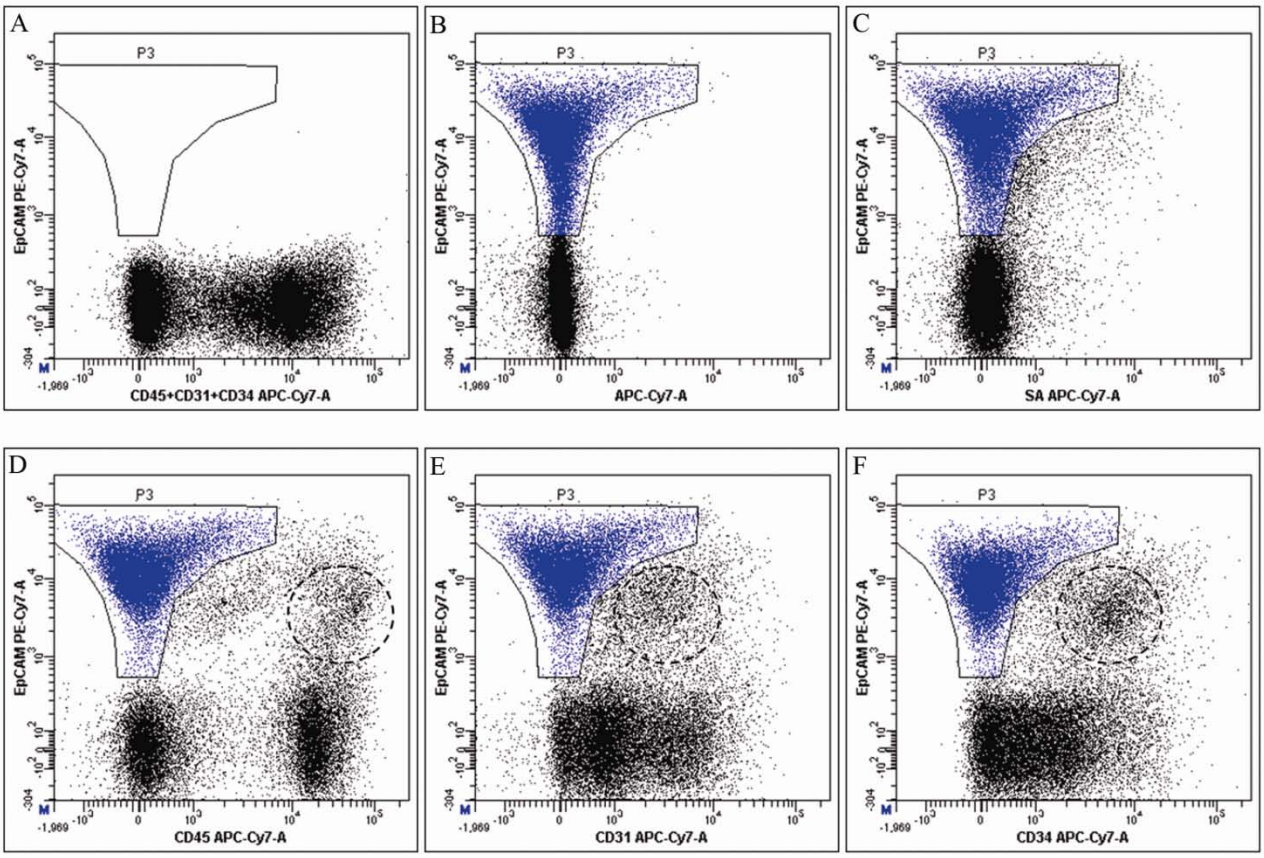

Figure 10. EpCAM expression in single cell suspension of lung epithelial cells

Cells isolated from wild type animals were analyzed for EpCAM, CD45, CD31 and CD34 expression. (A) No EpCAM control. Biotinylated CD45 CD31 CD34 (APC-eFuor780) in the live cell population (7AAD-negative) (B) No CD45 CD31 CD34 control. EpCAM PE-Cy7 expression in the live cell population. (C) Streptavidin only control. Non-specific binding of streptavidin APC-eFluor780 in the EpCAM PE-Cy7 stained sample. (D) EpCAM PE-Cy7 expression in a CD45 APC-eFluor780 stained sample. (E) EpCAM PE-Cy7 expression in a CD31 APC-eFluor780 stained sample. (F) EpCAM PE-Cy7 expression in a CD34 APC-eFluor780 stained sample. Dead cells have been excluded from the analysis based on 7AAD incorporation. Circled populations in (D)-(F) represent cells that co-express low levels of EpCAM PE-Cy7 and CD45 APC-eFluor780 (D), CD31 APC-eFluor780 (E) or CD34 APC-eFluor780 (F) respectively, most likely representing non-specific binding by macrophages. In each dot plot, x-axis represents fluorescence levels of APC-eFluor780 conjugated antibodies read in APC-Cy7 channel; y-axis represents fluorescence levels of PE-Cy7 EpCAM expression.

High levels of Integrin α6 expression have been described in some epithelial stem cell compartments allowing their prospective fractionation[139]. Thus, we interrogated the tissue expression of Integrin α6 and EpCAM. Immunolocalization of Integrin α6 and EpCAM in five micron sections from CCSPcre Rosa26LSL EYFP lungs showed that EpCAM expression is specific to the lung epithelium, while Integrin α6 is expressed by endothelial cells as well lung epithelial cells (Figure 12). Both antigens were expressed by bronchiolar epithelial cells (12B and D) and alveolar type II cells (12B and D). Flow cytometry analysis of the cell surface expression of EpCAM and Integrin α6 in isolated lung cells revealed that the majority of $EpCAM^{pos}$ cells also express Integrin α6 (Figure 12E). Thus, these data suggest that EpCAM and Integrin α6 are antigens commonly expressed on the surface of bronchiolar and alveolar epithelial cells. EpCAM is specifically expressed on the surface of epithelial cells only, allowing separation of epithelial from non-epithelial fractions of total lung cells. Therefore for the reminder of the study we will use EpCAM as a marker for lung epithelial cells.

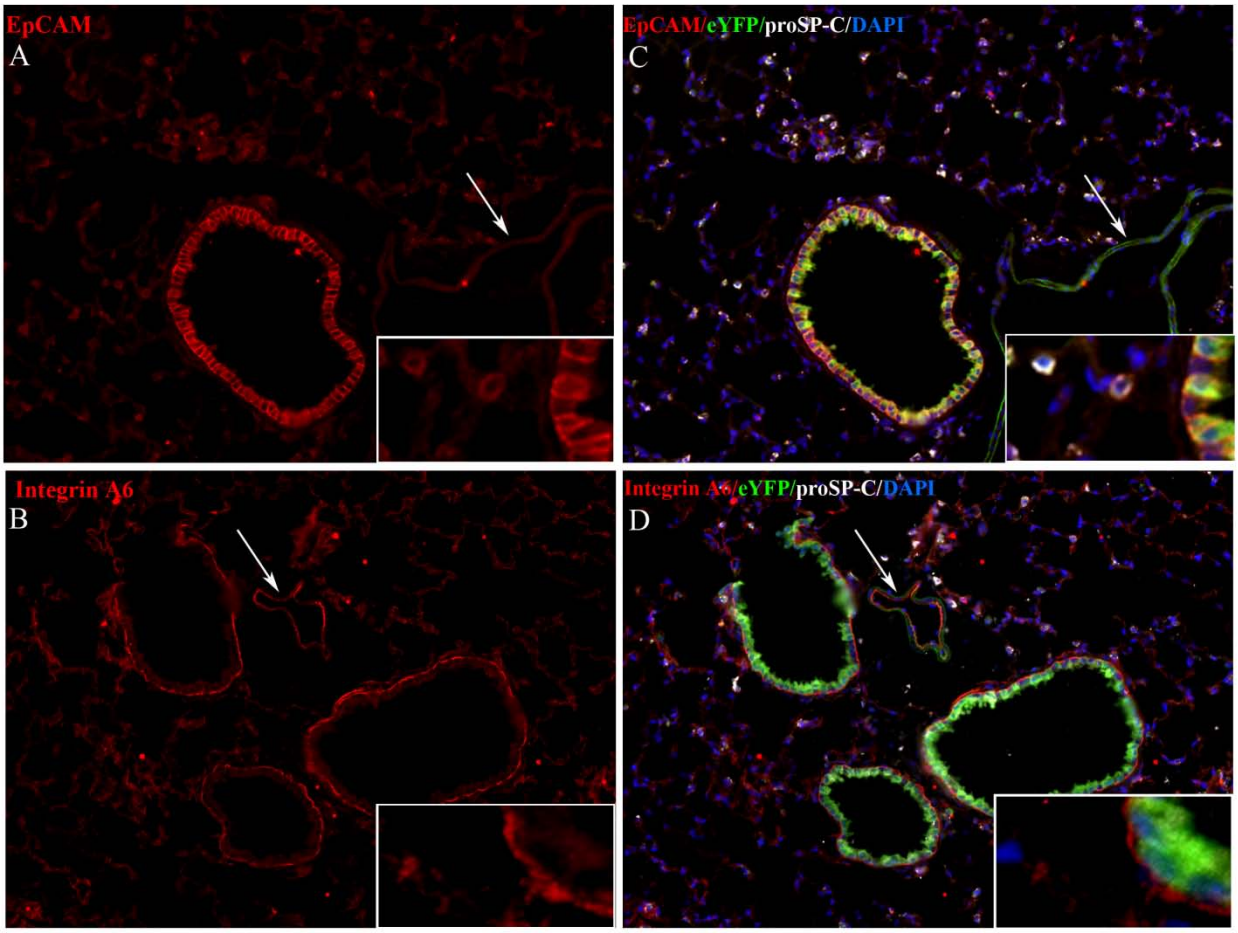
EpCAM
A
EpCAM/eYFP/proSP-C/DAPI
C
Integrin A6
B
Integrin A6/eYFP/proSP-C/DAPI
D

E

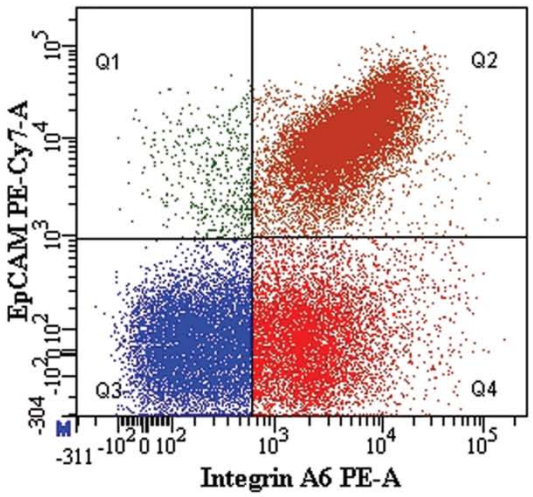
Q1
Q2
Q3
Q4
EpCAM PE-Cy7-A
Integrin A6 PE-A

Figure 11. EpCAM and Integrin alpha 6 expression in CCSP-Cre Rosa26-LSL-eYFP lung epithelium

Immunofluorescence staining of lung sections from CCSP-Cre Rosa26-LSL-eYFP transgenic animals demonstrating EpCAM (A) and Integrin A6 (B) expression (red). (C) and (D) overlay of native fluorescence of the airway epithelium (green), proSP-C (white) and EpCAM (C) or Integrin A6 (D) (200x magnification). (E) Flow cytometry analysis showing EpCAM PE-Cy7 (y-axis) and Integrin A6 PE (x-axis) expression on the cell surface of cells isolated from wild type animals showing that the majority of EpCAM positive cells also express Integrin α6 (gate Q2=49.9% of live cell population). Dead cells have been excluded from the analysis. $CD45^{pos}$ $CD31^{pos}$ $CD34^{pos}$ cells have not been excluded from the analysis. Arrows point at blood vessels in A-D.

4.2.2 Cell surface phenotype and autofluorescence characteristics of the alveolar and bronchiolar epithelium

We have previously shown that cell surface expression of Sca-1 is a property of the bronchiolar epithelium. Therefore, we asked whether exclusion of non-epithelial cells from the AF^{low} Sca-1^{low} $CD45^{neg}$ $CD31^{neg}$ $CD34^{neg}$ based on EpCAM expression allows for further enrichment in bronchiolar stem cells in wild type and ΔE3 animals and if Sca-1 expression distinguishes alveolar from bronchiolar epithelium. Thus, cells within the $EpCAM^{pos}$ $CD45^{neg}$ $CD31^{neg}$ $CD34^{neg}$ fraction of wild type and ΔE3 animals were analyzed by flow cytometry for cell surface expression of Sca-1 (Figure 12). Two populations were apparent in both genotypes: a Sca-1^{neg} $EpCAM^{pos}$ population and a Sca-1^{low} $EpCAM^{pos}$ population, neither of which varied with genotype (Figure 12 B and E). However, analysis of autofluorescence levels of the cells in the Sca-1^{low} $EpCAM^{pos}$ in the PerCP-Cy5.5 and FITC channels (Figure 12C and F) revealed a twofold enrichment in AF^{low} cells in ΔE3 genotype compared to wild type , paralleled by a corresponding decrease in the AF^{high} population (Figure 12 H).

To confirm the identity of cells in each fraction, we interrogated the gene expression level of cell-type specific markers in wild-type cells sorted according to their cell surface phenotype and autofluorescence characteristics. The abundance of CCSP, SP-C and FoxJ1 mRNAs was quantified by real-time PCR analysis of total RNA isolated from Sca-1^{neg} $EpCAM^{pos}$ $CD45^{neg}$ $CD31^{neg}$ $CD34^{neg}$ (Sca-1^{neg} $EpCAM^{pos}$), AF^{high} Sca-1^{low} $EpCAM^{pos}$ $CD45^{neg}$ $CD31^{neg}$ $CD34^{neg}$ (AF^{hi}) and AF^{low} Sca-1^{low} $EpCAM^{pos}$ $CD45^{neg}$ $CD31^{neg}$ $CD34^{neg}$ (AF^{low}) cell fractions (Figure 12 I-K). Sorted total live cells were used to show mRNA enrichment in each population and data was normalized to total lung mRNA purified from intact tissue. Thus CCSP

mRNA was expressed at highest levels in the AF^{hi} population (approximately 10 fold enrichment relative to total isolated cells) and at considerate levels in the AF^{low} population (approximately 3 fold enrichment relative to total isolated cells). This confirmed our previous data suggesting that CCSP expressing cells are enriched in the AF^{hi} fraction and that a distinct sub-population of CCSP expressing cells are present in the AF^{low} fraction (Figure 4D).

Ciliated cells and ATII cells represent fractions that potentially co-purify with bronchiolar stem or facultative TA (Clara) cell population. Therefore we sought to determine their presence in the cell populations described above. FoxJ1 is a transcription factor specifically expressed in ciliated cells of the bronchiolar epithelium[19,149]. Analysis of FoxJ1 mRNA levels (Figure 12K) demonstrated that ciliated cells are highly enriched in the AF^{low} fraction (approximately 50 fold enrichment relative to total isolated cells). In contrast, lower levels of FoxJ1 mRNA were detected in the AF^{hi} and Sca-1^{neg} $EpCAM^{pos}$ fractions suggesting that they were depleted of ciliated cells. This data suggested that ciliated cells co-purify with bronchiolar stem cells within the AF^{low} population.

In vivo, surfactant protein C is expressed by alveolar type II cells, rare putative bronchiolar stem cells[99,104]. We previously determined that isolated CCSP positive cells were also immunoreactive for proSP-C (previous chapter). Analysis of SPC mRNA levels in the sorted populations (Figure 12J) showed that the Sca-1^{neg} $EpCAM^{pos}$ population had the highest expression of SPC mRNA (approximately 6 fold enrichment relative to total isolated cells). Importantly, the AF^{low} population expressed approximately 3 times more SPC mRNA than the total cell population. The AF^{hi} population expressed undetectable levels of SPC mRNA, confirming that the facultative TA (Clara) cells do not express SPC mRNA. As mentioned above, low levels of proSP-C protein were expressed in many of the CCSP immunoreactive cells

found in the Sca-1^{low} CD45^{neg} CD31^{neg} fraction (Figure 8), which contained both AF^{hi} and AF^{low} populations. This is the most likely reason for the absence of SP-C mRNA from the AF^{hi} fraction of facultative TA (Clara) cells. Alternatively, this apparent divergence could be caused by differential regulation of SP-C mRNA and protein. Future experiments will address both possibilities. Results were confirmed using Integrin α6 as a selection marker replacing EpCAM (data not shown).

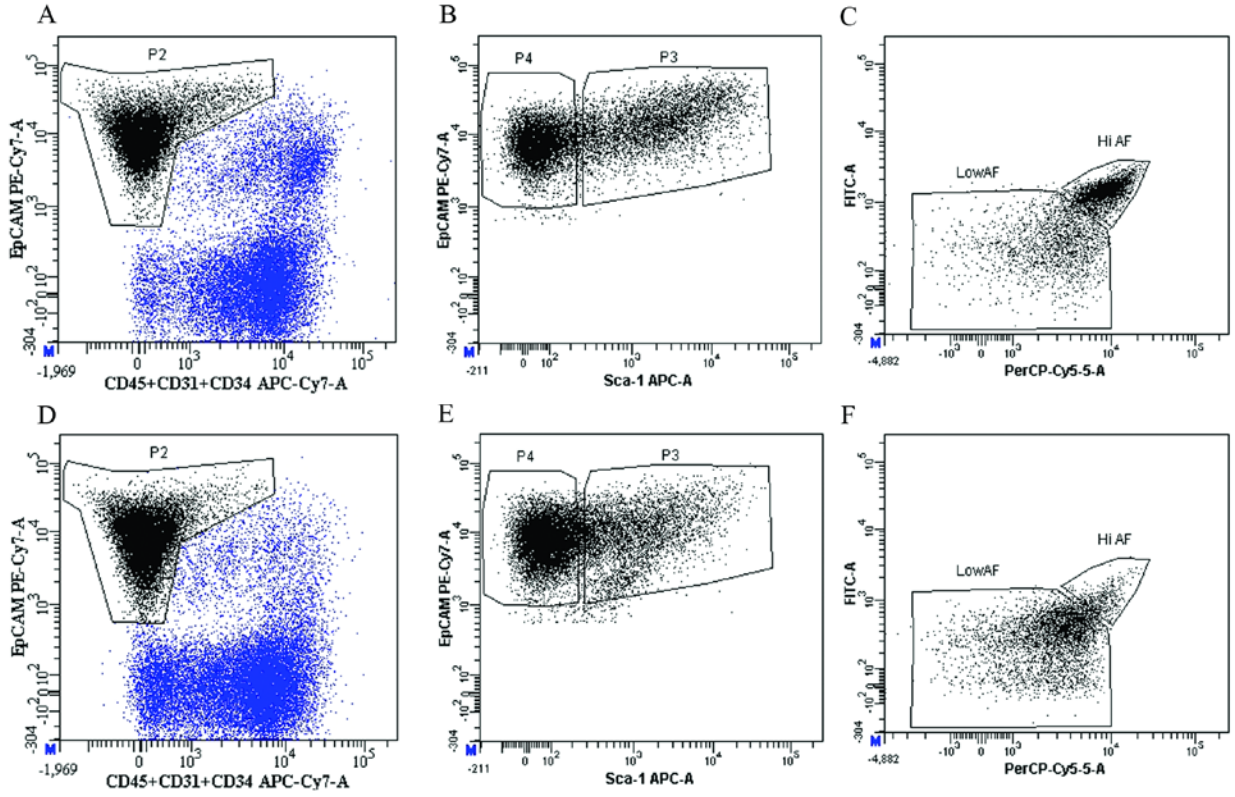
A
P2
EpCAM PE-Cy7-A
CD45+CD31+CD34 APC-Cy7-A
B
P4
P3
EpCAM PE-Cy7-A
Sca-1 APC-A
C
Hi AF
LowAF
FITC-A
PerCP-Cy5-5-A
D
P2
EpCAM PE-Cy7-A
CD45+CD31+CD34 APC-Cy7-A
E
P4
P3
EpCAM PE-Cy7-A
Sca-1 APC-A
F
Hi AF
LowAF
FITC-A
PerCP-Cy5-5-A

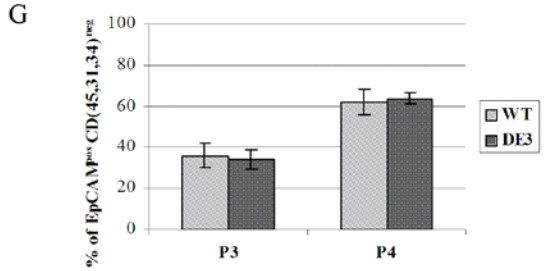
G
% of EpCAMpos CD(45,31,34)neg
WT
DE3
P3
P4

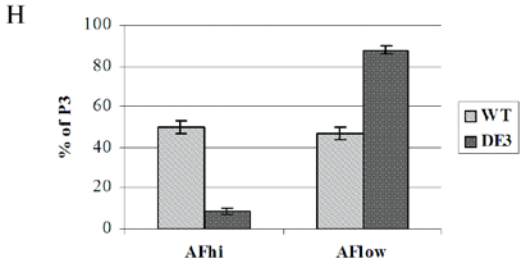
H
% of P3
WT
DE3
AFhi
AFlow

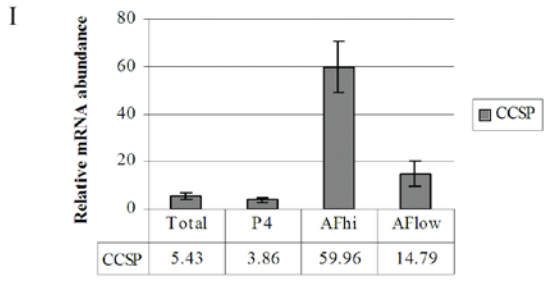
I
Relative mRNA abundance
CCSP
Total
P4
AFhi
AFlow
CCSP 5.43 3.86 59.96 14.79

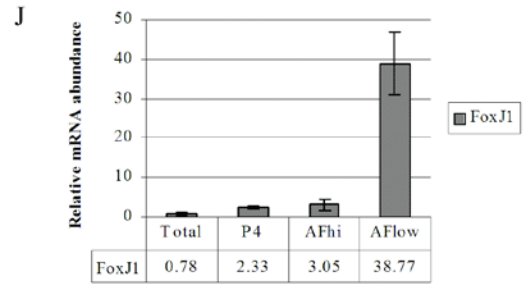
J
Relative mRNA abundance
FoxJ1
Total
P4
AFhi
AFlow
FoxJ1 0.78 2.33 3.05 38.77

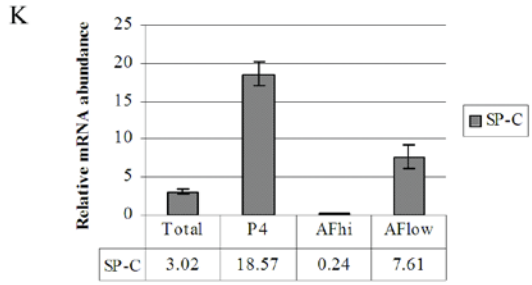
K
Relative mRNA abundance
SP-C
Total
P4
AFhi
AFlow
SP-C 3.02 18.57 0.24 7.61

Figure 12. Cell surface expression of EpCAM and Sca-1 defines subpopulations of lung epithelial cells belonging to the airway and alveolar epithelium.

Isolated cells from wild type (A)-(C) and ΔE3 mice (D)-(F) where analyzed by flow cytometry for cell surface expression of EpCAM PE-Cy7 and Sca-1 AF647 following exclusion of dead and CD45 CD31 CD34 positive cells. (A) and (D) EpCAM PE-Cy7 (y-axis) and CD45 CD31 CD34 APC-eFluor780 (x-axis) expression in cells isolated from wild type and ΔE3 mice respectively showing. Gate P2 represents EpCAM ^{pos} CD45^{neg} CD31^{neg} CD34^{neg} population (40.76% of live cells in (A) and 38.7% of live cells in (D)). (B) and (E) Sca-1 AF647 (x-axis) and EpCAM PE-Cy7 (y-axis) expression in the P2 population of wild type and ΔE3 cells respectively. Gate P3 defines Sca-1^{low} EpCAM^{pos} population and gate P4 defines the Sca-1^{neg} EpCAM^{pos} population. Quantification of the data is shown in (G) as percentage of P2. (C) and (F) Autofluorescence profile of the P3 population as seen in FITC and PerCP-Cy5.5 channels. HiAF and LowAF represent the high and the low autofluorescence populations respectively. Quantification of the data is shown in (H) as percentage of P3 population. Real time PCR data showing relative expression levels of CCSP(I), SPC (J) and FoxJ1 (K) in total cells (dead cells were excluded), EpCAM^{pos} Sca-1^{neg} CD45^{neg} CD31^{neg} CD34^{neg} (P4 in B), AFhi EpCAM^{pos} Sca-1^{low} CD45^{neg} CD31^{neg} CD34^{neg} (AFhi) and AFlow EpCAM^{pos} Sca-1^{low} CD45^{neg} CD31^{neg} CD34^{neg} (AFlow). Data were normalized to levels of each transcript in total lung RNA.

4.2.3 Cell surface phenotype and autofluorescence characteristics of ciliated cells of the bronchiolar epithelium

Ciliated cells represent a significant fraction of bronchiolar epithelial cells in the mouse lung. Thus identification of their cell surface and autofluorescence characteristics is necessary to allow their separation from the pools of lung stem and facultative TA (Clara) cells. Analysis of FoxJ1 mRNA levels (Figure 12) suggested that ciliated cells are enriched in the AF^{low} $EpCAM^{pos}$ $Sca\text{-}1^{low}$ $CD45^{neg}$ $CD31^{neg}$ $CD34^{neg}$ fraction.

To confirm the phenotypic characteristics of the ciliated cell population, cells were isolated from FoxJ1 GFP transgenic animals. In these animals, GFP is a faithful reporter of FoxJ1 expression, leading to specific fluorescent tagging of the majority of ciliated cells[19,149]. Exclusion of dead and $CD45^{pos}$ $CD31^{pos}$ $CD34^{pos}$ cells in these cell preparations allowed evaluation of GFP expression in different fractions of epithelial cells defined according to Sca-1 and EpCAM cell surface expression (Figure 13). Thus GFP^{pos} cells represented 7.46% of the total epithelial fraction (Figure 13B), 72% of which were present in the $Sca\text{-}1^{low}$ $EpCAM^{pos}$ fraction. Analysis of GFP expression in the $EpCAM^{pos}$ $Sca\text{-}1^{neg}$ fraction showed that only 2.56% of this fraction (P7 in Figure 13C) was represented by ciliated cells, a finding consistent with the low levels of FoxJ1 mRNA expression observed in the $Sca\text{-}1^{low}$ $EpCAM^{pos}$ population. Moreover, GFP^{pos} cells represented 19.03% of the $Sca\text{-}1^{low}$ $EpCAM^{pos}$ population (Figure 13D). Analysis of autofluorescence levels of the GFP^{pos} cells in the $Sca\text{-}1^{low}$ $EpCAM^{pos}$ population confirmed that the majority of ciliated cells belonged to the AF^{low} fraction, while only small numbers of GFP^{pos} cells were present in the AF^{hi} fraction (Figure 13E). GFP^{pos} ciliated cells fraction represented 33.73% of the AF^{low} $Sca\text{-}1^{low}$ $EpCAM^{pos}$ fraction, suggesting that ciliated cells co-purify with the putative bronchiolar stem cell fraction.

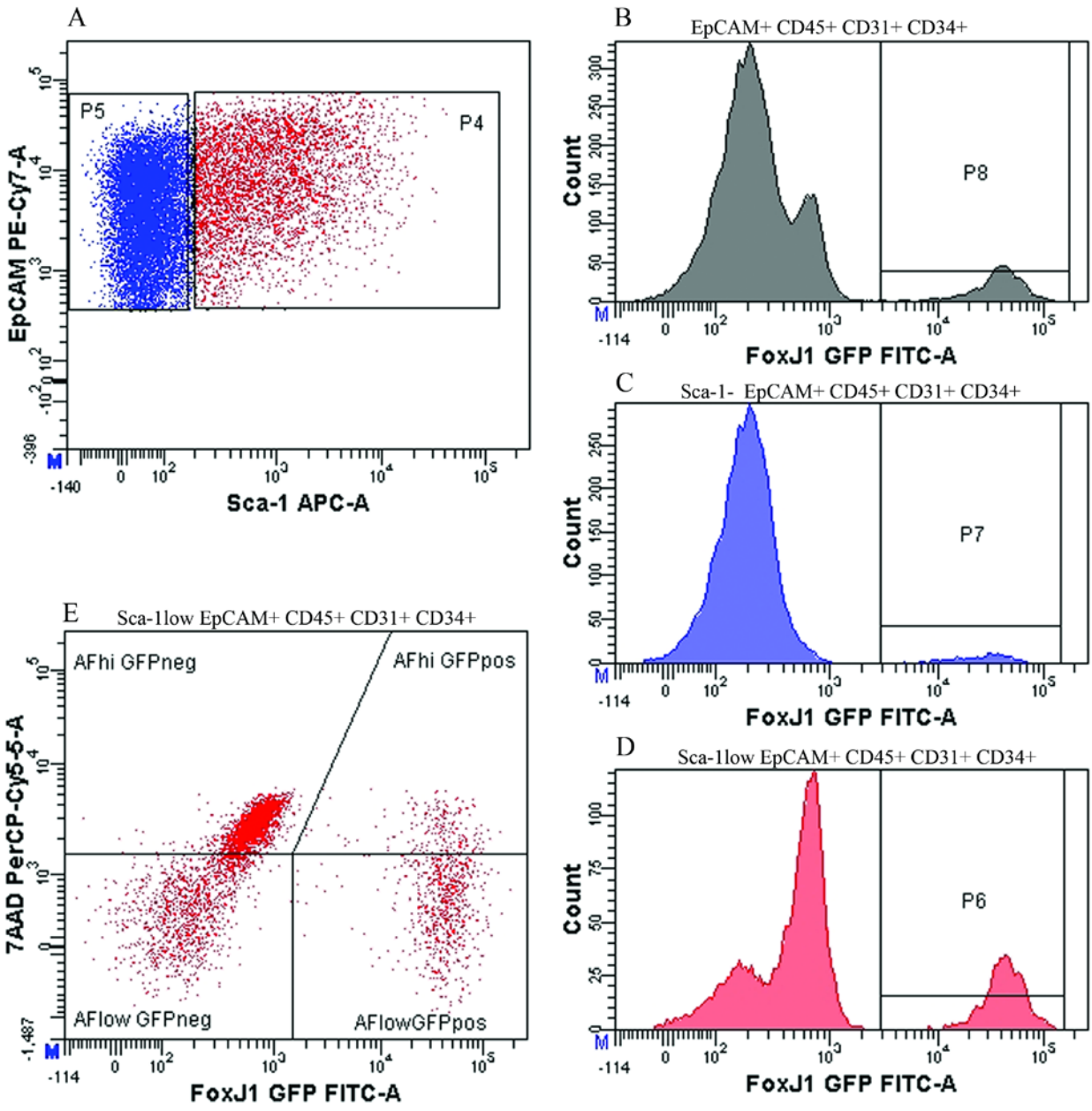
A
P5
P4
EpCAM PE-Cy7-A
Sca-1 APC-A
B
EpCAM+ CD45+ CD31+ CD34+
P8
Count
FoxJ1 GFP FITC-A
C
Sca-1- EpCAM+ CD45+ CD31+ CD34+
P7
Count
FoxJ1 GFP FITC-A
D
Sca-1low EpCAM+ CD45+ CD31+ CD34+
P6
Count
FoxJ1 GFP FITC-A
E
Sca-1low EpCAM+ CD45+ CD31+ CD34+
AFhi GFPneg
AFhi GFPpos
AFlow GFPneg
AFlowGFPpos
7AAD PerCP-Cy5-5-A
FoxJ1 GFP FITC-A

Figure 13. Cell surface phenotype and autofluorescence characteristics of ciliated cells of the bronchiolar epithelium

Lungs from FoxJ1GFP transgenic mice were dissociated and analyzed by flow cytometry for GFP expression in the context of EpCAM and Sca-1 expression. Dead and $CD45^{pos}$ $CD31^{pos}$ $CD34^{pos}$ cells were excluded from the analysis. (A) Flow cytometry data indicating the gating strategy for the Sca-1^{low} $EpCAM^{pos}$ (P4, red dots) and Sca-1^{neg} $EpCAM^{pos}$ (P5 blue dots) populations. (B) FoxJ1 GFP expression (P8=7.46%) in the epithelial cell population defined as $EpCAM^{pos}$ $CD45^{neg}$ $CD31^{neg}$ $CD34^{neg}$. (C) FoxJ1 GFP expression in the Sca-1^{neg} $EpCAM^{pos}$ cell population (P7=2.56%). (D) FoxJ1 GFP expression in the Sca-1^{low} $EpCAM^{pos}$ population (P6=19.03%). (E) Autofluorescence levels of the FoxJ1 GFP^{pos} cells within the Sca-1^{low} $EpCAM^{pos}$ population. $AF^{hi}GFP^{neg}$ population represents 50.83%, $AF^{hi}GFP^{pos}$ population represents 4.03%, $AF^{low}GFP^{pos}$ population represents 15.23% and $AF^{low}GFP^{neg}$ population represents 29.93% of the Sca-1^{low} $EpCAM^{pos}$ fraction. The quantitative analysis has been performed on three FoxJ1 GFP animals (n=3).

4.2.4 SP-C GFP expression in the lung

During development, SP-C is expressed at the tips of branching epithelium starting at E10.5 and its expression is restricted to the alveolar compartment late in development. In adult mouse lung, expression of surfactant protein C expression has long been considered a unique characteristic of ATII epithelial cells. Recent data suggests that bronchiolar stem cells associated with BADJs co-express CCSP and proSP-C in vivo[99,104](Figure 7). Consistent with these results, mRNA isolated from epithelial cells fractionated according to their Sca-1and EpCAM expression status and levels of autofluorescence showed that the AF^{low} $EpCAM^{pos}$ $Sca\text{-}1^{low}$ (AF^{low}) population expresses both CCSP and SPC mRNA (Figure 12). To confirm SP-C expression in different fractions of isolated cells, we used a transgenic mouse model in which GFP expression is controlled by the human SP-C promoter (SP-C GFP mice). Although these mice have been previously used for isolation of ATII cells, GFP expression has not been thoroughly characterized[150]. Consistent with the published data, high levels of GFP expression were noted in ATII cells. Surprisingly, analysis of native GFP fluorescence in frozen lung sections from SP-C GFP mice revealed GFP expression in the bronchiolar epithelium with a spatial distribution consistent with stem cell niches: neuro-epithelial bodies (NEBs) and broncho-alveolar duct junctions (BADJs). High levels of GFP were noted at BADJs and fluorescence intensity in bronchiolar epithelial cells decreased and disappeared gradually in proximal bronchiolar epithelium (Figure 14). Proximal bronchiolar epithelium did not express GFP with the exception of few clusters of cells surrounding NEBs (Figure 16). To confirm the identity of the cells expressing high levels of GFP found at BADJs, expression of CCSP and FoxJ1 was analyzed in frozen lung sections from SP-C GFP transgenic mice as markers for secretory and ciliated cells, respectively. High levels of GFP expression co-localized with CCSP expression (Figure 15 A-C)

while FoxJ1 expressing cells did not express detectable levels of GFP (Figure 15 D-E). To determine the identity of GFP expressing cells located in clusters in the more proximal airway epithelium, we analyzed CCSP, FoxJ1 and CGRP expression in those locations (Figure 16). Immunofluorescence staining demonstrated that CCSP expressing cells around NEBs have high levels of GFP (Figure 16A-C). Notably, none of the FoxJ1 (Figure 16 D-F) and CGRP (Figure 16 G-I) expressing cells expressed detectable levels of GFP. Together, these data show that in tissue sections of SP-C GFP lungs, GFP expression is not confined to the alveolar epithelium. Moreover, high levels of GFP expression were noted in CCSP expressing cells located in previously identified stem cell niches (NEBs and BADJs). Lower but detectable levels of GFP expression were noted in Clara cells of terminal bronchioles.

Next we sought to determine GFP expression in cells isolated from SP-C GFP transgenic mice. Epithelial cells obtained following exclusion of dead cells and $CD45^{pos}$ $CD31^{pos}$ $CD34^{pos}$ cells were analyzed for Sca-1 and EpCAM surface expression. Consistent with previous data, the analysis allowed the distinction between two populations characterized by Sca-1^{low} $EpCAM^{pos}$ (P4=28.93% of live $EpCAM^{pos}$ $CD45^{neg}$ $CD31^{neg}$ $CD34^{neg}$) and Sca-1^{neg} $EpCAM^{pos}$ (P6=63.7% of live $EpCAM^{pos}$ $CD45^{neg}$ $CD31^{neg}$ $CD34^{neg}$) (Figure 17A). Analysis of GFP expression in each fraction revealed that the majority of cells in the Sca-1^{neg} $EpCAM^{pos}$ fraction expressed high levels of GFP (GFPhi=90.26%) while very few cells were GFP low or negative (Figure 17B). Interestingly, analysis of GFP expression in the Sca-1^{low} $EpCAM^{pos}$ fraction revealed two distinct populations, one expressing high levels of GFP (GFPhi=18.7% of $EpCAM^{pos}$ Sca-1^{low}) and another one expressing lower levels of GFP (GFPlow=41.4% $EpCAM^{pos}$ Sca-1^{low}) (Figure 17C). Real time PCR data in Figure 12 suggested that the AF^{hi} Sca-1^{low} $EpCAM^{pos}$ population does not express significant levels of SP-C mRNA, while the AF^{low} Sca-1^{low} $EpCAM^{pos}$

population had high levels of SP-C mRNA. Analysis of autofluorescence levels of the GFP positive cells in the $EpCAM^{pos}$ $Sca\text{-}1^{low}$ population in the PerCP-Cy5.5 channel showed that a considerable number of AF^{hi} cells expressed intermediate levels of GFP and that the majority of GFP^{hi} cells belong to the AF^{low} population (Figure 17E). Together with the tissue analysis, this data suggests that the GFP^{hi} cells in the $EpCAM^{pos}$ $Sca\text{-}1^{low}$ fraction represent the *in vivo* counterpart of the GFP^{hi}, CCSP expressing cells found at BADJ and around NEBs. Future studies need to assess their properties during naphthalene-induced lung epithelium injury to determine if these cells are naphthalene resistant and if they can proliferate during the repair phase, characteristics previously ascribed to bronchiolar stem cells.

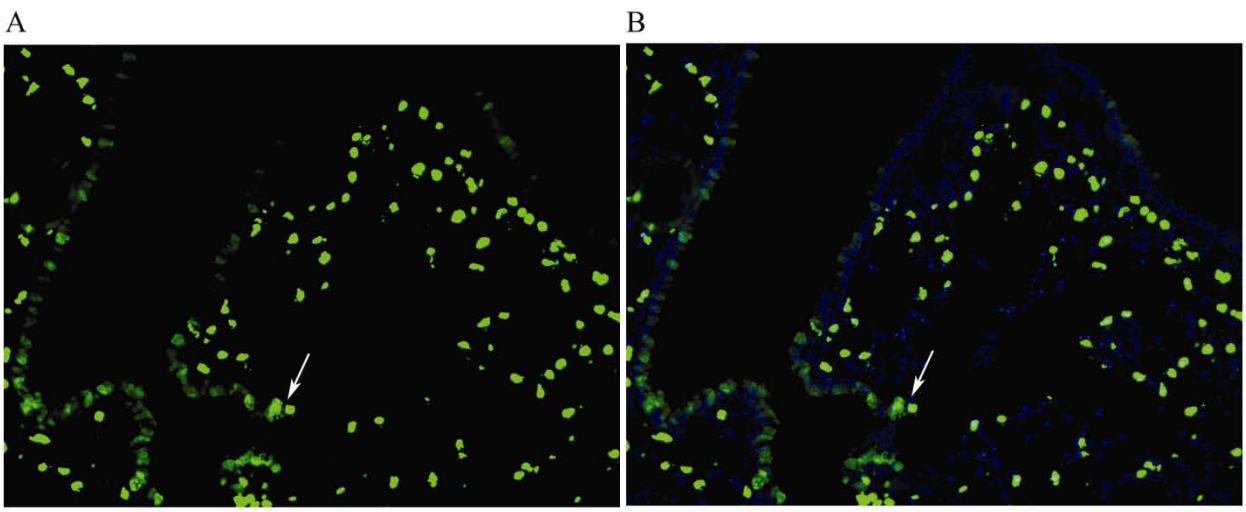

Figure 14. GFP expression in the bronchiolar epithelium of SPC GFP

Distribution of native GFP fluorescence (green) on the proximal to distal axis in the bronchioles of SPC GFP mice. (B) Overlay of native GFP fluorescence with DAPI (blue) as nuclear counterstain. Arrows in (A) and (B) indicate cells expressing high levels of GFP at the broncho-alveolar duct junction (200x magnification).

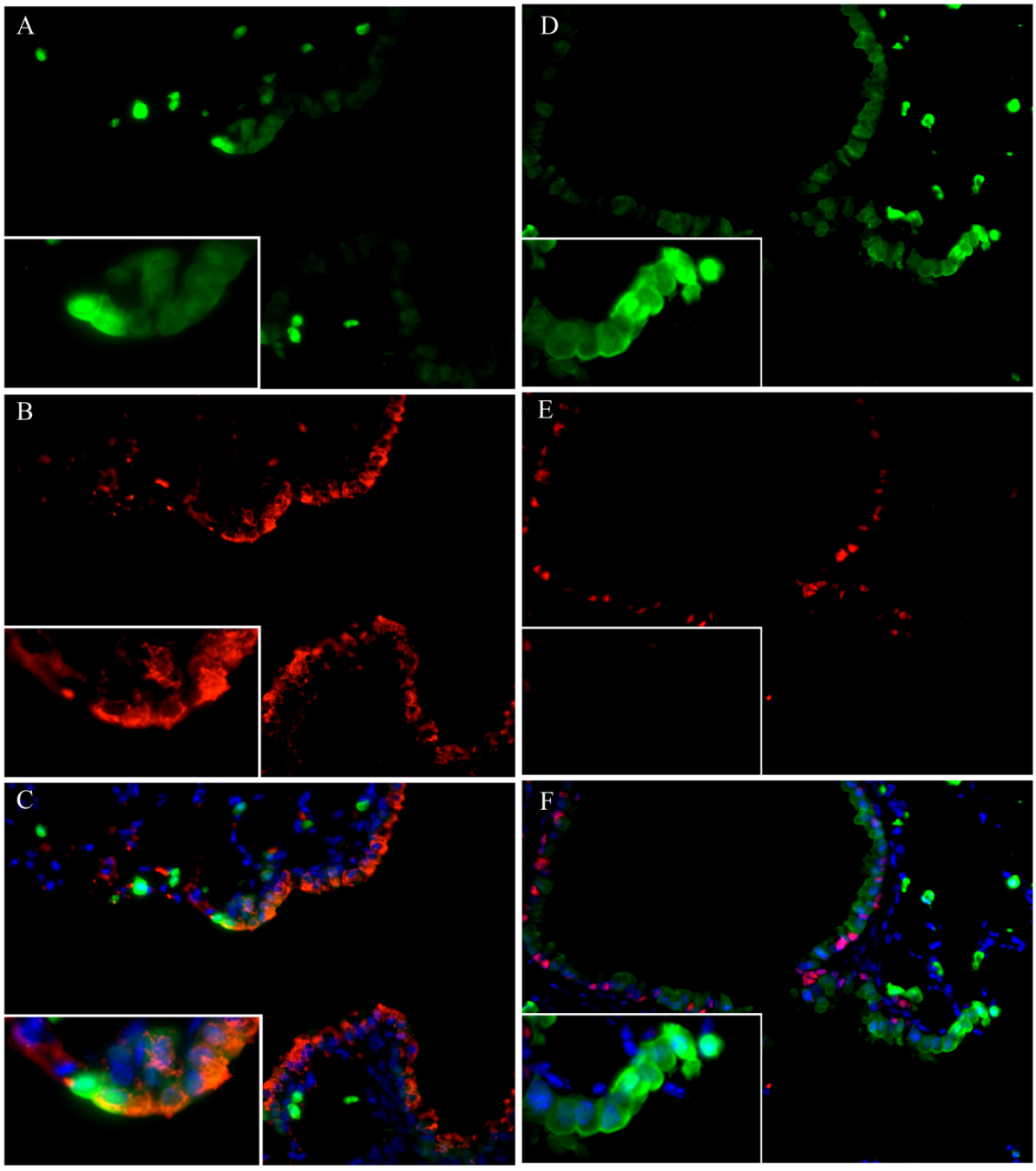
A
D
B
E
C
F

Figure 15. GFP expression in bronchiolar epithelial cells found at the broncho-alveolar duct junction (BADJ) of SPC GFP transgenic mice.

Immunolocalization of bronchiolar epithelium specific markers in the lungs of SPC GFP transgenic mice. (A)-(C) Co-localization of native GFP fluorescence (green signal in A) with CCSP (red signal in B) at the junction between the bronchiolar and alveolar compartment (BADJ). (C) represents overlay of (A), (B) and nuclear counterstain (blue signal – DAPI). (D)-(F) Immunofluorescence staining for GFP (green signal in D) and FoxJ1 (red signal in E) the of BADJs of SPC GFP transgenic mice. (F) represents overlay of (D), (E) and nuclear counterstain (blue signal – DAPI). Images were taken at 400x magnification. Insets represent higher magnifications of BADJ cells expressing high levels of GFP.

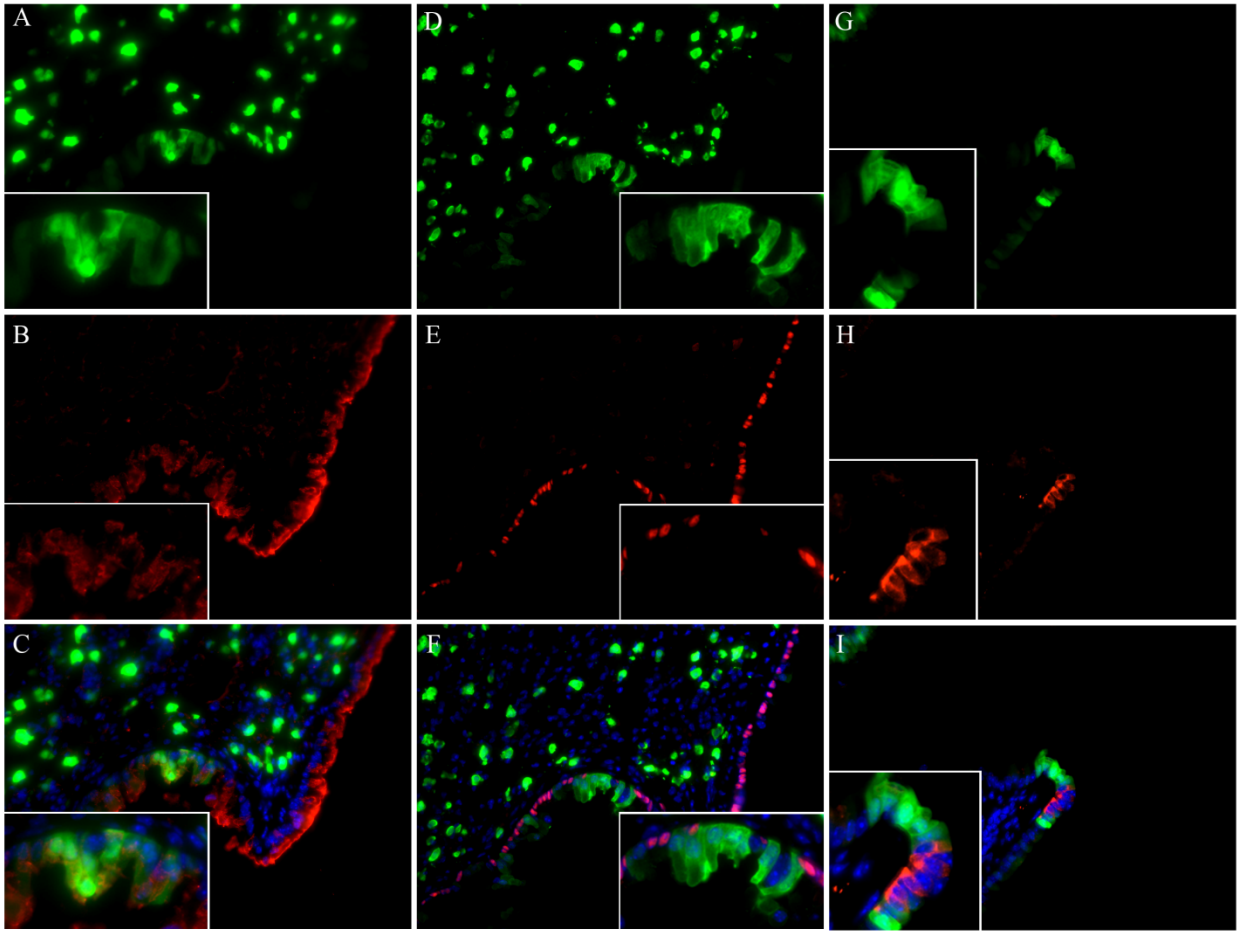
A
D
G
B
E
H
C
F
I

Figure 16. GFP expression in epithelial cells surrounding neuro-epithelial bodies (NEBs) of SPC GFP transgenic mice.

(A)-(C) Immunolocalization of CCSP (red in B) with the native GFP fluorescence of the bronchiolar epithelium around NEBs. (C) represents overlay of (A), (B) and DAPI as nuclear counterstain (blue). (D)-(F) Immunolocalization of FoxJ1 (red in E) and GFP (green in D) fluorescence in the bronchiolar epithelium surrounding NEBs. (E) represents overlay of (D), (F) and DAPI as nuclear counterstain (blue). In (A)-(E) NEBs were identified as CGRP expressing cell clusters in an adjacent section. (G)-(I) Immunolocalization of CGRP positive cells (red in H) in NEBs surrounded by GFP expressing cells (green in G – native fluorescence) demonstrating mutually exclusive expression. Images represent 400 x magnifications. Insets represent higher magnification of the NEB area.

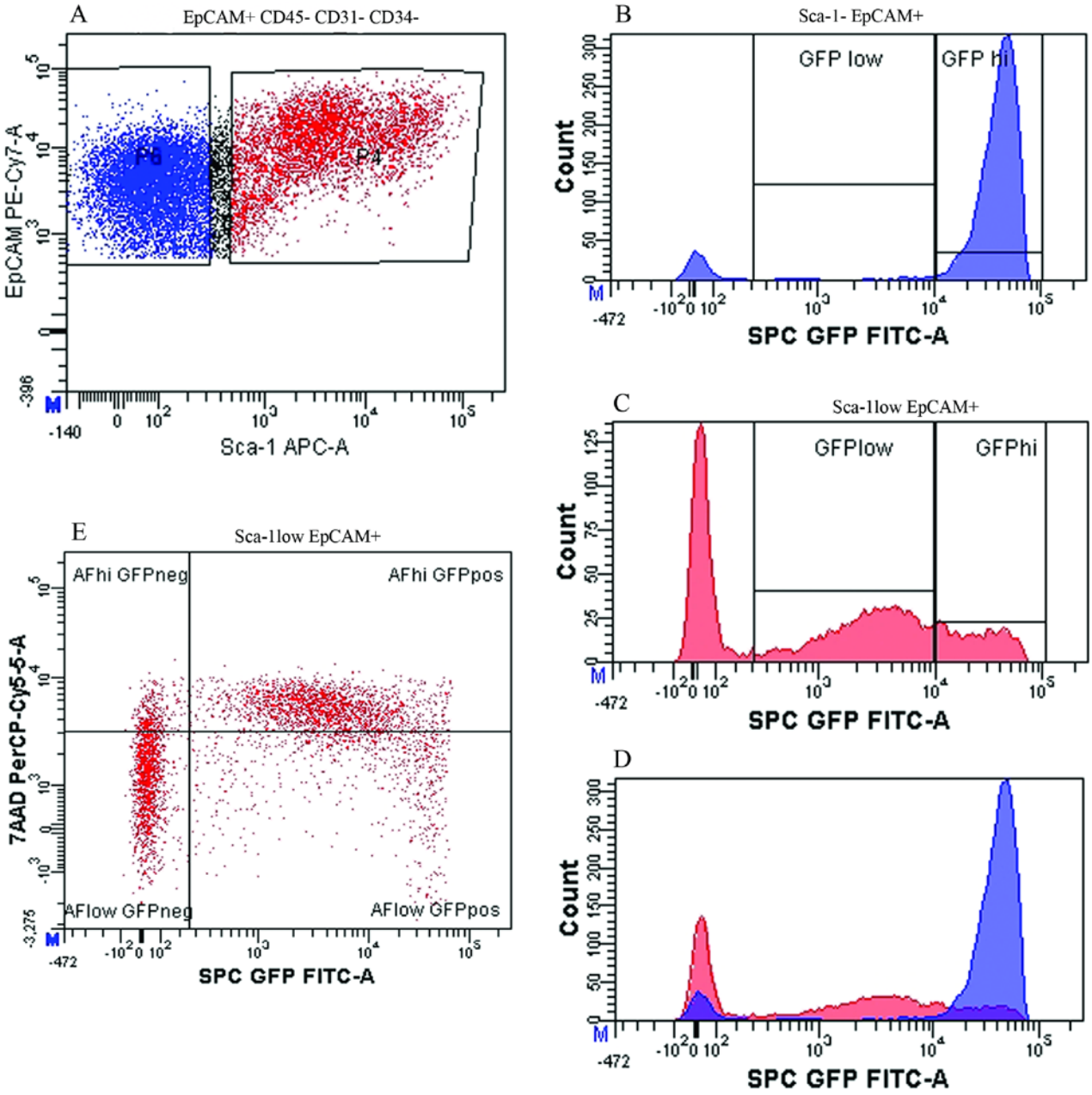
A
EpCAM+ CD45- CD31- CD34-
EpCAM PE-Cy7-A
Sca-1 APC-A
P3
P4
B
Sca-1- EpCAM+
GFP low
GFP hi
Count
SPC GFP FITC-A
C
Sca-1low EpCAM+
GFPlow
GFPhi
Count
SPC GFP FITC-A
D
Count
SPC GFP FITC-A
E
Sca-1low EpCAM+
AFhi GFPneg
AFhi GFPpos
AFlow GFPneg
AFlow GFPpos
7AAD PerCP-Cy5-5-A
SPC GFP FITC-A

Figure 17. Cell surface phenotype of cells isolated from SP-C GFP transgenic mice

Lungs from SP-C GFP transgenic mice were dissociated and analyzed by flow cytometry for GFP expression in the context of EpCAM and Sca-1 expression.(A) Flow cytometry dot plot showing the gating strategy for the $EpCAM^{pos}$ $Sca\text{-}1^{low}$ (P4 = 28.96%, red dots) and $EpCAM^{pos}$ $Sca\text{-}1^{neg}$ (P6 = 63.7%, blue dots) populations. To minimize the cross-contamination of cells from the two different fractions gates were drawn further apart. (B) Histogram representation of GFP expression in the $EpCAM^{pos}$ $Sca\text{-}1^{neg}$ fraction showing that the majority of cells express high levels of GFP (GFPhi = 90.26% and GFPlow = 2.26% of the $EpCAM^{pos}$ $Sca\text{-}1^{neg}$ fraction). (C) Histogram representation of GFP expression in the $EpCAM^{pos}$ $Sca\text{-}1^{low}$ fraction showing the distribution of cells between GFPhi and GFPlow fractions (GFPhi = 18.7% and GFPlow = 41.4% of the $EpCAM^{pos}$ $Sca\text{-}1^{low}$ fraction). (D) Overlay of (B) and (C) allows the comparison of GFP fluorescence levels and number of GFP expressing cells in each population. (E) Analysis of autofluorescence levels as a function of GFP expression in the $EpCAM^{pos}$ $Sca\text{-}1^{low}$ fraction. Quadrants are labeled according to their autofluorescence and GFP status as follows: AFhi GFPneg = 7.93%, AFhi GFPpos = 46.33%, AFlow GFPneg = 29.86%, AFlow GFPpos = 15.86% of the $EpCAM^{pos}$ $Sca\text{-}1^{low}$ population. Dead cells and $EpCAM^{neg}$ $CD45^{pos}$ $CD31^{pos}$ $CD34^{pos}$ cells were excluded from the analysis. Quantitative analysis represents the results from cells isolated from three SP-C GFP transgenic mice.

4.2.5 Functional analysis of the proliferative behavior of the AF^{hi} and AF^{low} populations during naphthalene injury and repair

Data presented in the previous chapter suggest that the two components of the $EpCAM^{pos}$ Sca-1^{low} population, the AF^{hi} and the AF^{low} fractions, represent functionally distinct progenitor pools of facultative TA (Clara) cells and bronchiolar stem cells, respectively. The main distinction between Clara and stem cell populations *in vivo* is their behavior in response to airway injury. Thus, the facultative TA (Clara) cells metabolize naphthalene and are depleted within the first 24 hours after naphthalene administration. In contrast, the bronchiolar stem cells are naphthalene resistant and proliferate to repair naphthalene injured airways. Ciliated cells, which co-purify with bronchiolar stem cells in the AF^{low} fraction, survive naphthalene injury and squamate to cover the basement membrane until epithelial integrity is restored[18,55,151].

Thus, to reveal functional differences between cell types represented within the AF^{hi} and AF^{low} populations, the abundance and proliferative capacity of cells within the two fractions were studied during naphthalene injury and repair. Changes in the abundance of the AF^{hi} population during naphthalene injury were assessed by flow cytometry. Cells were isolated from lungs of C57B6 male mice two days after exposure to 250mg/kg naphthalene (Figure 18). In control animals, analysis of autofluorescence levels in the PE and APC channels revealed a distinct AF^{hi} population that accounted for 12.1% of the live $CD45^{neg}$ $CD31^{neg}$ population (Figure 18A). In contrast, autofluorescence analysis of cells isolated from naphthalene treated mice revealed an approximate 70% decrease in the size of the AF^{hi} population which accounted for only 3.56% of the live $CD45^{neg}$ $CD31^{neg}$ population (Figure 18B and C) confirming that cells within the AF^{hi} fraction represent mostly naphthalene-sensitive Clara cells.

To study the proliferative capacity of cells within the AF^{hi} and AF^{low} fractionss, mice were exposed to naphthalene followed by a 72 hour period of BrdU administration. Cells isolated from lungs of uninjured control mice and mice recovered for 3 days after naphthalene administration were analyzed for EpCAM and Sca-1 expression (Figure 19). EpCAM expression is limited to the epithelial compartment of the lung, thus making exclusion of CD45, CD31 and CD34 expressing cells unnecessary. Analysis of the abundance of $EpCAM^{pos}$ $Sca\text{-}1^{low}$ cells showed a drastic decrease in this fraction in naphthalene injured compared to control animals. A slight decrease in the number of $Sca\text{-}1^{neg}$ $EpCAM^{pos}$ cells was noticed representing a dilution caused most probably by an influx of inflammatory cells (Figure 19 A-C). This data demonstrated efficient injury of the bronchiolar epithelium. Next, the number of cells that proliferated during the first 72 hours after naphthalene administration was determined in the $Sca\text{-}1^{low}$ $EpCAM^{pos}$ and $Sca\text{-}1^{neg}$ $EpCAM^{pos}$ populations by analysis of BrdU incorporation. Very low numbers of BrdU incorporating cells were detected in control animals (P4=2.7% of $Sca\text{-}1^{low}$ $EpCAM^{pos}$ population and P5=0.766% of $Sca\text{-}1^{neg}$ $EpCAM^{pos}$ population in Figure 19 D and E respectively), confirming the quiescence of the steady state lung epithelium. The number of BrdU incorporating cells in the $Sca\text{-}1^{low}$ $EpCAM^{pos}$ population 3 days after naphthalene injury was significantly increased (P4= 20.33% of $Sca\text{-}1^{low}$ $EpCAM^{pos}$ population Figure 19 F). This demonstrates that naphthalene resistant cells in the $EpCAM^{pos}$ $Sca\text{-}1^{low}$ fraction have a high proliferative potential, consistent with the expected behavior of the bronchiolar stem cell population. We next sought to determine the autofluorescence levels of BrdU incorporating cells in the $EpCAM^{pos}$ $Sca\text{-}1^{low}$ fraction of control and injured mice. Analysis of BrdU positive cells (FITC channel) as a function of autofluorescence in PerCP-Cy5.5 channel revealed four populations (Q1- $BrdU^{neg}$ AF^{hi}, Q2- $BrdU^{pos}$ AF^{hi}, Q3 – $BrdU^{neg}$ AF^{low} and Q4 – $BrdU^{pos}$ AF^{low}

populations, Figure 19 I-L). In cells isolated from uninjured animals, the few $BrdU^{pos}$ cells were uniformly distributed between the AF^{low} and AF^{hi} fractions (Q2 and Q4) suggesting that both populations participate, albeit at very low levels, to normal homeostatic maintenance of the airway epithelium. Whether BrdU incorporating cells in the AF^{low} fraction represent proliferating stem cells or nascent ciliated cells, remains to be determined. Comparison of the $BrdU^{neg}$ fractions (Q1 and Q3 in Figure 19 I, J and K) between uninjured and injured animals confirmed the decrease in the AF^{hi} population following injury as shown in Figure 18. Interestingly, analysis of the distribution of BrdU incorporating cells in injured animals demonstrated that the majority of $BrdU^{pos}$ cells were present in the AF^{low} fraction, with an almost 10 fold increase in number compared with uninjured controls (Q2 and Q4 in Figure 19 I, J and L). Together these data demonstrate that the AF^{hi} $EpCAM^{pos}$ Sca-1^{low} population represents the naphthalene-sensitive facultative TA (Clara) cell population and that the AF^{low} fraction of the $EpCAM^{pos}$ Sca-1^{low} population represents naphthalene resistant, highly proliferative stem cell population responsible for the initiation of the repair process following naphthalene injury.

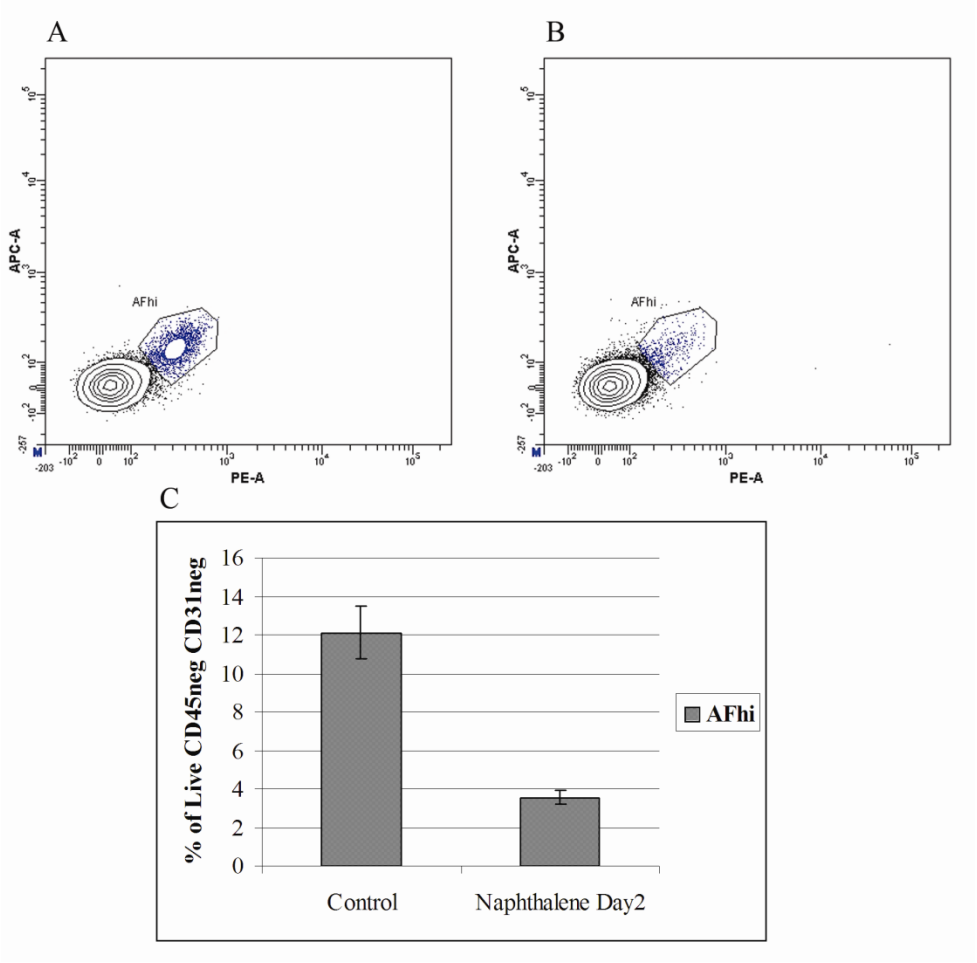

Figure 18. Changes in the abundance of AFhi population during naphthalene injury.

Adult male mice were treated with naphthalene (250mg/kg). Two days later cells were isolated from naphthalene treated and untreated (control) lungs (n=3 mice per condition) and the abundance of the AFhi population in the live cell population was analyzed and compared between groups. (A) Flow cytometry analysis of autofluorescence levels of cells isolated from a control (untreated) mouse. (B) Flow cytometry analysis of autofluorescence levels of cells isolated two days after naphthalene administration. The gate defines the high autofluorescence (AFhi) population in (A) and (B). (C) Quantitative representation of data in figure (A) and (B).

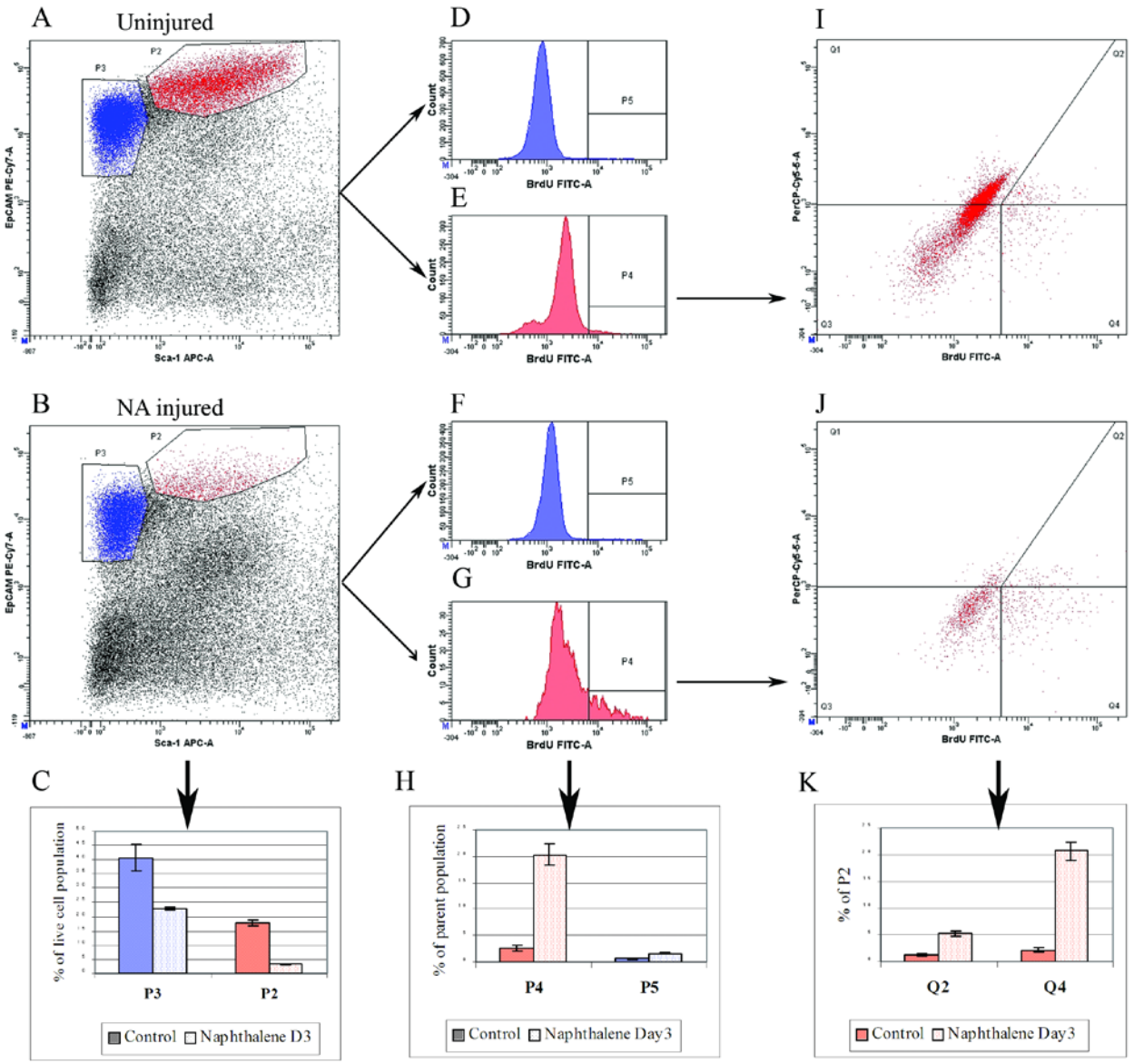
A
Uninjured
P2
P3
EpCAM PE-Cy7-A
Sca-1 APC-A
D
Count
P5
BrdU FITC-A
E
P4
I
Q1
Q2
Q3
Q4
PerCP-Cy5-5-A
B
NA injured
F
G
J
C
% of live cell population
P3
P2
Control
Naphthalene D3
H
% of parent population
P4
P5
Naphthalene Day3
K
% of P2
Q2
Q4

Figure 19. Proliferation during the repair process following naphthalene injury.

Adult male mice were treated with naphthalene (250mg/kg). BrdU was administered i.p. to treated and untreated controls every 12 hours for 72 hours after naphthalene administration. Mice were sacrificed 2 hours after the last i.p. administration, cells were isolated and analyzed by flow cytometry for BrdU incorporation in the context of the Sca-1 and EpCAM cell surface expression. (A)-(C) Flow cytometry analysis of EpCAM PE-Cy7 (y axis) and Sca-1 Alexa Fluor 647 (x axis) in the live cell population of control (A) and day3 after naphthalene injury (B) animals. P2 gate (red dots) represents the Sca-1^{low} $EpCAM^{pos}$ population and P3 gate (blue dots) represents the Sca-1^{neg} $EpCAM^{pos}$ population. (C) Quantitative representation of data in (A) and (B) showing the abundance of cells in P2 and P3 populations in cells isolated from control (dark red and blue bars) and day 3 after naphthalene injury (light red and blue bars). (D) – (H) Proliferation in the P2 (red histograms) and P3 (blue histograms) cell populations in control and naphthalene treated mice. Flow cytometry histograms demonstrating the number of BrdU incorporating cells in cells isolated from control (D and E) or day 3 after naphthalene treatment (F and G) mice. Gates P4 and P5 represent the $BrdU^{pos}$ fractions of the Sca-1^{low} $EpCAM^{pos}$ (P2) population and Sca-1^{neg} $EpCAM^{pos}$ (P3) respectively. (H) Quantitative analysis of the number of $BrdU^{pos}$ cells in (D) – (G) in control (dark blue and red bars) and naphthalene treated (light blue and red bars) mice. (I) – (L) Analysis of autofluorescence levels of the Sca-1^{low} $EpCAM^{pos}$ (P2 in A and B) in the PerCP-Cy5.5 and FITC channels in control (I) and naphthalene treated animals (J). Q1- AF^{hi} $BrdU^{neg}$, Q2 - AF^{hi} $BrdU^{pos}$, Q3 – AF^{low} $BrdU^{neg}$, and Q4 – AF^{low} $BrdU^{pos}$. (K) Quantitative representation of gates Q2 and Q4 in control (dark red bars) and naphthalene treated animals (light red bars).

4.2.6 Functional analysis of the proliferative behavior of the AF^{hi} and AF^{low} populations during ozone injury and repair

The progenitor function of the abundant pool of Clara cells (termed here facultative TA cells) in the rodent lung has been demonstrated in classical studies involving ozone injury[2]. Ozone exposure causes lung epithelial cell damage, ciliated cells being the most sensitive cells. Evans et al. demonstrated that ablation of ciliated cells by exposure to ozone causes Clara cells to undergo morphological changes, proliferate and restore the ciliated cell pool. Thus the progenitor-progeny relationship between Clara cells and ciliated cells was established[2]. We have shown in the previous chapter that the AF^{hi} $EpCAM^{pos}$ $Sca\text{-}1^{low}$ $CD45^{neg}$ $CD31^{neg}$ $CD34^{neg}$ population consists of naphthalene-sensitive cells and that AF^{low} $EpCAM^{pos}$ $Sca\text{-}1^{low}$ $CD45^{neg}$ $CD31^{neg}$ $CD34^{neg}$ cells represent the naphthalene resistant stem cells that proliferate during the repair response. To demonstrate the facultative progenitor function of the AF^{hi} $EpCAM^{pos}$ $Sca\text{-}1^{low}$ fraction, ciliated cells were depleted by means of ozone exposure. Adult male mice were exposed to 1.5ppm Ozone for 12 hours, and control mice were exposed to filtered air (FA) for the same length of time. To label proliferating cells, mice in both groups were treated with BrdU for the first 48 hours of recovery and sacrificed 2 hours after the last BrdU administration (Figure 19). As expected, analysis of EpCAM and Sca-1 expression in the live cell population revealed two populations of $EpCAM^{pos}$ $Sca\text{-}1^{low}$ and $EpCAM^{pos}$ $Sca\text{-}1^{neg}$. Interestingly, the $EpCAM^{pos}$ $Sca\text{-}1^{low}$ population showed a significant increase 48 hours after ozone exposure (P2=10.25% vs 15.23% of live cells in FA exposed and ozone treated mice respectively), while the $EpCAM^{pos}$ $Sca\text{-}1^{neg}$ population did not change significantly (P3=26.75% vs 29.26% of live cells population in FA and ozone treated mice respectively). This increase was most likely caused by an ample proliferative response of the Clara cell population that exceeded the needs for ciliated cell

replacement, thus resulting in an overall increase in number of bronchiolar epithelial cells. Thus, the number of cells that proliferated during the 48hours of BrdU administration was evaluated in each fraction. The number of BrdU incorporating cells in the $EpCAM^{pos}$ $Sca\text{-}1^{neg}$ fraction was very low in FA controls and did not increase significantly following ozone exposure (P5=0.6% versus 0.46%), suggesting that the alveolar compartment was not impacted by ozone exposure. However, evaluation of the proliferating pool in the $EpCAM^{pos}$ $Sca\text{-}1^{low}$ population showed an almost four fold increase in percentage of $BrdU^{pos}$ cells in ozone treated mice compared with FA controls (P5=3.1% versus 11.06%), consistent with the expected behavior of bronchiolar epithelial cells. To determine the autofluorescence characteristics of $BrdU^{pos}$ cells in the $EpCAM^{pos}$ $Sca\text{-}1^{low}$ population, BrdU FITC expression in that fraction was evaluated as a function of autofluorescence in PerCP-Cy5.5 channel. The number of $BrdU^{neg}$ cells in the AF^{low} and AF^{hi} populations (Q1 and Q3 in figure 20K) was not altered in response to ozone injury, thus demonstrating that the increase in total number of cells in the $EpCAM^{pos}$ $Sca\text{-}1^{low}$ fraction observed in ozone exposed mice is indeed the result of proliferative events that took place in the 48hours of BrdU administration. Interestingly, $BrdU^{pos}$ cells in ozone treated mice were present in both AF^{hi} and AF^{low} fractions, suggesting that both the stem and the facultative TA compartments participate to the repair response following ozone injury (populations Q2 and Q4 in figure 20L). However, BrdU incorporating facultative TA (Clara) cells that differentiated and gave rise to ciliated cells represent another possible source of $BrdU^{pos}$ cells in the AF^{low} fraction. Importantly though, the significant number of cells in the AF^{hi} fraction incorporated BrdU label following ozone injury, demonstrating its proliferative ability and progenitor function.

Ozone injury has been shown to induce proliferation in CCSP expressing secretory cells in the bronchiolar epithelium, without distinguishing between stem and facultative TA (Clara)

cells. Analysis of the autofluorescence levels of cells proliferating in response to ozone injury suggested that both the stem and the facultative TA (Clara) cell pools participate in the repair process. Thus we analyzed the localization of BrdU incorporating cells in lung sections from FA and ozone exposed mice as a function of known lung epithelial specific markers (Figure 21). As expected, the number of proliferating cells in FA exposed animals was very low. Interestingly though, exposure to ozone induced proliferation preferentially in the distal bronchiolar epithelium, while the proximal epithelium was mainly quiescent with the exception of occasional foci of proliferating CCSP expressing cells (Figure 21 A-F). Importantly, we were able to demonstrate the presence of proliferating cells within both previously characterized stem cell niches, BADJs and NEBs (Figure 21 F and L) as well as CCSP expressing cells outside of these niches. Consistent with the flow cytometry analysis, proliferation in the alveolar epithelium compartment was very low; the majority of proliferating cells in that location most likely represented inflammatory cells (Figure 21 G-J).

Thus, we used two distinct injury models to reveal the functional differences between the AF^{hi} and the AF^{low} fractions of the $EpCAM^{pos}$ $Sca\text{-}1^{low}$ population of bronchiolar epithelial cells. Together, these data demonstrate that the AF^{low} population represents naphthalene resistant cells, that participates in the repair response following both naphthalene and ozone injury, validating their stem cell characteristics. The AF^{hi} population consists of naphthalene sensitive cells that have proliferative capacity in response to ozone exposure demonstrating their facultative progenitor behavior.

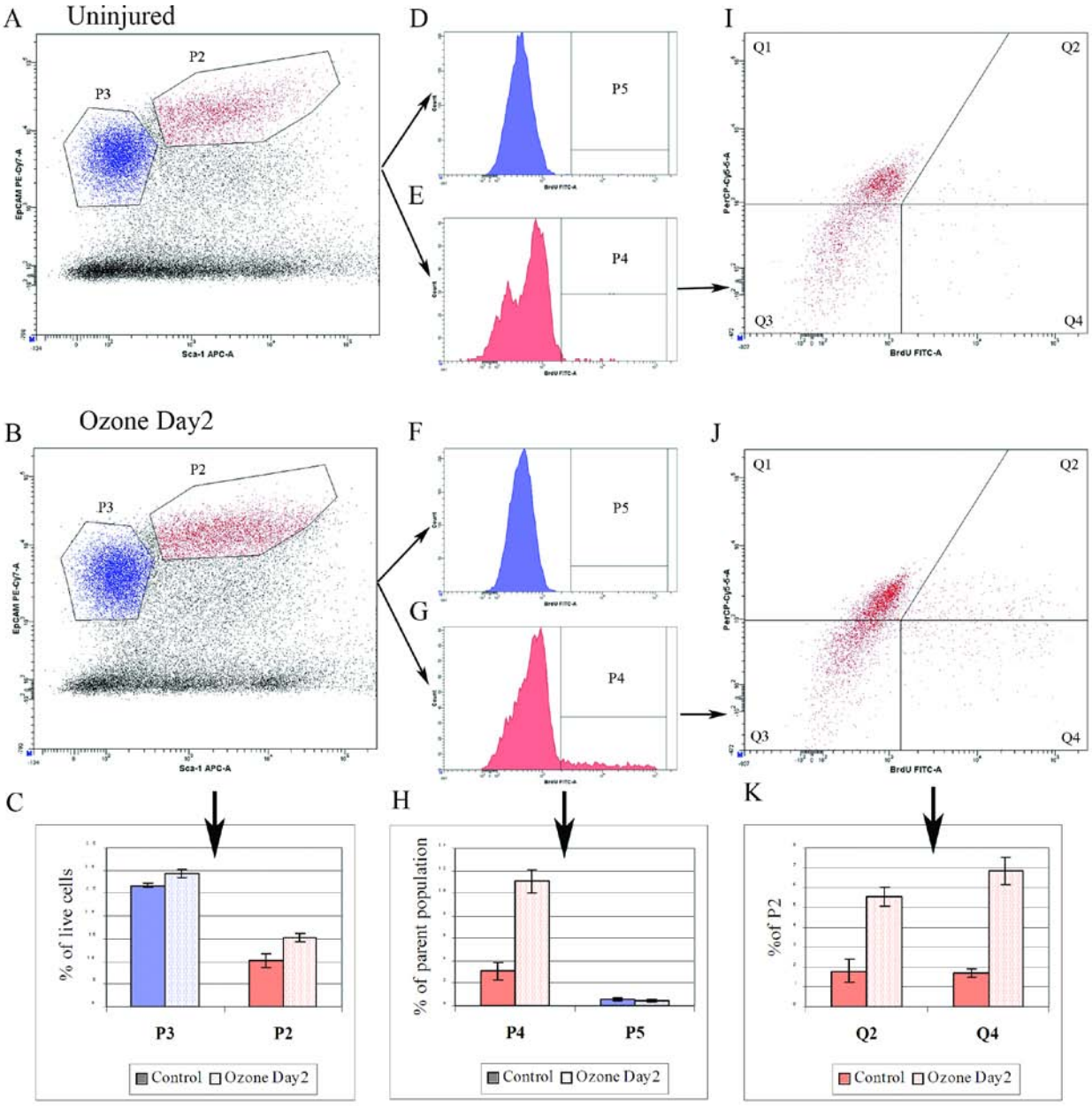
A
Uninjured
P2
P3
EpCAM PE-Cy7-A
Sca-1 APC-A
D
P5
E
P4
BrdU FITC-A
I
Q1
Q2
Q3
Q4
PerCP-Cy5-5-A
BrdU FITC-A
B
Ozone Day2
F
G
J
C
% of live cells
P3
P2
Control
Ozone Day2
H
% of parent population
P4
P5
K
%of P2
Q2
Q4

Figure 20. Proliferation during the repair process following ozone injury.

Adult male mice were exposed to 1.5ppm ozone for 12 hours and recovered for 48 hours in room air. Control mice were exposed to 1.5ppm filtered air (FA) for 12 hours and recovered for 48 hours in room air. BrdU was administered i.p. to animals in both groups every 12 hours for the 48 hours of recovery. Mice were sacrificed 2 hours after the last i.p. administration, cells were isolated and analyzed by flow cytometry for BrdU incorporation in the context of the Sca-1 and EpCAM cell surface expression. (A)-(C) Flow cytometry analysis of EpCAM PE-Cy7 (y axis) and Sca-1 Alexa Fluor 647 (x axis) in the live cell population of control FA (A) and ozone exposed animals (B). P2 gate (red dots) represents the Sca-1^{low} $EpCAM^{pos}$ population and P3 gate (blue dots) represents the Sca-1^{neg} $EpCAM^{pos}$ population. (C) Quantitative representation of data in (A) and (B) showing the abundance of cells in P2 and P3 populations in cells isolated from control FA (dark blue and red bars) and ozone exposed mice (light blue and red bars)(P2=10.25% and 15.23% and P3=26.72% and 29.26% of live cell population in FA or ozone expose mice respectively). (D) – (H) Proliferation in the P2 (red histograms) and P3 (blue histograms) cell populations in control FA and ozone exposed mice. Flow cytometry histograms demonstrating the number of BrdU incorporating cells in control FA (D and E) or ozone treated (F and G) mice. Gates P4 and P5 represent the $BrdU^{pos}$ fractions of the Sca-1^{low} $EpCAM^{pos}$ (P2) population and Sca-1^{neg} $EpCAM^{pos}$ (P3) respectively. (H) Quantitative analysis of the number of $BrdU^{pos}$ cells in (D) – (G) in control FA (dark red and blue bars) and ozone treated (light red and blue bars) mice (P4=3.1% and 11.06% and P5=0.6% and 0.466%). (I) – (L) Analysis of autofluorescence levels of the Sca-1^{low} $EpCAM^{pos}$ (P2 in A and B) in the PerCP-Cy5.5 and FITC channels in control FA (I) and ozone exposed mice (J). Q1- AF^{hi} $BrdU^{neg}$, Q2 - AF^{hi} $BrdU^{pos}$, Q3 – AF^{low} $BrdU^{neg}$, and Q4 – AF^{low} $BrdU^{pos}$. (K) Quantitative representation of gates Q2 and Q4 in FA (dark red bars) and ozone treated animals (light red bars) (Q2=1.8% and 5.56% and Q4=1.7% and 6.83%).

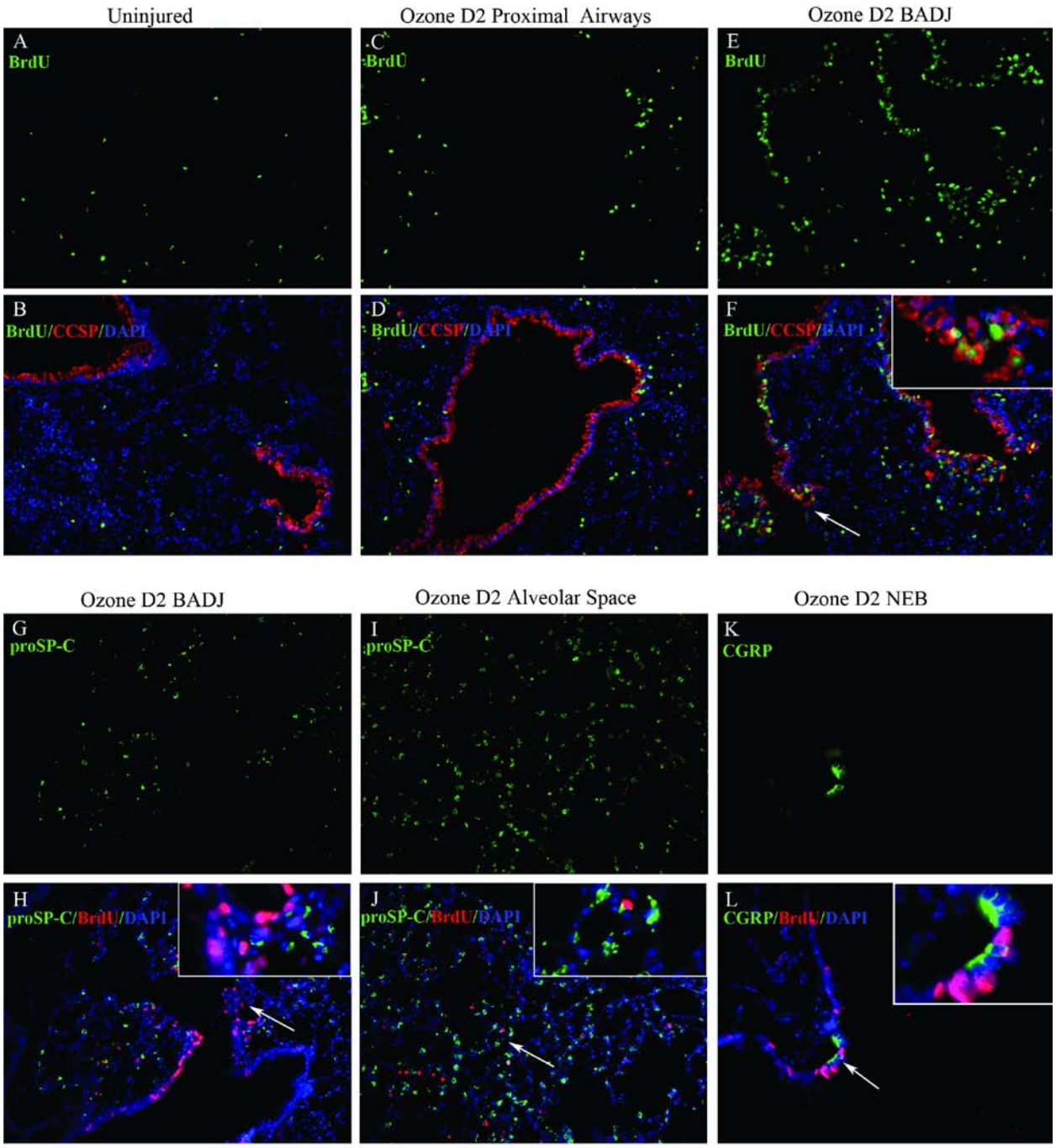
Uninjured
Ozone D2 Proximal Airways
Ozone D2 BADJ
A
BrdU
C
BrdU
E
BrdU
B
BrdU/CCSP/DAPI
D
BrdU/CCSP/DAPI
F
BrdU/CCSP/DAPI
Ozone D2 BADJ
Ozone D2 Alveolar Space
Ozone D2 NEB
G
proSP-C
I
proSP-C
K
CGRP
H
proSP-C/BrdU/DAPI
J
proSP-C/BrdU/DAPI
L
CGRP/BrdU/DAPI

Figure 21. Tissue localization of cells proliferating in response to ozone injury

Adult male mice were exposed to 1.5ppm ozone for 12 hours and recovered for 2 or 10 days in room air. Control mice were exposed to filtered air (FA) for 12 hours and recovered for the same amount of time in room air. BrdU was administered i.p. to animals in all groups every 12 hours for the first 48 hours of recovery. The identity of the proliferating cells was determined by immunofluorescence co-localization of BrdU (green signal) and other cell type specific markers (red signal). (A) – (F) Proliferation in the airway epithelium. BrdU (green A-F) CCSP (red B, D and F) immunolocalization in lung sections of control FA exposed mice (A and B), proximal airways of ozone exposed mice (C and D) and distal airways of ozone exposed mice (E and F). Inset in F shows higher magnification of a BADJ area (200 x magnification). (G) – (J) Immunofluorescence staining for BrdU (green) and proSP-C (red) of terminal bronchioles (G and H) and gas exchange area (I and J) of ozone exposed mice (200x magnification). Insets in (H) and (J) represent higher magnifications of a BADJ (H) and gas exchange area (J). (K) and (L) Immunofluorescence detection of BrdU (green) and CGRP (red) in neuro-endocrine bodies of ozone exposed mice (400x magnification). Inset in (L) represents higher magnification of the NEB area. DAPI – nuclear counterstain (blue signal in overlayed images). Arrows in F, H, J and L point at areas magnified in insets.

4.3 DISCUSSION

Expression of a unique repertoire of cell surface markers has been extensively used as a tool to prospectively isolate and characterize stem and progenitor populations in several organs. Moreover, it represents a pre-requisite of stem cell isolation aimed at development of cell-based therapies. The goal of this study was to define characteristics of bronchiolar stem cells that allow their prospective isolation to better understand their functional behavior in steady state and injured lung. In this chapter we provide evidence for expression of Sca-1, EpCAM and Integrin α6 on the cell surface of distinct populations of lung epithelial cells. EpCAM and Integrin α6 allow the distinction between epithelial and non-epithelial cells within the Sca-1^{low} population. Gene expression analysis validated by the use of transgenic mouse models expressing fluorescent reporters allowed the identification of cell surface phenotype and autofluorescence characteristics of most epithelial cell types in the lung. Thus we define an $EpCAM^{pos}$, Integrin $\alpha6^{pos}$, Sca-1^{neg}, $CD45^{neg}$, $CD31^{neg}$, $CD34^{neg}$ population that represents mostly alveolar epithelial cells. Bronchiolar epithelial cells are characterized by $EpCAM^{pos}$, Integrin $\alpha6^{pos}$, Sca-1^{low}, $CD45^{neg}$, $CD31^{neg}$, $CD34^{neg}$ phenotype and they can be further fractionated according to their autofluorescence characteristics into AF^{hi} and AF^{low} populations. Epithelial injury and repair models demonstrate that cells within the two populations are functionally distinct. The AF^{hi} fraction behavior was indicative of a facultative progenitor population, while the behavior of the AF^{low} fraction suggested a stem cell phenotype. Ciliated cells of the bronchiolar epithelium were present in the AF^{low} fraction, indicating that they are a significant fraction that co-purifies with the bronchiolar stem cell population.

Validation of stem cell characteristics of a specific cell population includes analysis of its *in vivo, in vitro* and transplantation properties that would confirm their progenitor cell function.

Self renewal and differentiation abilities of a putative stem cell population can be demonstrated in clonogenic and serial passage in cultured and transplanted cells[30, 51]. Unfortunately, robust and reproducible *in vitro* and transplantation assays for lung epithelial cells do not exist, thus making it impossible to test the functional properties of the AF^{hi} and AF^{low} fractions of the $EpCAM^{pos}$ Sca-1^{low} $CD45^{neg}$ $CD31^{neg}$ $CD34^{neg}$ cell populations in such assays. *In vivo* bronchiolar stem cells have been identified based on their resistance to naphthalene injury and proliferative capacity during airway repair response[18, 55]. Thus we have been able to demonstrate that the AF^{hi} population is naphthalene sensitive and that the AF^{low} population is naphthalene resistant and it incorporates BrdU label during the initial phases of the repair response (Figure 22 C). Moreover, Clara cells have been shown to serve as progenitors for the terminally differentiated ciliated cells following ozone injury[2]. In our studies, we used a relative high concentration of ozone for extended periods of time (1.5ppm ozone for 12 hours) and we can show that we elicited a proliferative response from both the stem and the facultative TA (Clara) cell populations (Figure 22 B). Although these data does demonstrate the progenitor functions of the AF^{hi} fraction, it also shows for the first time that ozone can induce proliferation in the stem cell compartment. Future studies will evaluate the dose dependency and the types of injury that ozone causes as well as the proliferative response it induces. Naphthalene and ozone injury and repair studies were designed to determine the characteristics of cells that incorporated BrdU label during the initial repair response (Figure 22). However, our analysis does not indicate the number and phenotype of cells that actively proliferate at the time of the analysis, but it allows us to determine the fate and phenotype of cells that have proliferated during the labeling period. It is possible, for example, that a stem cell originally belonging to the AF^{low} population, incorporated BrdU early during the labeling period and matured into a facultative TA (Clara) cell, found in the AF^{hi} population at the

time of the analysis. Conversely, a facultative TA (Clara) cell in the AF^{hi} fraction can incorporate BrdU during a proliferation event that generates a $BrdU^{pos}$ ciliated cell, found in the AF^{low} fraction at the time of the analysis. Pulse labeling experiments (one i.p. administration of BrdU 2 hours before sacrificing the animal) will accurately determine the size of the actively proliferating pool. Comparison of the results from continuous and instantaneous labeling following naphthalene and ozone injury will reveal important information about the number and the fate of proliferating cells in each fraction.

Another proposed *in vivo* characteristic of the bronchiolar stem cell found at BADJs is dual expression of two proteins characteristic for ATII and bronchiolar secretory cells, SP-C and CCSP respectively[99,104]. Their presence *in vivo* and their direct relationship with bronchiolar stem cells are still a matter of debate. Technical hurdles related to the quality of antibodies used, the low levels of expression of both proteins and the autofluorescence of the bronchiolar epithelium made it difficult to draw definitive conclusions in regard to their existence and functional properties. Moreover, the existence of such dual expressing cells in the other stem cell niche (NEBs) has not been assessed before. To confirm the presence of dual expressing cells in the AF^{low} fraction, we used a transgenic animal model expressing GFP under the human SP-C promoter[150]. Interestingly, analysis of native fluorescence showed GFP expression in the airways of SP-C GFP transgenic mice. Fluorescence levels were high at BADJs and faded proximally, with the exception of CCSP expressing cells located around NEBs. Whether those cells represent naphthalene resistant cells and proliferate to repair the epithelium remains to be addressed in future studies. Expression of the GFP transgene does not necessarily parallel the endogenous gene or protein expression but it does raise the interesting possibility that the SP-C promoter is active and can be activated in certain circumstances. Most importantly, the value of this

transgenic animal model is that together with the cell surface characteristics described in the chapter, it will allow the prospective isolation of cells located in stem cell niches. Future studies will evaluate the *in vitro* and in vivo functional properties as well as the gene expression signature of the cell populations described in this chapter.

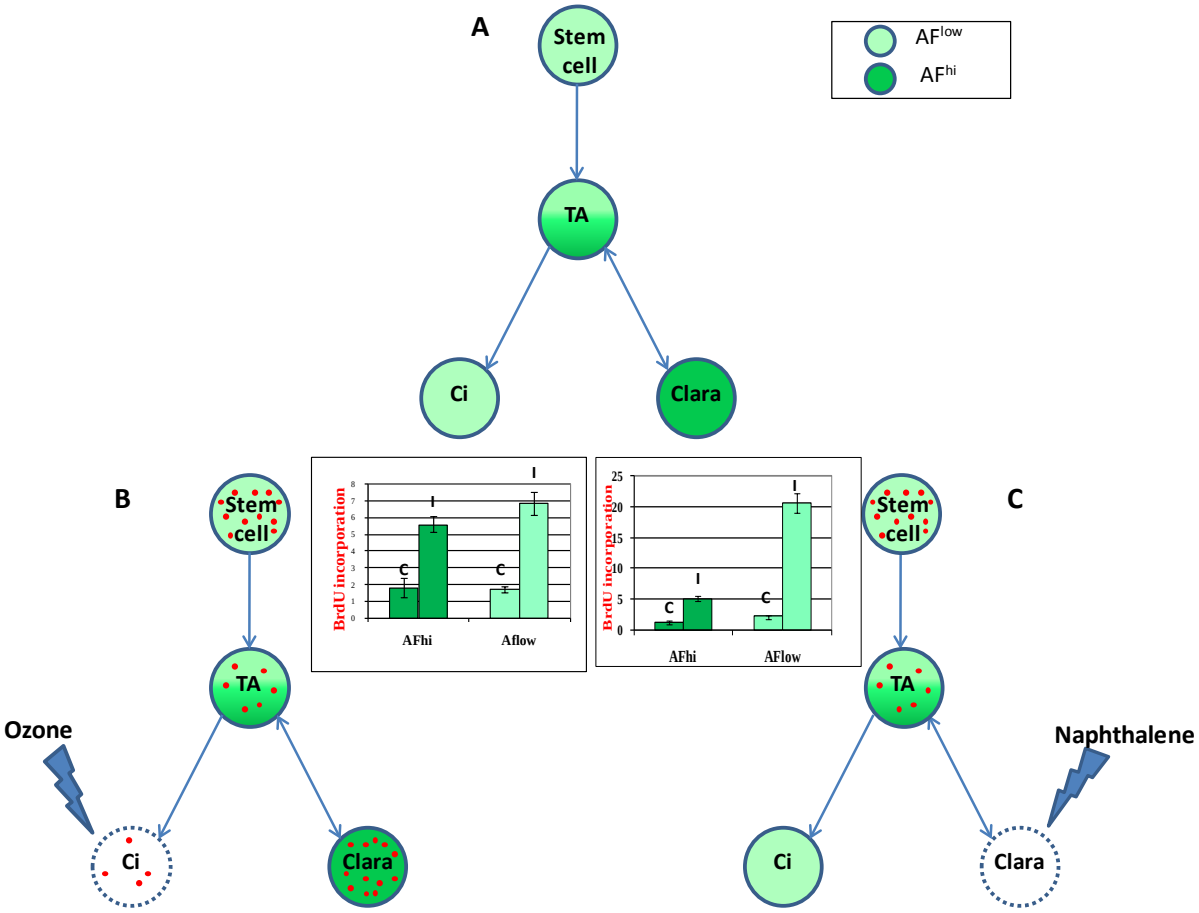

Figure 22. Schematic representation of the structure of the bronchiolar stem cell hierarchy

The model represents hierarchical organization of the bronchiolar stem cell hierarchy based upon autofluorescence and functional characteristics in steady state (A) and injured (B) and (C) airway epithelium. (A) Steady state airway epithelium encompasses two distinct populations based upon autofluorescence characteristics: a population characterized by high autofluorescence (AF^{hi} – light green) that comprises of facultative TA (Clara) cells and a population characterized by low autofluorescence (AF^{low} – dark green) comprising of bronchiolar stem cells (Stem cell) and terminally differentiated ciliated cells (Ci). The transit amplifying population (TA) represents an intermediate between the stem and the facultative TA (Clara) cells that holds the ability to generate terminally differentiated ciliated cells. (B) Representation of the functional behavior of BrdU (red dots) incorporating cells in the AF^{hi} and AF^{low} fractions during the repair response following ozone exposure shows that both stem and facultative TA can give rise to the TA intermediate that replenishes the pool of terminally differentiated ciliated cells. Graph: see Figure 20K, in each group, left bar represents BrdU incorporation in FA controls (C) and right bar represents BrdU incorporation in O3 injured mice (I). (C) Representation of the functional behavior of BrdU (red dots) incorporating cells in the AF^{hi} and AF^{low} fractions during the repair response following naphthalene injury showing that the AF^{low} population of stem cells is responsible for the majority of BrdU incorporating cells. Graph: see Figure 19K; in each group left bar represents BrdU incorporation in uninjured controls (C) and right bar represents BrdU incorporation in naphthalene injured mice (I). Cells lined by dotted line represent cells depleted during injury (ozone sensitive (B) and naphthalene sensitive (C) cells).

5.0 SUMMARY, CONCLUDING REMARKS, AND FUTURE DIRECTIONS

The main goal of our study was to define characteristics specific to the bronchiolar stem cell population that would allow their prospective isolation and further characterization towards a better understanding of how they participate in lung disease pathogenesis and of their therapeutic potential. We have been able to demonstrate that previously proposed cell surface markers do not accurately define the bronchiolar stem cell population. In the absence of robust *in vitro* and transplantation assays, we used transgenic animal models associated with stem cell expansion, ablation and lineage tracing to validate fractionation strategies leading to enrichment of distinct populations of lung progenitor and stem cells. The stem and progenitor properties of these populations have been validated using previously established injury and repair models. Thus, we have been able to identify three distinct populations of lung epithelial cells: 1) a population defined by $EpCAM^{pos}$ $Sca\text{-}1^{neg}$ $CD45^{neg}$ $CD31^{neg}$ $CD34^{neg}$ phenotype that consists mostly of alveolar type II cells; 2) a population defined by AF^{hi} $EpCAM^{pos}$ $Sca\text{-}1^{low}$ $CD45^{neg}$ $CD31^{neg}$ $CD34^{neg}$ that consists mainly of the facultative TA (Clara) cell population and 3) a population defined by AF^{low} $EpCAM^{pos}$ $Sca\text{-}1^{low}$ $CD45^{neg}$ $CD31^{neg}$ $CD34^{neg}$ that contains the majority of ciliated cells as well as the bronchiolar stem cell population.

Future studies need to assess the functional properties of prospectively isolated stem and progenitor cell populations *in vitro* and in transplantation assays, and define the gene expression signature of the stem cell population.

Culture conditions supporting the growth and expansion of mouse bronchiolar epithelial cells are currently unknown. In other systems, cell culture experiments were able to reveal differences between stem cells and more differentiated progenitors based on the size of the generated clones (holoclones vs meroclones in the skin[65]), their clonogenic frequency, i.e. the frequency with which cells give rise to colonies, and serial passage ability, the ability to re-form colonies upon passaging[51,152].We are currently conducting experiments towards defining culturing conditions for bronchiolar epithelial cells. The cell specific markers available to determine the identity of cultured epithelial cells are mostly secreted proteins (CCSP and SP-C) and their expression is down-regulated in culture, making it impossible to determine the identity of the growing cells. In that regard, transgenic animal models that allow lineage tracing of cells within the bronchiolar epithelium represent an invaluable tool to follow the fate of cultured epithelial cells. In bronchiolar epithelium both stem and facultative TA (Clara) cells have proliferative ability and the distinction between the two has been established *in vivo* based upon the relative resistance of the stem cells to naphthalene injury. It is currently unknown whether this stem cell property is conferred by the protective environment of the stem cell niche or if it is a cell-intrinsic property. Therefore, there is a strong possibility that when removed from their native environment, functional differences between stem and facultative TA (Clara) cells are abrogated. Culture conditions have a profound influence on the proliferative and differentiation choices of cells that are not necessarily reflective of their *in vivo* properties. Thus, interpretation of cell culture outcome must be approached with caution and all the above mentioned factors must be taken into consideration. The appropriate combination of substrates and medium components will need to be defined for self renewal and differentiation assays. Preliminary studies have been successful in the propagation of lineage tagged cells on Matrigel basement

membrane extract and on NIH 3T3 J2 cells (Figure 23). Lineage tagged epithelial cells formed sphere-like structures when grown on Matrigel and three dimensional colonies of cells when grown on NIH 3T3 J2 cells. Both of these substrates were previously used for propagation of other stem cell populations like epidermal stem cells (NIH 3T3 J2) and mammary and prostate stem cells (Matrigel) [51, 52,153,154]. Ongoing studies aim at optimizing culturing conditions permissive for propagation and serial passage of bronchiolar epithelial cells that would reflect the functional differences between stem and facultative TA cells observed *in vivo*.

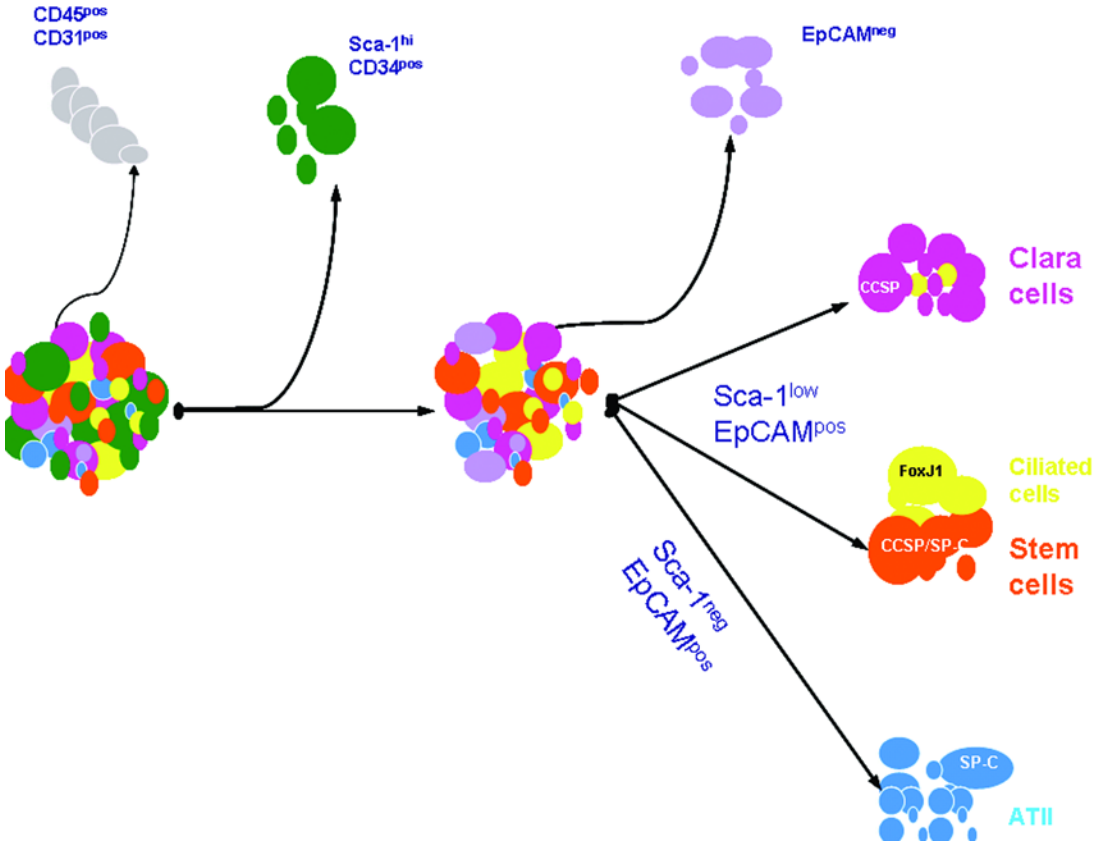

Figure 23. Outline of the selection strategy leading to prospective isolation of sub-populations of lung epithelial cells.

The model summarizes steps taken towards identification of positive and negative selection markers used to prospectively isolate facultative TA (Clara) cells (purple discs), alveolar type II (ATII) cells (blue discs), ciliated cells (yellow discs) and bronchiolar stem cells (orange discs). The selection strategy includes negative selection of cells of hematopoietic ($CD45^{pos}$) and endothelial ($CD31^{pos}$) origin (grey discs, Figure 1C), $CD34^{pos}$ cells (green discs, Figures 6 and 9) and non-epithelial cells ($EpCAM^{neg}$ purple discs, Figures 10-13). Sca-1 expression distinguishes alveolar epithelium ($Sca\text{-}1^{neg}$, blue discs, Figures12 and 17) from bronchiolar epithelial cells ($Sca\text{-}1^{low}$, Figure 12). Amongst airway epithelial cells, autofluorescence characteristics distinguish facultative TA (Clara) cells which are AF^{hi} (magenta discs, Figure 12) from bronchiolar stem cells (orange discs) and ciliated cells (yellow discs) which are AF^{low} (Figures 12 and 17).

A

B

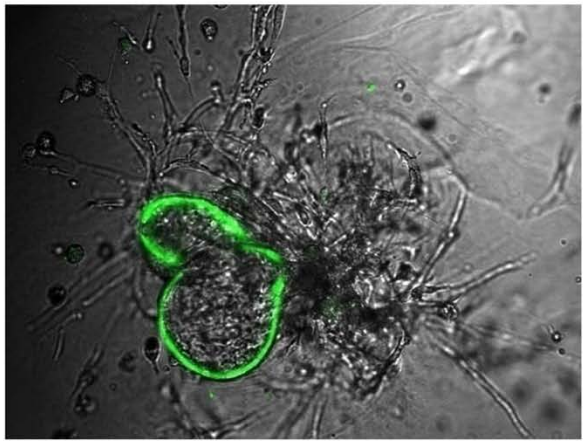

C

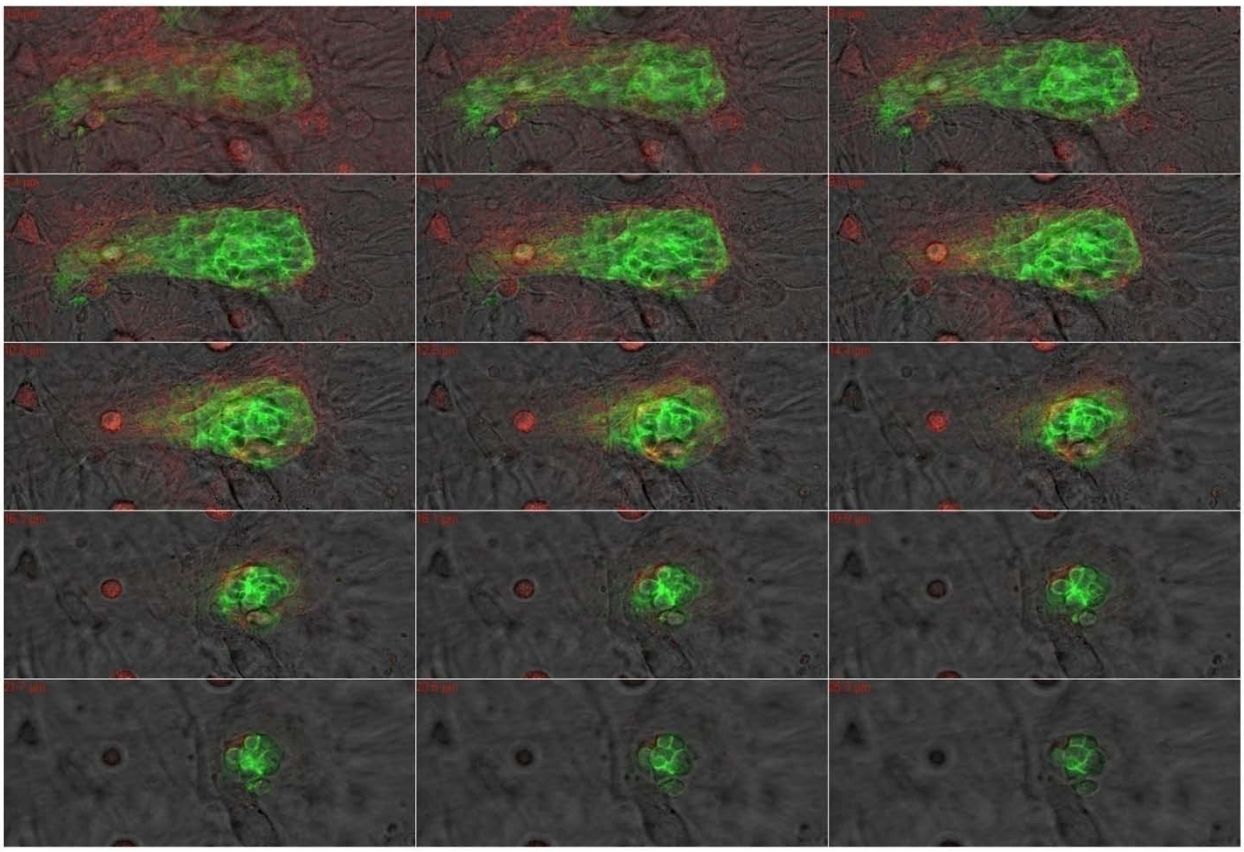

Figure 24. Cell culture assays supporting growth of lung epithelial cells

Cells were isolated from the lungs of wild-type (A), CCSPcre Rosa26 LSL EYFP (B) and SP-Ccre Rosa26 TdTomato$^{flox/flox\ EGFP}$ (C) and cultured on Matrigel (A) and (B) and on NIH3T3 J2 fibronblasts (C).

(A). Nuclear fast red staining of a spheroid 21days into the Matrigel culture. (B) Confocal microscopy image of a spheroid derived from lineage traced airway epithelial cells (CCSPcre Rosa26 LSL EYFP) demonstrating the airway epithelium origin of cells forming spheroids. (C) Z-stack confocal images of cells from lineage traced lung epithelial cells (SP-Ccre Rosa26 TdTomato$^{flox/flox\ EGFP}$) cultured on Mitomycin C treated NIH 3T3 J2 for 7 days. Red cells (TdTomato) represent unrecombined non-epithelial cells and green cells (EGFP) recombined lung epithelial cells. The SP-Ccre transgene is activated in lung epithelium early in development (approximately E10.5), thus inducing recombination and lineage tracing of the entire intra-pulmonary lung epithelium (airways and alveolar epithelium).

Transplantation assays are critical to demonstrate the functional properties of a stem cell population as they provide an environment more closely related to the native environment of the population studied. Future studies need to define the optimal conditions that promote propagation of lung epithelial cells. Good examples include intra-tracheal administration of cells or injecting cells subcutaneously or under the kidney capsule. Survival, proliferation and differentiation of bronchiolar stem cells are expected to be greatly influenced by the environment. The properties of the bronchiolar stem cell niche are largely unknown and the mechanisms involved in stem cell maintenance and activation remain to be explored. To provide the best chances for the bronchiolar stem cell to survive and proliferate we used a novel technique involving subcutaneous co-transplantation of mixed fluorescently tagged bronchiolar epithelial cells and untagged undifferentiated mouse embryonic (ES) stem cells. When transplanted subcutaneously, undifferentiated ES cells randomly differentiate towards all known lineages and give rise to teratomas. We hypothesized that on their way to differentiating towards endodermal lineage the ES cells would provide an environment appropriate for maintenance and growth of bronchiolar stem cells. Thus we isolated lung epithelial cells from transgenic mice expressing ubiquitously TdTomato, mixed them with untagged undifferentiated ES cells and transplanted them subcutaneously under the skin of immuno-deficient mice. Teratomas were collected three weeks later and analyzed for the presence of TdTomato positive cells. Interestingly, clusters of TdTomato positive cells were found organized in tubular structures that expressed CCSP, proSP-C or both (Figure 24). Moreover, ES cell derived tubular structures that expressed proSP-C were also present. They were underlined by TdTomato mesenchymal cells, suggesting that lung fibroblasts can influence the differentiation of ES cells towards lung

epithelium. Future experiments performed with sorted population (AF^{hi} and AF^{low}) will address the functional properties of the stem and facultative progenitor cell pools.

Our studies indicate that the AF^{hi} and AF^{low} populations are functionally and phenotypically different. In order to refine our understanding of the differences between these populations and find novel cell surface markers that would allow further enrichment in bronchiolar stem cells in the AF^{low} fraction, we will perform microarray analysis on mRNA isolated from sorted populations. Ciliated cells, which are also present in the AF^{low} population, will be excluded using FoxJ1 GFP transgenic mice.

In conclusion, the work presented here provides new information defining bronchiolar cells with phenotypic characteristics of stem cells, opening the door for development of novel assays to evaluate the status of the bronchiolar stem cell compartment in healthy and disease states. An important future direction consists of translational research that will eventually lead to improved therapeutic interventions and a better understanding of pathogenetic mechanisms of human lung disease. In that regard, solid *in vitro* and transplantation assays become instrumental in transitioning from mouse to human lung science to improve our understanding of human lung biology.

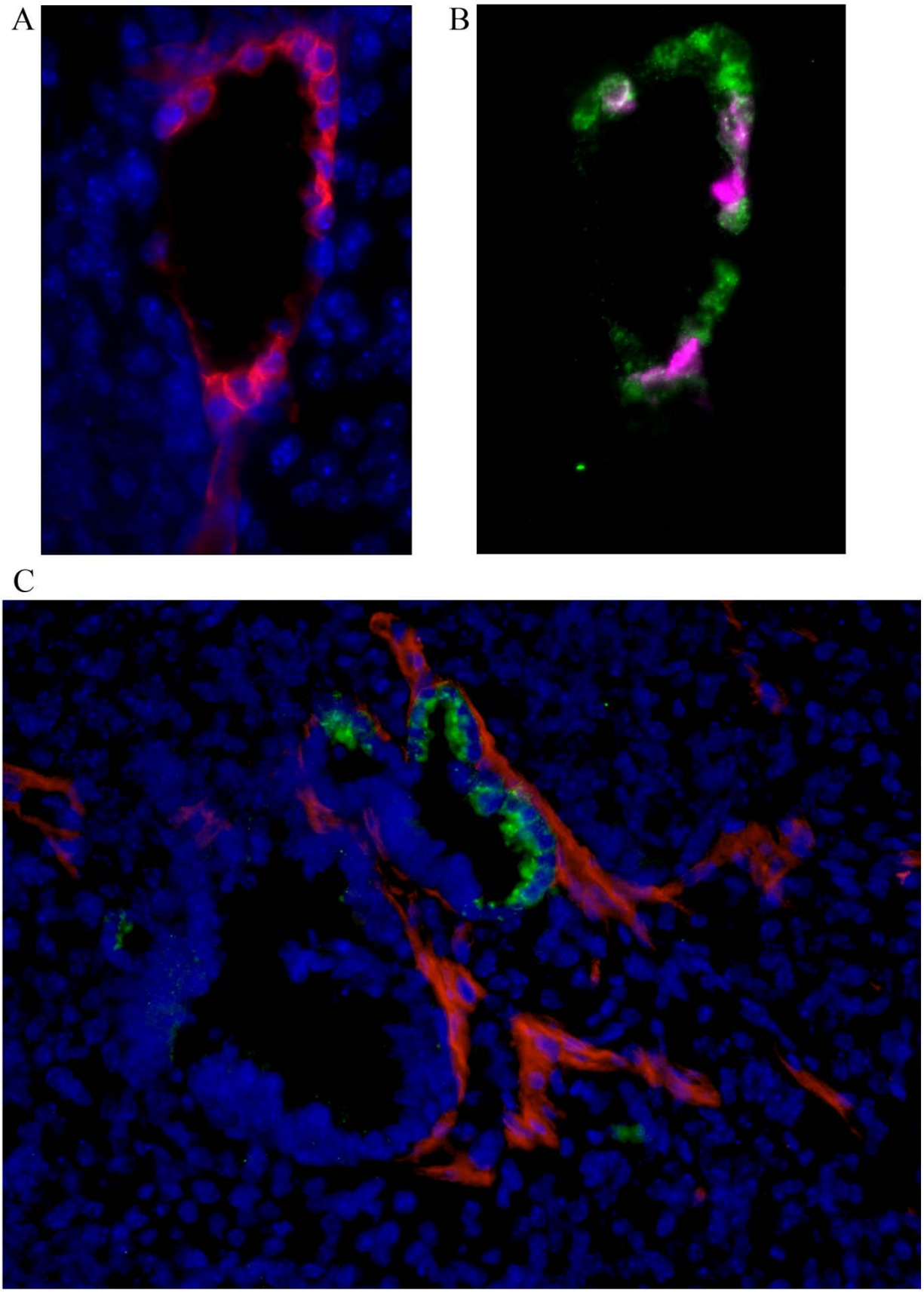
A
B
C

Figure 25. Lung epithelial cells transplantation assay

Cells isolated from lungs (total cell population) of ubiquitous TdTomato expressing mice (Rosa26 TdTomato$^{flox/flox\ EGFP}$) were mixed with undifferentiated ES cells and transplanted under the skin of immuno-deficient mice. Three weeks later the teratomas were harvested, sectioned and stained for CCSP (purple), proSP-C (green). (A) (B) Immunofluorescence staining for CCSP (purple) and proSP-C (green) of an epithelial tubular structure derived from transplanted lung cells (red – TdTomato) showing that teratomas are permissive for airway epithelial cells growth. (C) Immunofluorescence staining for CCSP (purple) and proSP-C (green) of an epithelial structure derived from differentiating ES cells underlined by lung derived mesenchymal cells (red – TdTomato), suggesting that adult lung mesenchyme can direct differentiation of ES cells into lung epithelium. Blue signal represents DAPI counterstain. (A) and (B) 400x magnification and (C) 200x magnification.

APPENDIX A

A.1 CELL ISOLATION PROCEDURE

Materials:

- Dissection instruments
- Dissection board
- Canula: 20GA 1.16IN (BD)
- 2 X 1ml seringe
- 1X 10ml seringe
- 4-0 silk
- Anesthetic
- Ice bucket
- 50ml conical tubes
- 1XPBS (perfusion)
- 1XPBS 0.2mM EGTA (Lavage)
- Ham's F12
- 0.2um Syringe filter (Nalgene)
- 70um Nylon Cell Strainer (BD Falcon)
- HBSS
- HBSS+ (HBSS, 10mMHEPES pH 7, 2%FBS)
- FBS
- DNase I
- Elastase (4U/ml in Ham's F12) – Worthington
- Pen/Strep

- 2l beaker
- 2l saline at 37C
- 1.5ml tube floater
- Razor blades
- Petri dishes
- 100 ul 2 N HCl
- 100 ul 2 N NaOH

Mice:

1. anesthetize mouse
2. pin mouse using 5-point method
3. spray fur with 70% EtOH
4. open abdominal cavity
5. exsanguinate
6. nick diaphragm to deflate lungs
7. cut diaphragm along the bottom of the rib cage
8. open thoracic cavity on left side
9. cut under left clavicle to reveal trachea
10. mop up blood around trachea with gauze
11. cannulate trachea just below the larynx
12. tie in cannula with 4-0 silk
13. attach air-filled 1 ml syringe to cannula
14. nick the right atrium
15. perfuse with 10 ml 1X PBS
    a. left hand:
        i. forceps
        ii. grab heart along junction between ventricles
        iii. do not pull as this will occlude the pulmonary artery
    b. right hand:
        i. 26g needle attached to 10 ml syringe filled with 1X PBS

ii. Puncture right ventricle. Right ventricle wall is very thin.
iii. You should feel a “pop” if you are in the right spot
iv. You should be able to see the tip of the needle through the heart tissue
v. Inject 10 ml PBS into ventricle
vi. If all is well the lung will become white immediately
vii. If the perfusion is going poorly try:
    1. Make sure the right atrium is cut and dark red blood is coming out.
    2. repositioning the needle (the ventricle is a rather small target and seems to collapse under these conditions).
    3. inflate the lungs with air via the tracheal cannula
    4. perfuse more slowly
    5. perfuse with another 10 ml PBS

16. Lavage the lung with 4-1 ml 1XPBS/0.2 mM EGTA
    a. Attach a 1 ml syringe filled with PBS/EGTA to the tracheal cannula
    b. Instill PBS slowly over 5 seconds
    c. Withdraw PBS over 5 seconds
    d. Repeat 3 times
17. Collect tissue
    a. remove heart lung block with cannula attached
    b. make sure the cannula is numbered
    c. immerse tissue in ice cold PBS in a 50 ml conical test tube
    d. store on ice

Cell isolation procedure:

18. Elastase solution:
    a. 3mls/animal (1X1 ml instillation and 4X0.5mls instillation) make about 10% extra
    b. Ham’s F12 at 37C
    c. Figure out stock concentration of Elastase (U/ml)

d. Add the necessary volume of enzyme to get to 4U/ml
e. Bring the pH of the solution up using NaOH to 8.5 or 9 or until the solution starts clearing up. Make sure you don't go over 10, because that might denature the enzyme. Once the solution is clear, add the necessary amount of HCl to bring the pH back down to 7.4. Filter through the 0.2um syringe filter.

19. Pour saline into 2L beaker
20. place float into beaker
21. attach tissue to float by passing cannula flange through hole in float
22. fill 1 ml syringe with 4 u/ml elastase
23. instill 1 ml elastase into each lung
24. incubate 5 minutes
25. repeat 4 times with 0.5mls elastase
26. remove digested tissue from float by pulling through hole
27. place each lung in a separate bacterial grade Petri plate
28. cut off lung tissue and place in a pile on a dry section of the Petri plate
29. discard heart, thymus, and trachea in red bag
30. drain/aspirate residual liquid (get tissue as try as possible)
31. collect tissue in the "corner" of the plate
32. mince tissue with scissors until about 2 mm^2
33. mince tissue with razor blade
34. add 5 ml DNAse I to tissue
35. incubate 5-10 minutes at 37°C in the incubator
36. add 10mls cold HBSS and triturate tissue by pipetting up and down
37. transfer to cell strainer positioned in a 50 ml conical test tube
38. rinse plate and tissue in strainer with 2X10 ml HBSS
39. underlay cell suspension with 5ml FBS
40. centrifuge 500g, 8 min, 4°C
    a. use the break to clean the hood
41. pour off supernatant
42. disperse cells by "racking"

43. resuspend cells in 1 ml RBC lysis buffer
44. incubate 1.5 minutes
    b. time this with a watch
    c. **a longer incubation will result in epithelial cell lysis**
45. add 10 ml HBSS+ to cells
46. centrifuge 700g, 8 min, 4°C
47. aspirate supernatant
48. disperse cells by "racking"
49. resuspend cells in 1ml cold HBSS+
50. count in trypan blue. I usually use a 1:10 dilution in HBSS+, 10ul cells and 10ul Trypan blue. Count 5 squares, average and multiply by 20X10*4.
51. Use for further applications.
52. Expected yield: average 6X10*6 cells, or between 4X10*6 and 13X10*6 cells.

A.2 CELLS SURFACE STAINING FOR FLOW CYTOMETRY

Materials:

- cells, HBSS+(HBSS 10mM HEPES 2%FBS), Antibodies, viability dye (7AAD or PI)

Method:

1. Resuspend cells at 10*6 cells in 100ul of HBSS+
2. Add the desired amount of antibody
3. Incubate on ice in the dark for 30 min
4. Add 1ml of HBSS+

5. Spin down 500g for 7min
6. Remove supernatant by inverting the tube and placing it upside down on a piece of paper towel so that most of the supernatant is absorbed
7. Resuspend in 300ul HBSS+
8. Add viability dye. I use 7AAD, 2ul per 100ul HBSS+
9. Read tubes.

Notes:

Blocking: I usually do not use Fc Block. Most of the cells that have Fc receptors are in the CD45 CD31 positive fraction and I exclude those from the analysis anyway. I tried with or without block and I did not see much of a difference. I block when I do intracellular staining with unconjugated antibodies.

Isotype controls: I usually do them the first time I use a new antibody, and if they look clean, I do not use them again. They do not bring any information about the non-specific binding of the antibody used, they only tell us about the non-specific fraction of that particular Ig fraction of the serum.

Always stain 10*6 cells in 100ul HBSS+. Scale up or down if needed (for sorts for example, where I usually stain about 10X10*6 cells).

Always titrate antibodies. Pick the concentration that gives the best signal to noise ratio. Ideally, every time you change the LotNo of the antibody, even if it's an antibody you've used before, you should do a titer run.

For intracellular staining see protocol in Current protocols in immunology. It works well.

For Biotinylated antibodies, after the first incubation with the primary antibody, wash and incubate for 15- 30 min with SA. Remember to titrate SA and include a SA only control. Lung has a lot of endogenous biotin, thus keep the SA concentration to a minimum.

Controls:

1. Compensation controls: single color tubes. Be aware of the high autofluorescence of the airway epithelium. Make sure you compensate on populations of equal autofluorescence and adjust compensation values before analysis. For sorting experiments ALWAYS compensate manually. Always use biexponential display of the data to see events under the axis.
2. FMO's: fluorescence minus one controls. Have samples that have all but one of the antibodies added (take out one antibody at a time). These controls allow the proper discrimination between the positive and negative populations.
3. BrdU: always include cells isolated from a mouse that did not receive BrdU as control. It is the most valid control, much better than the Isotype and no primary antibody controls.
4. Streptavidin only controls and No primary controls. When I use Zenon kits, I include Zenon complexes alone, without the primary antibody. In my experience, the kit is not cleaner than regular primary/secondary staining.

A.3 NAPHTHALENE TREATMENT PROTOCOL

Reagents

Naphthalene: Fisher Scientific N134-500; store at room temperature; use gloves and work in chemical fume hood when working with naphthalene

Corn oil: Just buy Mazola corn oil. Aliquot @ 25 mL in 50 mL conical tubes and store at -20 C (thaw on day of use)

Naphthalene solution

1. Estimate the overall volume that you need to deliver. This is based on mouse mass. Assume about 35 grams for the average mouse (change if need for different mouse lines).

A) 35 grams/mouse X # of mice in study = X grams of "mouse mass"

B) Assume that you will deliver 10 µL of NA solution per gram of mouse mass.

µL of solution needed =

(g of mouse mass from 1A) (10 µL of NA solution / g mouse mass)

Then, it's actually best to add volume; say that you needed 4.5 mL; you should plan to make 5 or 6 mL, to allow for extra and loss during transfers.

2. Estimating Naphthalene (solute) mass needed

Notes on dose are elsewhere; say you are planning on 250 mg NA/kg of mouse mass. This means that you need to prepare a working solution that is 25 mg NA/mL. This results from our assumed volume of delivery:

10 µL 10,000 µL 10 mL

---------- = ---------- = ----------

1 gram mouse mass 1 Kg mouse mass 1 Kg mouse mass

250 mg NA 1 Kg mouse mass 25 mg mouse mass

So: ---------- X ---------- = ----------

1 Kg mouse mass 10 mL mL

So, (25 mg/mL) (Volume from 1B) = mass of NA needed

3. USING GLOVES, weigh out naphthalene. The best procedure here is to work with Naphthalene in a chemical fume hood. However, most people do not have their analytical balance in their chemical fume hood. The easiest way around this is to: A) Place a small beaker on the balance; place an empty 50 ml conical tube in the beaker; tare the balance B) take the tube to the hood and put in your best estimate of the amount of naphthalene needed; recap the tube C) bring the CLOSED tube back to the balance, place in the beaker, and weigh it. Repeat until you have exactly enough naphthalene (which rarely happens) or you have more than enough. You can easily compensate for having more than enough in the next step.

4. A) Calculate amount of Mazola corn oil solvent needed. Just set up a proportion to correct for the excess NA you probably have from step 3.

1 mL of solution X mL

---------- = ----------

25 mg NA mass actually weighed

Solve for X.

B) You would think you would now just add the volume, X, to the tube with the naphthalene in it. Unfortunately, corn oil is difficult to pipet in accurate volumes due to viscosity, and the fact that it sticks to the sides of the pipets, leaving a residue that would create large volumetric errors. Instead, it is easier to add the necessary mass of corn oil. Place the conical with the naphthalene on the balance, zero it, and pipet corn oil until the correct final mass is reached. To calculate the mass needed, you need to know the approximate density of Mazola corn oil, which is 0.9185 g/mL.

Calculate:

(X from step 3) (0.9185 g/mL) = mass of corn oil needed.

5. Cap tube, use tape or strong rubber bands to attach to vortexer, vortex on high for 20 minutes or until NA is reasonable well dissolved, or at least a well-dispersed slurry.

Preparation of syringes

1. Obtain 1 mL syringes ("tuberculin" syringes). Remove the normal 26 gauge needle; replace with 18G needle.
2. Load working NA solution (a full 1 mL per syringe). Carefully remove needle, and rigorously clean the end of the syringe; clean it until it squeaks, leaving no slippery residue!

3. Only then should the original 26G needle be replaced. If there is a residue, when you are trying to inject, the needle will very likely just pop off, leaving a mess, and leaving you unsure how much NA was actually delivered to the animal; the animal would have to be removed from the study. Cap needles; take to mouse colony.

Injection

1. Always inject before 10:00 am to take advantage of the daily minimum in mouse glutathione levels.
2. Weigh animals to the nearest 0.1 gram. A small, light plastic container on a portable top-loading balance works best. Bouncy mice are hard to weigh; some people use light anesthesia with halothane to get accurate weights. RECORD animal's weight. Weight loss data is an invaluable method to make preliminary assessments of injury.
3. Inject working NA solution at 10 μL/g of mouse body weight.
4. Make sure that the injection is intraperitoneal and not subcutaneous. If a bubble raises in the skin, it's sc. Do not nick the viscera, etc. If you inject the bladder, the mouse will die almost instantly!

Dose

1. We have not done a formal study of all strains, but some information is available from GW Lawson et al., AJ Path 160(1):315-27, Jan 2002.
2. Females are more sensitive than males.

3. For FVB/n: 275-300mg/kg results in extensive injury from the bronchi through the terminal bronchioles. Some lethality is observed at 300 mg/kg. At all doses the animals will exhibit ruffled fur at about 36 hours and will have reddened eyes at 48 hours.
4. Large animals will require a larger dose to achieve the same level of injury due to partitioning of the naphthalene to the fat stores.

BIBLIOGRAPHY

1. Evans, M.J., Cabral-Anderson, L.J. & Freeman, G. Role of the Clara cell in renewal of the bronchiolar epithelium. *Lab Invest* **38**, 648-653 (1978).
2. Evans, M.J., Johnson, L.V., Stephens, R.J. & Freeman, G. Renewal of the terminal bronchiolar epithelium in the rat following exposure to NO2 or O3. *Lab Invest* **35**, 246-257 (1976).
3. Evans, M.J., Cabral, L.J., Stephens, R.J. & Freeman, G. Transformation of alveolar type 2 cells to type 1 cells following exposure to NO2. *Exp Mol Pathol* **22**, 142-150 (1975).
4. Lourenco, R.V., Klimek, M.F. & Borowski, C.J. Deposition and clearance of 2 micron particles in the tracheobronchial tree of normal subjects--smokers and nonsmokers. *J Clin Invest* **50**, 1411-1420 (1971).
5. Massaro, D. & Massaro, G.D. Biochemical and anatomical adaptation of the lung to oxygen-induced injury. *Fed Proc* **37**, 2485-2488 (1978).
6. Massaro, G.D., Amado, C., Clerch, L. & Massaro, D. Studies on the regulation of secretion in Clara cells with evidence for chemical nonautonomic mediation of the secretory response to increased ventilation in rat lungs. *J Clin Invest* **70**, 608-613 (1982).
7. Buonarati, M., Morin, D., Plopper, C. & Buckpitt, A. Glutathione depletion and cytotoxicity by naphthalene 1,2-oxide in isolated hepatocytes. *Chem Biol Interact* **71**, 147-165 (1989).
8. Chichester, C.H., Philpot, R.M., Weir, A.J., Buckpitt, A.R. & Plopper, C.G. Characterization of the cytochrome P-450 monooxygenase system in nonciliated bronchiolar epithelial (Clara) cells isolated from mouse lung. *Am J Respir Cell Mol Biol* **4**, 179-186 (1991).
9. Devereux, T.R. Alveolar type II and Clara cells: isolation and xenobiotic metabolism. *Environ Health Perspect* **56**, 95-101 (1984).
10. Reid, L.M. & Jones, R. Mucous membrane of respiratory epithelium. *Environ Health Perspect* **35**, 113-120 (1980).
11. Pack, R.J., Al-Ugaily, L.H. & Morris, G. The cells of the tracheobronchial epithelium of the mouse: a quantitative light and electron microscope study. *J Anat* **132**, 71-84 (1981).
12. Boers, J.E., Ambergen, A.W. & Thunnissen, F.B. Number and proliferation of basal and parabasal cells in normal human airway epithelium. *Am J Respir Crit Care Med* **157**, 2000-2006 (1998).
13. Boers, J.E., Ambergen, A.W. & Thunnissen, F.B. Number and proliferation of clara cells in normal human airway epithelium. *Am J Respir Crit Care Med* **159**, 1585-1591 (1999).
14. Boers, J.E., den Brok, J.L., Koudstaal, J., Arends, J.W. & Thunnissen, F.B. Number and proliferation of neuroendocrine cells in normal human airway epithelium. *Am J Respir Crit Care Med* **154**, 758-763 (1996).

15. Herzog, E.L., Brody, A.R., Colby, T.V., Mason, R. & Williams, M.C. Knowns and unknowns of the alveolus. *Proc Am Thorac Soc* **5**, 778-782 (2008).
16. Borthwick, D.W., Shahbazian, M., Krantz, Q.T., Dorin, J.R. & Randell, S.H. Evidence for stem-cell niches in the tracheal epithelium. *Am J Respir Cell Mol Biol* **24**, 662-670 (2001).
17. Reynolds, S.D., Giangreco, A., Power, J.H. & Stripp, B.R. Neuroepithelial bodies of pulmonary airways serve as a reservoir of progenitor cells capable of epithelial regeneration. *Am J Pathol* **156**, 269-278 (2000).
18. Hong, K.U., Reynolds, S.D., Giangreco, A., Hurley, C.M. & Stripp, B.R. Clara cell secretory protein-expressing cells of the airway neuroepithelial body microenvironment include a label-retaining subset and are critical for epithelial renewal after progenitor cell depletion. *Am J Respir Cell Mol Biol* **24**, 671-681 (2001).
19. Rawlins, E.L. & Hogan, B.L. Ciliated epithelial cell lifespan in the mouse trachea and lung. *Am J Physiol Lung Cell Mol Physiol* **295**, L231-234 (2008).
20. Knowles, M.R. & Boucher, R.C. Mucus clearance as a primary innate defense mechanism for mammalian airways. *J Clin Invest* **109**, 571-577 (2002).
21. Cheng, D.S., *et al.* Airway Epithelium Controls Lung Inflammation and Injury through the NF-{kappa}B Pathway. *J Immunol* **178**, 6504-6513 (2007).
22. Sadikot, R.T., *et al.* Targeted immunomodulation of the NF-kappaB pathway in airway epithelium impacts host defense against Pseudomonas aeruginosa. *J Immunol* **176**, 4923-4930 (2006).
23. Elizur, A., *et al.* Clara cells impact the pulmonary innate immune response to LPS. *Am J Physiol Lung Cell Mol Physiol* **293**, L383-392 (2007).
24. Elizur, A., *et al.* Tumor necrosis factor-alpha from macrophages enhances LPS-induced clara cell expression of keratinocyte-derived chemokine. *Am J Respir Cell Mol Biol* **38**, 8-15 (2008).
25. Reynolds, S.D., *et al.* CCSP regulates cross talk between secretory cells and both ciliated cells and macrophages of the conducting airway. *Am J Physiol Lung Cell Mol Physiol* **293**, L114-123 (2007).
26. Holgate, S.T., *et al.* Epithelial-mesenchymal communication in the pathogenesis of chronic asthma. *Proc Am Thorac Soc* **1**, 93-98 (2004).
27. Reynolds, S.D., *et al.* Airway injury in lung disease pathophysiology: selective depletion of airway stem and progenitor cell pools potentiates lung inflammation and alveolar dysfunction. *Am J Physiol Lung Cell Mol Physiol* **287**, L1256-1265 (2004).
28. Snyder, J.C., Zemke, A.C. & Stripp, B.R. Reparative Capacity of Airway Epithelium Impacts Deposition and Remodeling of Extracellular Matrix. *Am J Respir Cell Mol Biol* (2008).
29. Zhu, L., *et al.* Prominin 1 marks intestinal stem cells that are susceptible to neoplastic transformation. *Nature* (2008).
30. Dick, J.E. Stem cell concepts renew cancer research. *Blood* **112**, 4793-4807 (2008).
31. Bagby, G.C., Lipton, J.M., Sloand, E.M. & Schiffer, C.A. Marrow failure. *Hematology Am Soc Hematol Educ Program*, 318-336 (2004).
32. Cardoso, W.V. & Lu, J. Regulation of early lung morphogenesis: questions, facts and controversies. *Development* **133**, 1611-1624 (2006).
33. Sekine, K., *et al.* Fgf10 is essential for limb and lung formation. *Nat Genet* **21**, 138-141 (1999).

34. Bellusci, S., Grindley, J., Emoto, H., Itoh, N. & Hogan, B.L. Fibroblast growth factor 10 (FGF10) and branching morphogenesis in the embryonic mouse lung. *Development* **124**, 4867-4878 (1997).
35. Weaver, M., Dunn, N.R. & Hogan, B.L. Bmp4 and Fgf10 play opposing roles during lung bud morphogenesis. *Development* **127**, 2695-2704 (2000).
36. Loscertales, M., Mikels, A.J., Hu, J.K., Donahoe, P.K. & Roberts, D.J. Chick pulmonary Wnt5a directs airway and vascular tubulogenesis. *Development* **135**, 1365-1376 (2008).
37. Yin, Y., *et al.* An FGF-WNT gene regulatory network controls lung mesenchyme development. *Dev Biol* **319**, 426-436 (2008).
38. Shannon, J.M. Induction of alveolar type II cell differentiation in fetal tracheal epithelium by grafted distal lung mesenchyme. *Dev Biol* **166**, 600-614 (1994).
39. Shannon, J.M., Nielsen, L.D., Gebb, S.A. & Randell, S.H. Mesenchyme specifies epithelial differentiation in reciprocal recombinants of embryonic lung and trachea. *Dev Dyn* **212**, 482-494 (1998).
40. Donovan, P.J. & Gearhart, J. The end of the beginning for pluripotent stem cells. *Nature* **414**, 92-97 (2001).
41. Slack, J.M. Origin of stem cells in organogenesis. *Science* **322**, 1498-1501 (2008).
42. McCulloch, E.A. & Till, J.E. The radiation sensitivity of normal mouse bone marrow cells, determined by quantitative marrow transplantation into irradiated mice. *Radiat Res* **13**, 115-125 (1960).
43. Becker, A.J., Mc, C.E. & Till, J.E. Cytological demonstration of the clonal nature of spleen colonies derived from transplanted mouse marrow cells. *Nature* **197**, 452-454 (1963).
44. Barker, N., van de Wetering, M. & Clevers, H. The intestinal stem cell. *Genes Dev* **22**, 1856-1864 (2008).
45. Barker, N., *et al.* Identification of stem cells in small intestine and colon by marker gene Lgr5. *Nature* **449**, 1003-1007 (2007).
46. Potten, C.S., *et al.* Identification of a putative intestinal stem cell and early lineage marker; musashi-1. *Differentiation* **71**, 28-41 (2003).
47. Clarke, D.L., *et al.* Generalized potential of adult neural stem cells. *Science* **288**, 1660-1663 (2000).
48. Tumbar, T., *et al.* Defining the epithelial stem cell niche in skin. *Science* **303**, 359-363 (2004).
49. Fuchs, E. & Horsley, V. More than one way to skin. *Genes Dev* **22**, 976-985 (2008).
50. Majo, F., Rochat, A., Nicolas, M., Jaoude, G.A. & Barrandon, Y. Oligopotent stem cells are distributed throughout the mammalian ocular surface. *Nature* **456**, 250-254 (2008).
51. Shackleton, M., *et al.* Generation of a functional mammary gland from a single stem cell. *Nature* **439**, 84-88 (2006).
52. Stingl, J., *et al.* Purification and unique properties of mammary epithelial stem cells. *Nature* **439**, 993-997 (2006).
53. Eirew, P., *et al.* A method for quantifying normal human mammary epithelial stem cells with in vivo regenerative ability. *Nat Med* **14**, 1384-1389 (2008).
54. Giangreco, A., Groot, K.R. & Janes, S.M. Lung cancer and lung stem cells: strange bedfellows? *Am J Respir Crit Care Med* **175**, 547-553 (2007).

55. Giangreco, A., Reynolds, S.D. & Stripp, B.R. Terminal bronchioles harbor a unique airway stem cell population that localizes to the bronchoalveolar duct junction. *Am J Pathol* **161**, 173-182 (2002).
56. Jakubowski, A., *et al.* TWEAK induces liver progenitor cell proliferation. *J Clin Invest* **115**, 2330-2340 (2005).
57. Petkov, P.M., Kim, K., Sandhu, J., Shafritz, D.A. & Dabeva, M.D. Identification of differentially expressed genes in epithelial stem/progenitor cells of fetal rat liver. *Genomics* **68**, 197-209 (2000).
58. Xu, X., *et al.* Beta cells can be generated from endogenous progenitors in injured adult mouse pancreas. *Cell* **132**, 197-207 (2008).
59. Leong, K.G., Wang, B.E., Johnson, L. & Gao, W.Q. Generation of a prostate from a single adult stem cell. *Nature* **456**, 804-808 (2008).
60. Lajtha, L.G. Stem cell concepts. *Differentiation* **14**, 23-34 (1979).
61. Potten, C.S. & Loeffler, M. Stem cells: attributes, cycles, spirals, pitfalls and uncertainties. Lessons for and from the crypt. *Development* **110**, 1001-1020 (1990).
62. Lechler, T. & Fuchs, E. Asymmetric cell divisions promote stratification and differentiation of mammalian skin. *Nature* **437**, 275-280 (2005).
63. Wu, M., *et al.* Imaging hematopoietic precursor division in real time. *Cell Stem Cell* **1**, 541-554 (2007).
64. Song, X., Zhu, C.H., Doan, C. & Xie, T. Germline stem cells anchored by adherens junctions in the Drosophila ovary niches. *Science* **296**, 1855-1857 (2002).
65. Clayton, E., *et al.* A single type of progenitor cell maintains normal epidermis. *Nature* **446**, 185-189 (2007).
66. Jones, P. & Simons, B.D. Epidermal homeostasis: do committed progenitors work while stem cells sleep? *Nat Rev Mol Cell Biol* **9**, 82-88 (2008).
67. Evans, M.J., Cabral-Anderson, L.J. & Freeman, G. Effects of NO2 on the lungs of aging rats. II. Cell proliferation. *Exp Mol Pathol* **27**, 366-376 (1977).
68. Evans, M.J. & Hackney, J.D. Cell proliferation in lungs of mice exposed to elevated concentrations of oxygen. *Aerosp Med* **43**, 620-622 (1972).
69. Teta, M., Rankin, M.M., Long, S.Y., Stein, G.M. & Kushner, J.A. Growth and regeneration of adult beta cells does not involve specialized progenitors. *Dev Cell* **12**, 817-826 (2007).
70. Cepko, C., Ryder, E.F., Austin, C.P., Walsh, C. & Fekete, D.M. Lineage analysis using retrovirus vectors. *Methods Enzymol* **254**, 387-419 (1995).
71. Rompani, S.B. & Cepko, C.L. Retinal progenitor cells can produce restricted subsets of horizontal cells. *Proc Natl Acad Sci U S A* **105**, 192-197 (2008).
72. Joyner, A.L. & Zervas, M. Genetic inducible fate mapping in mouse: establishing genetic lineages and defining genetic neuroanatomy in the nervous system. *Dev Dyn* **235**, 2376-2385 (2006).
73. Rawlins, E.L., Ostrowski, L.E., Randell, S.H. & Hogan, B.L. Lung development and repair: contribution of the ciliated lineage. *Proc Natl Acad Sci U S A* **104**, 410-417 (2007).
74. Cotsarelis, G., Sun, T.T. & Lavker, R.M. Label-retaining cells reside in the bulge area of pilosebaceous unit: implications for follicular stem cells, hair cycle, and skin carcinogenesis. *Cell* **61**, 1329-1337 (1990).

75. Marshman, E., Booth, C. & Potten, C.S. The intestinal epithelial stem cell. *Bioessays* **24**, 91-98 (2002).
76. Alison, M.R., Islam, S. & Lim, S. Stem cells in liver regeneration, fibrosis and cancer: the good, the bad and the ugly. *J Pathol* **217**, 282-298 (2009).
77. Zaret, K.S. & Grompe, M. Generation and regeneration of cells of the liver and pancreas. *Science* **322**, 1490-1494 (2008).
78. Bonnet, D. & Dick, J.E. Human acute myeloid leukemia is organized as a hierarchy that originates from a primitive hematopoietic cell. *Nat Med* **3**, 730-737 (1997).
79. Sieburg, H.B., Cho, R.H. & Muller-Sieburg, C.E. Limiting dilution analysis for estimating the frequency of hematopoietic stem cells: uncertainty and significance. *Exp Hematol* **30**, 1436-1443 (2002).
80. You, Y., Richer, E.J., Huang, T. & Brody, S.L. Growth and differentiation of mouse tracheal epithelial cells: selection of a proliferative population. *Am J Physiol Lung Cell Mol Physiol* **283**, L1315-1321 (2002).
81. Liu, J.Y., Nettesheim, P. & Randell, S.H. Growth and differentiation of tracheal epithelial progenitor cells. *Am J Physiol* **266**, L296-307 (1994).
82. Evans, M.J., Shami, S.G., Cabral-Anderson, L.J. & Dekker, N.P. Role of nonciliated cells in renewal of the bronchial epithelium of rats exposed to NO2. *Am J Pathol* **123**, 126-133 (1986).
83. Randell, S.H., Comment, C.E., Ramaekers, F.C. & Nettesheim, P. Properties of rat tracheal epithelial cells separated based on expression of cell surface alpha-galactosyl end groups. *Am J Respir Cell Mol Biol* **4**, 544-554 (1991).
84. Engelhardt, J.F., Schlossberg, H., Yankaskas, J.R. & Dudus, L. Progenitor cells of the adult human airway involved in submucosal gland development. *Development* **121**, 2031-2046 (1995).
85. Schoch, K.G., *et al.* A subset of mouse tracheal epithelial basal cells generates large colonies in vitro. *Am J Physiol Lung Cell Mol Physiol* **286**, L631-642 (2004).
86. Hong, K.U., Reynolds, S.D., Watkins, S., Fuchs, E. & Stripp, B.R. Basal cells are a multipotent progenitor capable of renewing the bronchial epithelium. *Am J Pathol* **164**, 577-588 (2004).
87. Hong, K.U., Reynolds, S.D., Watkins, S., Fuchs, E. & Stripp, B.R. In vivo differentiation potential of tracheal basal cells: evidence for multipotent and unipotent subpopulations. *Am J Physiol Lung Cell Mol Physiol* **286**, L643-649 (2004).
88. Goodell, M.A., Brose, K., Paradis, G., Conner, A.S. & Mulligan, R.C. Isolation and functional properties of murine hematopoietic stem cells that are replicating in vivo. *J Exp Med* **183**, 1797-1806 (1996).
89. Giangreco, A., Shen, H., Reynolds, S.D. & Stripp, B.R. Molecular phenotype of airway side population cells. *Am J Physiol Lung Cell Mol Physiol* **286**, L624-630 (2004).
90. Reynolds, S.D., *et al.* Molecular and functional properties of lung SP cells. *Am J Physiol Lung Cell Mol Physiol* **292**, L972-983 (2007).
91. Hackett, T.L., *et al.* Characterization of side population cells from human airway epithelium. *Stem Cells* **26**, 2576-2585 (2008).
92. Castillon, N., *et al.* Regeneration of a well-differentiated human airway surface epithelium by spheroid and lentivirus vector-transduced airway cells. *J Gene Med* **6**, 846-856 (2004).

93. Avril-Delplanque, A., *et al.* Aquaporin-3 expression in human fetal airway epithelial progenitor cells. *Stem Cells* **23**, 992-1001 (2005).
94. Macchiarini, P., *et al.* Clinical transplantation of a tissue-engineered airway. *Lancet* **372**, 2023-2030 (2008).
95. O'Brien, K.A., Suverkropp, C., Kanekal, S., Plopper, C.G. & Buckpitt, A.R. Tolerance to multiple doses of the pulmonary toxicant, naphthalene. *Toxicol Appl Pharmacol* **99**, 487-500 (1989).
96. Reynolds, S.D., *et al.* Conditional clara cell ablation reveals a self-renewing progenitor function of pulmonary neuroendocrine cells. *Am J Physiol Lung Cell Mol Physiol* **278**, L1256-1263 (2000).
97. Stripp, B.R., Maxson, K., Mera, R. & Singh, G. Plasticity of airway cell proliferation and gene expression after acute naphthalene injury. *Am J Physiol* **269**, L791-799 (1995).
98. Stevens, T.P., McBride, J.T., Peake, J.L., Pinkerton, K.E. & Stripp, B.R. Cell proliferation contributes to PNEC hyperplasia after acute airway injury. *Am J Physiol* **272**, L486-493 (1997).
99. Kim, C.F., *et al.* Identification of bronchioalveolar stem cells in normal lung and lung cancer. *Cell* **121**, 823-835 (2005).
100. Van Winkle, L.S., Buckpitt, A.R., Nishio, S.J., Isaac, J.M. & Plopper, C.G. Cellular response in naphthalene-induced Clara cell injury and bronchiolar epithelial repair in mice. *Am J Physiol* **269**, L800-818 (1995).
101. Fuchs, E., Tumbar, T. & Guasch, G. Socializing with the neighbors: stem cells and their niche. *Cell* **116**, 769-778 (2004).
102. De Proost, I., *et al.* Functional live cell imaging of the pulmonary neuroepithelial body microenvironment. *Am J Respir Cell Mol Biol* **39**, 180-189 (2008).
103. Jackson, E.L., *et al.* Analysis of lung tumor initiation and progression using conditional expression of oncogenic K-ras. *Genes Dev* **15**, 3243-3248 (2001).
104. Reynolds, S.D., *et al.* Conditional stabilization of beta-catenin expands the pool of lung stem cells. *Stem Cells* **26**, 1337-1346 (2008).
105. Mucenski, M.L., *et al.* Beta-catenin regulates differentiation of respiratory epithelial cells in vivo. *Am J Physiol Lung Cell Mol Physiol* **289**, L971-979 (2005).
106. Zemke, A.C., *et al.* {beta}-Catenin is not Necessary for Maintenance or Repair of the Bronchiolar Epithelium. *Am J Respir Cell Mol Biol* (2009).
107. Zhang, Y., *et al.* A Gata6-Wnt pathway required for epithelial stem cell development and airway regeneration. *Nat Genet* **40**, 862-870 (2008).
108. Yang, Y., *et al.* Phosphatidylinositol 3-kinase mediates bronchioalveolar stem cell expansion in mouse models of oncogenic K-ras-induced lung cancer. *PLoS ONE* **3**, e2220 (2008).
109. Ventura, J.J., *et al.* p38alpha MAP kinase is essential in lung stem and progenitor cell proliferation and differentiation. *Nat Genet* **39**, 750-758 (2007).
110. Dovey, J.S., Zacharek, S.J., Kim, C.F. & Lees, J.A. Bmi1 is critical for lung tumorigenesis and bronchioalveolar stem cell expansion. *Proc Natl Acad Sci U S A* **105**, 11857-11862 (2008).
111. Yanagi, S., *et al.* Pten controls lung morphogenesis, bronchioalveolar stem cells, and onset of lung adenocarcinomas in mice. *J Clin Invest* **117**, 2929-2940 (2007).
112. Corti, M., Brody, A.R. & Harrison, J.H. Isolation and primary culture of murine alveolar type II cells. *Am J Respir Cell Mol Biol* **14**, 309-315 (1996).

113. McQualter, J.L., *et al.* Endogenous fibroblastic progenitor cells in the adult mouse lung are highly enriched in the Sca-1 positive cell fraction. *Stem Cells* (2008).
114. Summer, R., *et al.* SP (Side Population) Cells and Bcrp1 Expression in Lung. *Am J Physiol Lung Cell Mol Physiol* (2003).
115. Teisanu, R.M., Lagasse, E., Whitesides, J.F. & Stripp, B.R. Prospective isolation of bronchiolar stem cells based upon immunophenotypic and autofluorescence characteristics. *Stem Cells* (2008).
116. Zemke, A.C., *et al.* Molecular Staging of Epithlieial Maturation Using Secretory Cell-Specific Genes as Markers. *Am J Respir Cell Mol Biol* (2008).
117. Hatasa, K. & Nakamura, T. Electron microscopic observations of lung alveolar epithelial cells of normal young mice, with special reference to formation and secretion of osmiophilic lamellar bodies. *Z Zellforsch Mikrosk Anat* **68**, 266-277 (1965).
118. Shannon, J.M., Jennings, S.D. & Nielsen, L.D. Modulation of alveolar type II cell differentiated function in vitro. *Am J Physiol* **262**, L427-436 (1992).
119. Fehrenbach, H., *et al.* Keratinocyte growth factor-induced hyperplasia of rat alveolar type II cells in vivo is resolved by differentiation into type I cells and by apoptosis. *Eur Respir J* **14**, 534-544 (1999).
120. Evans, M.J., Stephens, R.J., Cabral, L.J. & Freeman, G. Cell renewal in the lungs of rats exposed to low levels of NO2. *Arch Environ Health* **24**, 180-188 (1972).
121. Yee, M., *et al.* Type II epithelial cells are critical target for hyperoxia-mediated impairment of postnatal lung development. *Am J Physiol Lung Cell Mol Physiol* **291**, L1101-1111 (2006).
122. Dobbs, L.G., Pian, M.S., Maglio, M., Dumars, S. & Allen, L. Maintenance of the differentiated type II cell phenotype by culture with an apical air surface. *Am J Physiol* **273**, L347-354 (1997).
123. Danto, S.I., Shannon, J.M., Borok, Z., Zabski, S.M. & Crandall, E.D. Reversible transdifferentiation of alveolar epithelial cells. *Am J Respir Cell Mol Biol* **12**, 497-502 (1995).
124. Roper, J.M., *et al.* In vivo exposure to hyperoxia induces DNA damage in a population of alveolar type II epithelial cells. *Am J Physiol Lung Cell Mol Physiol* **286**, L1045-1054 (2004).
125. Roper, J.M., Staversky, R.J., Finkelstein, J.N., Keng, P.C. & O'Reilly, M.A. Identification and isolation of mouse type II cells on the basis of intrinsic expression of enhanced green fluorescent protein. *Am J Physiol Lung Cell Mol Physiol* **285**, L691-700 (2003).
126. Randell, S.H. Airway epithelial stem cells and the pathophysiology of chronic obstructive pulmonary disease. *Proc Am Thorac Soc* **3**, 718-725 (2006).
127. Muzumdar, M.D., Tasic, B., Miyamichi, K., Li, L. & Luo, L. A global double-fluorescent Cre reporter mouse. *Genesis* **45**, 593-605 (2007).
128. Soriano, P. Generalized lacZ expression with the ROSA26 Cre reporter strain. *Nat Genet* **21**, 70-71 (1999).
129. Savov, J.D., *et al.* Ozone-induced acute pulmonary injury in inbred mouse strains. *Am J Respir Cell Mol Biol* **31**, 69-77 (2004).
130. Hollingsworth, J.W., 2nd, *et al.* The role of Toll-like receptor 4 in environmental airway injury in mice. *Am J Respir Crit Care Med* **170**, 126-132 (2004).

131. Hollingsworth, J.W., *et al.* Ambient ozone primes pulmonary innate immunity in mice. *J Immunol* **179**, 4367-4375 (2007).
132. Srinivas, S., *et al.* Cre reporter strains produced by targeted insertion of EYFP and ECFP into the ROSA26 locus. *BMC Dev Biol* **1**, 4 (2001).
133. Kotton, D.N., Summer, R.S., Sun, X., Ma, B.Y. & Fine, A. Stem cell antigen-1 expression in the pulmonary vascular endothelium. *Am J Physiol Lung Cell Mol Physiol* **284**, L990-996 (2003).
134. Ikeda, N., *et al.* Comprehensive diagnostic bronchoscopy of central type early stage lung cancer. *Lung Cancer* **56**, 295-302 (2007).
135. Leonhard, M. New incoherent autofluorescence/fluorescence system for early detection of lung cancer. *Diagn Ther Endosc* **5**, 71-75 (1999).
136. Lam, B., *et al.* The clinical value of autofluorescence bronchoscopy for the diagnosis of lung cancer. *Eur Respir J* **28**, 915-919 (2006).
137. Müller, E.J., Williamson, L., Kolly, C. & Suter, M.M. Outside-in signaling through integrins and cadherins: a central mechanism to control epidermal growth and differentiation? *The Journal of investigative dermatology* **128**, 501-516 (2008).
138. Watt, F.M., Lo Celso, C. & Silva-Vargas, V. Epidermal stem cells: an update. *Curr Opin Genet Dev* **16**, 518-524 (2006).
139. Tani, H., Morris, R.J. & Kaur, P. Enrichment for murine keratinocyte stem cells based on cell surface phenotype. *Proceedings of the National Academy of Sciences of the United States of America* **97**, 10960-10965 (2000).
140. Li, A., Simmons, P.J. & Kaur, P. Identification and isolation of candidate human keratinocyte stem cells based on cell surface phenotype. *Proceedings of the National Academy of Sciences of the United States of America* **95**, 3902-3907 (1998).
141. Maetzel, D., *et al.* Nuclear signalling by tumour-associated antigen EpCAM. *Nat Cell Biol* **11**, 162-171 (2009).
142. Kasper, M., Behrens, J., Schuh, D. & Müller, M. Distribution of E-cadherin and Ep-CAM in the human lung during development and after injury. *Histochemistry and Cell Biology* **103**, 281-286 (1995).
143. Bevilacqua, S., *et al.* A "live" biopsy in a small-cell lung cancer patient by detection of circulating tumor cells. *Lung Cancer* (2009).
144. Went, P., *et al.* Frequent high-level expression of the immunotherapeutic target Ep-CAM in colon, stomach, prostate and lung cancers. *Br J Cancer* **94**, 128-135 (2006).
145. Amann, M., *et al.* Therapeutic window of MuS110, a single-chain antibody construct bispecific for murine EpCAM and murine CD3. *Cancer research* **68**, 143-151 (2008).
146. Yovchev, M.I., *et al.* Identification of adult hepatic progenitor cells capable of repopulating injured rat liver. *Hepatology* **47**, 636-647 (2008).
147. Stingl, J., Raouf, A., Emerman, J.T. & Eaves, C.J. Epithelial progenitors in the normal human mammary gland. *Journal of Mammary Gland Biology and Neoplasia* **10**, 49-59 (2005).
148. Stingl, J., Eaves, C.J., Zandieh, I. & Emerman, J.T. Characterization of bipotent mammary epithelial progenitor cells in normal adult human breast tissue. *Breast cancer research and treatment* **67**, 93-109 (2001).
149. Ostrowski, L.E., Hutchins, J.R., Zakel, K. & O'Neal, W.K. Targeting expression of a transgene to the airway surface epithelium using a ciliated cell-specific promoter. *Molecular therapy* **8**, 637-645 (2003).

150. Lo, B., Hansen, S., Evans, K., Heath, J.K. & Wright, J.R. Alveolar epithelial type II cells induce T cell tolerance to specific antigen. *The journal of immunology* **180**, 881-888 (2008).
151. Van Winkle, L.S., Johnson, Z.A., Nishio, S.J., Brown, C.D. & Plopper, C.G. Early events in naphthalene-induced acute Clara cell toxicity: comparison of membrane permeability and ultrastructure. *Am J Respir Cell Mol Biol* **21**, 44-53 (1999).
152. Xin, L., Lukacs, R.U., Lawson, D.A., Cheng, D. & Witte, O.N. Self-renewal and multilineage differentiation in vitro from murine prostate stem cells. *Stem Cells* **25**, 2760-2769 (2007).
153. Azuma, M., *et al.* A quantitative matrigel assay for assessing repopulating capacity of prostate stem cells. *Biochem Biophys Res Commun* **338**, 1164-1170 (2005).
154. Claudinot, S., Nicolas, M., Oshima, H., Rochat, A. & Barrandon, Y. Long-term renewal of hair follicles from clonogenic multipotent stem cells. *Proc Natl Acad Sci U S A* **102**, 14677-14682 (2005).